The Henryk Niewodniczański

Institute of Nuclear Physics

Polish Academy of Sciences

Ph.D. thesis

"Study of interactions of copper-phenanthroline complexes with biomolecules by the X-ray Absorption Spectroscopy"

Wiktoria Idalia Stańczyk

Thesis submitted for the degree of
Doctor of Philosophy in Physics

Supervisor: prof. dr hab. Wojciech Maria Kwiatek
Auxiliary supervisor: dr hab. inż. Joanna Czapla-Masztafiak

Kraków, 2024

To my grandparents

Acknowledgments

Firstly, I would like to share my greatest gratitude to my supervisors – **prof. dr hab. Wojciech M. Kwiatek** and **dr hab. inż. Joanna Czapla-Masztafiak**, for their support, sharing with me their experience, and giving advices. For their kindness, understanding, and openness to letting me realize many scientific and social activities.

Secondly, I would like to thank **dr hab. Jakub Szlachetko, prof. UJ**, for supporting me many times during my Ph.D. studies, and giving me opportunities to learn and take part in many experiments abroad. For his supervision and giving inspiration, especially while being the Director of Department of Applied Spectroscopy at IFJ PAN.

I also would like to thank the scientific community that I could work with and learn from. Especially, people that I met in the Department of the Applied Spectroscopy of IFJ PAN: **dr hab. inż. Janusz Lekki, dr Wojciech Błachucki, dr Anna Wach, dr inż. Gabriela Imbir, dr Krzysztof Tyrała, dr Klaudia Wojtaszek, dr Artem Yakovliev, mgr Rafał Fanselow, tech. Tomasz Pieprzyca, and tech. Zbigniew Szklarz**, who helped me many times in my doctoral struggles, shared time for many discussions and supported me during my research.

People that I met during my internships and experiments in external facilities, especially **dr Christopher Milne** from the FXE station of the European XFEL and **dr Pieter Glatzel** from ID26 beamline of the ESRF synchrotron, for letting me learn from the bests and get experience in working with advanced equipment in the prestigious scientific facilities.

Staff from the DESY and SOLARIS synchrotron, that enabled me to conduct experiments during the ongoing pandemic of SARS-COVID-19.

Dr Ewa Pięta for her help in performing ATR-FTIR experiments, data analysis, and being so good-tempered and friendly.

Dr Michał Nowakowski for his support in the most crucial part of this research, for performing theoretical calculations, and for sharing with me his knowledge. Also, for his kindness and having with me many discussions during conferences and other occasions.

I would like to thank my colleagues from the doctoral community. People from the **IFJ PAN Doctoral Council**, with whom I spent all my Ph.D. student years at the IFJ PAN, planning many activities and sharing memories.

People that I met during my work for the Doctoral Council of PAN and Krajowa Reprezentacja Doktorantów. Especially, **dr Joanna Beck, mgr Piotr Skowron, mgr Patrycja Uram, and mgr Hubert Kasprzak**, for the unforgettable cooperation and nice time spent together on work for the doctoral community.

Dr Katarzyna Mikołajczak, dr inż. Jan Albert Zienkiewicz and mgr inż. Dawid Drozdowski, and many other friends, for our daily conversations about Ph.D. students' life and for providing an atmosphere of good humor and understanding.

Mgr inż. Ewa Borsuk and her husband **mgr inż. Józef Borsuk,** for our friendship and accompaniment during Ph.D. students' journey, from the very beginning.

Finally, I would like to thank **my family**, for their support and always believing in me.

My Love - Marcin, for being the best companion I could only imagine, even during my hardest times. For cheering me, always being on my side, for giving me the peace and support, that I needed.

And I would like to thank **God**, for His presence, giving me the strength to survive and to overcome problems, and enabling me to fulfill my dream to get a Ph.D. title.

NATIONAL SCIENCE CENTRE
POLAND

Doctoral research was realised with the financial support from the National Science Centre Poland (NCN), from SONATA 11 grant no. **2016/21/D/ST4/00378**.

Table of contents

ABSTRACT **11**

STRESZCZENIE (PL) **13**

LIST OF TABLES **17**

LIST OF FIGURES **19**

THESIS HYPOTHESIS, GOALS, AND STRUCTURE **25**

CHAPTER 1 ..... **27**

1.1. Properties of copper and its behavior in the human body **27**

1.2. Copper in anticancer therapy **30**

1.3. Synthesis of the copper-phenanthroline complex with triazole **35**

1.4. Verification of the results of synthesis by performing ATR-FTIR measurements **38**

1.5. Discussion **41**

1.6. Materials and laboratory **42**

1.7. Bibliography **43**

CHAPTER 2 ..... **49**

2.1. X-ray interactions with matter **49**
2.1.1. Elastic and non-elastic scattering 50
2.1.2. Photoelectric effect 51
2.1.3. Diffraction 56

2.2. Sources of X-rays **57**
2.2.1. X-ray tube 57
2.2.2. Synchrotron 58

2.3. X-ray Absorption Spectroscopy (XAS) **65**
2.3.1. Introduction to the method 65
2.3.2. XAS spectrum 69
2.3.3. XAS laboratory setup 71
2.3.4. XAS synchrotron setup 76

2.4. XAS measurements of copper referential samples in laboratory conditions **81**
2.4.1. Sample preparation 81
2.4.2. Data acquisition 83
2.4.3. Energetic calibration and data analysis procedure 84
2.4.4. Results 86

2.5. XAS measurements of copper solid samples at synchrotron facilities 97
2.5.1. Setup preparation 97
2.5.2. XAS data analysis 99
2.5.3. Results 101
2.5.4. Verification of XAS results obtained in laboratory conditions 103

2.6. Comparison of copper-complexes XAS spectra obtained with different radiation sources 105

2.7. Discussion 112

2.8. Materials and used programs 115

2.9. Bibliography 116

CHAPTER 3 119

3.1. Studies of interactions of metal complexes with biomolecules 119

3.2. XAS examination of biological samples - BioXAS 121

3.3. Development of the setup for the delivery of liquids 124

3.4. BioXAS examination of copper(II) compounds interactions with biomolecules 128
3.4.1. Data acquisition and analysis 128
3.4.2. Comparison of the XAS spectra of solid and liquid copper(II) samples 129
3.4.3. Examination of copper(II)-phenanthroline complexes' interactions with DNA 135
3.4.4. Examination of copper(II)-phenanthroline complexes' interactions with BSA 141

3.5. Discussion 144

3.6. Materials 146

3.7. Bibliography 148

FINAL DISCUSSION 151

LIST OF SCIENTIFIC ACHIEVEMENTS 159

Abstract

The motivation to investigate a topic presented in this doctoral dissertation originated from the still ongoing studies on new chemotherapeutic drugs. Nowadays, the problem of the side effects after application of the available medicines or the nonefficiency of some anticancer therapies is getting an importance, due to the still increasing number of diagnosed cancer cases worldwide. Commonly used compounds based on platinum, like cisplatin, are found to cause nausea, and lead to hearing impairment or problems with the digestive system, just to mention a few. Additionally, platinum is quite an expensive element to possess, what results in the high costs of drug production. Therefore, other alternatives are being explored, including complexes based on copper. This research concentrated on the examination of two copper-phenanthroline complexes, which were: Cu(1,10-phenanthroline)Cl_2, and synthesized Cu(1,10-phenanthroline)-(1H-1,2,4-triazole-1-yl)$Cl_2 \cdot H_2O$, with the use of the X-ray Absorption Spectroscopy (XAS) method.

The first part of the thesis focused on the review of copper's presence in the human body and its possible applications in anticancer treatment. The most important part focused on the process of synthesis of the copper-phenanthroline complex with triazole, basing on the publication by Tabassum et al. (2012). After many repetitions and attempts to optimize the synthesis procedure, it was found, that two different products are being obtained. To verify what are these products, an infrared spectroscopy examination was performed. It was found, that the secondary compound was in fact Cu(1,10-phenanthroline)Cl_2, already chosen before examination. The main product was recognized as the expected copper complex with triazole.

The second part was dedicated to the theory of X-ray absorption spectroscopy and various X-ray sources used in studies with this method. The experimental part concentrated on the XAS examination of both copper-phenanthroline compounds in a solid state, including additional referential compounds. The important part of this examination involved the application of the laboratory XAS setup, which is yet not so commonly used. The parameters of the measurements, especially acquisition time and concentration of the compound in the sample, were optimized, followed by the complex data analysis. XAS spectra, which were obtained in laboratory conditions, gave insight into the shape of the spectra and possible position of the absorption edge, yet, were lacking in less pronounced features, like pre-edge peaks. Therefore, it was decided to move the examination to the synchrotron facility, to obtain more detailed spectra.

Studies with the use of synchrotron radiation were performed in three facilities, that were: Swiss Light Source (SLS) of the Paul Scherrer Institut (PSI) in Villigen, Switzerland; PETRA III of the Deutsches Elektronen-Synchrotron (DESY) complex, in Hamburg, Germany; and SOLARIS synchrotron, in Kraków, Poland. Results provided information, that the studied compounds are not prone to photoreduction, and revealed the spectral features, that were absent in the laboratory XAS spectra. Analysis of the identified pre-edge peaks confirmed the expected geometry of the complexes, that were described in the crystallographic data found in the literature. This part of the examination also provided spectra, that were used as a reference in the analysis of the spectra of solutions of these two compounds.

The final part of the doctoral research concerned on the XAS studies of solutions. The important aspect involved the design of a liquid delivery setup, that enabled measurements of solutions over many hours, without a loss of the sample and reducing the possibility of radiation damage. Three different setups were tested, from which two having dedicated cells were found to be the most efficient.

Results of XAS studies of the copper-phenanthroline compounds dissolved in aqueous solutions, supported by the theoretical calculations, revealed the undergoing exchange of the ligands attached to copper. This process was also taken into consideration in the analysis of spectra of solutions incubated with DNA and bovine serum albumin (BSA). After analysis of the results of XAS spectra subtraction, the changes within the absorption edge region suggested a change in the electronic structure of both complexes, being a result of the weak noncovalent interactions with DNA. Additional electrostatic interactions were also found to be possible. In the case of examination involving BSA, it was found, that the copper-triazole complex seems to more preferably interact with this biomolecule than the first compound, probably because of the presence of the second planar organic group, which can be involved in hydrophobic interactions.

Summing all the results and discussions presented in this thesis, X-ray Absorption Spectroscopy was found to be a useful method for studying interactions of prospective copper-based chemotherapeutics with chosen biomolecules. Additionally, it revealed the information, that was lacking in the previous publications, which described a copper-triazole complex. Yet, this information was found to be crucial in understanding the mechanism of the interactions between copper-phenanthroline complexes with DNA and BSA molecules.

Streszczenie (PL)

Motywacją do podjęcia tematu projektu doktorskiego były wciąż trwające badania nad nowymi lekami chemioterapeutycznymi. W dzisiejszych czasach problem skutków ubocznych, pojawiających się w wyniku stosowania dostępnych leków, lub braku skuteczności niektórych terapii przeciwnowotworowych, nabiera szczególnego znaczenia w związku ze stale rosnącą liczbą diagnozowanych przypadków nowotworów na świecie. Stwierdzono, że powszechnie stosowane związki na bazie platyny, takie jak cisplatyna, powodują nudności i prowadzą do upośledzenia słuchu lub problemów z układem trawiennym, ale problemów tych jest dużo więcej. Dodatkowo platyna jest pierwiastkiem dość drogim w pozyskiwaniu, co przenosi się na wysokie koszty produkcji leków. Dlatego też badane są innego rodzaju związki, w tym kompleksy na bazie miedzi. Opisywane w rozprawie badania skupiły się na charakteryzacji dwóch kompleksów miedzi z fenantroliną, którymi były: Cu(1,10-fenantrolina)Cl_2 oraz zsyntetyzowany Cu(1,10-fenantrolina)-(1H-1,2,4-triazolo-1-yl)$Cl_2 \cdot H_2O$, metodą rentgenowskiej spektroskopii absorpcyjnej (ang. **X-ray Absorption Spectroscopy**, **XAS**).

Pierwsza część pracy skupiła się na przeglądzie literatury dotyczącej obecności miedzi w organizmie człowieka i jej możliwych zastosowaniach w leczeniu przeciwnowotworowym. Najważniejsza jednak część dotyczyła procesu syntezy kompleksu miedzi z triazolem, na podstawie publikacji Tabassum i inni (2012). Po wielu powtórzeniach i próbach optymalizacji procedury syntezy stwierdzono, że otrzymywane są dwa różne produkty reakcji. Aby scharakteryzować te produkty, wykonano badania metodą spektroskopii w podczerwieni. Stwierdzono, że drugim produktem okazał się wybrany już wcześniej do badań związek Cu(1,10-fenantrolina)Cl_2. Jako główny produkt rozpoznano oczekiwany kompleks miedzi z triazolem.

Część drugą rozprawy poświęcono teorii rentgenowskiej spektroskopii absorpcyjnej oraz różnym źródłom promieniowania rentgenowskiego, wykorzystywanym w badaniach tą metodą. Część doświadczalna skupiła się na badaniach XAS obu związków miedzi z fenantroliną w stanie stałym, z uwzględnieniem dodatkowych związków referencyjnych. Ważnym aspektem tego badania było zastosowanie laboratoryjnego układu XAS, który nie jest jeszcze tak powszechnie stosowany. Zoptymalizowano także parametry pomiarów, zwłaszcza czas akwizycji widm i stężenie związku w próbce, a następnie poddano wyniki kompleksowej analizie.

Uzyskane w warunkach laboratoryjnych widma XAS dały wgląd w kształt widm i możliwe położenie krawędzi absorpcji, jednakże brakowało w nich mniej intensywnych

struktur, takich jak piki przedkrawędziowe. W związku z tym, zdecydowano się przenieść badania do centrów synchrotronowych, w celu uzyskania bardziej szczegółowych widm.

Badania z wykorzystaniem promieniowania synchrotronowego przeprowadzono w trzech ośrodkach, którymi były: Swiss Light Source (SLS) Instytutu Paul'a Scherrer'a (PSI) w Villigen w Szwajcarii; PETRA III kompleksu Deutsches Elektronen-Synchrotron (DESY) w Hamburgu, w Niemczech; i synchrotron SOLARIS w Krakowie. Wyniki dostarczyły informacji, że badane związki nie ulegały redukcji pod wpływem napromieniowania, a także ujawniły struktury widmowe, których brakowało w laboratoryjnych widmach XAS. Analiza zidentyfikowanych pików przedkrawędziowych potwierdziła oczekiwaną geometrię kompleksów, która została zawarta w danych krystalograficznych dostępnych w literaturze. W tej części badań otrzymano także widma, które posłużyły jako referencja do analizy widm roztworów badanych dwóch związków.

Ostatnia część pracy doktorskiej dotyczyła badań cieczy. Ważnym aspektem było zaprojektowanie układu dostarczania cieczy, który umożliwiłby wielogodzinne pomiary roztworów bez strat próbki i ograniczałby możliwość uszkodzeń radiacyjnych badanego materiału. Przetestowano trzy różne układy, z których dwa z dedykowanymi celkami okazały się najbardziej wydajne.

Wyniki badań XAS związków miedzi z fenantroliną, rozpuszczonych w roztworach wodnych, poparte obliczeniami teoretycznymi, wykazały zachodzącą wymianę ligandów przyłączonych do miedzi. Proces ten uwzględniono w analizie widm roztworów inkubowanych z DNA i albuminą surowicy bydlęcej (ang. **bovine serum albumin, BSA**). Po analizie wyników odejmowania widm XAS, zmiany w obszarze krawędzi absorpcji sugerują zmianę w strukturze elektronowej obu kompleksów, będącą efektem zachodzących słabych, niekowalencyjnych oddziaływań z DNA. Stwierdzono również, że mogą także zachodzić dodatkowe oddziaływania elektrostatyczne. W przypadku badań z udziałem albuminy stwierdzono, że kompleks miedzi z triazolem wydaje się chętniej oddziaływać z tą biomolekułą niż pierwszy badany związek, prawdopodobnie ze względu na obecność drugiej grupy organicznej, która może brać udział w oddziaływaniach hydrofobowych.

Podsumowując wszystkie wyniki i dyskusje przedstawione w rozprawie, stwierdzono, że rentgenowska spektroskopia absorpcyjna jest użyteczną metodą badania oddziaływań potencjalnych chemioterapeutyków na bazie miedzi z wybranymi biomolekułami. Dodatkowo uzyskano informacje, których brakowało we wcześniejszych publikacjach, opisujących kompleks miedzi z triazolem. Stwierdzono jednak, że są one

kluczowe dla zrozumienia mechanizmu oddziaływań między kompleksami miedzi z fenantroliną z cząsteczkami DNA i albuminy.

List of tables

Table 1 Proportions of reagents for Cu(phen.triaz)Cl_2 synthesis 35

Table 2 Mass ratios of the used compounds to create a pellet sample 82

Table 3 Determined values of the energy of the absorption edge obtained by analyzing the derivatives of the XAS spectra 91

Table 4 Determined values of energy of the absorption edge from taking the energy of the point in half of the height of the edge 94

Table 5 Determined values characteristic for pre-edge peaks of XAS spectra of copper complexes with the indication of its crystallographic system 102

Table 6 Determined values of the energy of the absorption edge for copper samples 103

Table 7 Comparison of the obtained energies of the absorption edge for all copper(II) samples, determined from he results of the measurements using different sources of X-rays 109

Table 8 Determined values of parameters characteristic for pre-edge peaks of XAS spectra of copper complexes with the indication of its crystallographic system 111

Table 9 Determined values of the energy of the absorption edge for solid and liquid copper-phenanthroline samples 132

Table 10 Proportions of the used materials to prepare sample with copper-phenanthroline complex with DNA for incubation 136

Table 11 Determined values of the energy of the absorption edge for liquid copper-phenanthroline samples with or without DNA 136

Table 12 Proportions of the used materials to prepare sample with copper-phenanthroline complex and BSA for incubation 141

Table 13 Determined values of the energy of the absorption edge for liquid copper-phenanthroline samples with or without BSA 143

List of figures

Figure 1 Cooper distribution inside a human body [6] 27
Figure 2 Application of copper nanoparticles in various fields of medicine [35] 31
Figure 3 Chemical structure of 1,10-phenanthroline 31
Figure 4 Chemical structure of 1,2,4-triazole 32
Figure 5 Spatial structure of $Cu(phen)Cl_2$ 33
Figure 6 Spatial structure of $Cu(phen,triaz)Cl_2$ 33
Figure 7 Dimeric structure of $Cu(phen,triaz)Cl_2$, created via hydrogen bondings with water molecule [53] 33
Figure 8 Scheme of the ATR-FTIR setup [55] 34
Figure 9 Chemical reaction scheme of $Cu(phen,triaz)Cl_2$ synthesis 35
Figure 10 Reaction mixture before (left) and after (right) adding phenanthroline and triazole solutions 36
Figure 11 Filtration setup connected to the water pump 36
Figure 12 Filtrate of the performed synthesis 36
Figure 13 ATR-FTIR spectrum of the performed synthesis product 38
Figure 14 Comparison of ATR-FTIR spectra of $Cu(phen)Cl_2$ and sediment from performed synthesis 39
Figure 15 Comparison of fingerprint region of spectra of all studied samples 40
Figure 16 Proposed correction of the chemical reaction scheme of $Cu(phen,triaz)Cl_2$ synthesis 41
Figure 17 Cross sections for different interactions of photons with Cu atom [1] 49
Figure 18 Scheme of the elastic scattering process 51
Figure 19 Scheme of the non-elastic scattering process 51
Figure 20 Scheme of the photoelectric effect, with irradiation followed by absorption of the radiation (left) and ejection of the electron (right). For clarity of these and following figures, the number of draw electrons bounded to edges was reduced and the ejected electron's path was marked on the side 52
Figure 21 Scheme of the generation of the X-ray fluorescence radiation 53
Figure 22 Scheme of the Auger effect 54
Figure 23 Scheme of the Coster-Kronig effect 54
Figure 24 Scheme of possible processes, followed by the interactions of the incident X-rays with the matter in the given material [2] 55
Figure 25 Scheme of the diffraction of X-rays on the crystallographic planes 56
Figure 26 Schemes of the angular distribution of emitted radiation by the accelerated electron 60
Figure 27 Comparison of the synchrotron radiation brightness generated by different X-ray sources [2] 60
Figure 28 Example of synchrotron machine scheme [3] 61
Figure 29 Scheme of the magnets setup in an insertion device [4] 62
Figure 30 Configuration of the XAS setup, operating in the transmission mode 66
Figure 31 Configuration of the XAS setup operating in the fluorescence mode 67

Figure 32 Configuration of the XAS setup operating in the electron yield mode 67

Figure 33 Cu K-edge XAS spectrum of the copper foil, with marked XANES and EXAFS regions... 70

Figure 34 Configuration of the XAS laboratory setup. With letters: S - X-ray tube, B - sample holder station, C – crystal analyser, D – detector were marked. The red line shows the possible propagation pathway of the emitted X-rays from the X-ray source 72

Figure 35 Scheme of the position of the elements of laboratory XAS setup..... 73

Figure 36 View on the SLS and SwissFEL facilities [18]..... 77

Figure 37 Scheme of the SuperXAS beamline [19] 77

Figure 38 View on the experimental table of the SuperXAS beamline..... 78

Figure 39 View on the DESY facility with PETRA III synchrotron [22] 78

Figure 40 View on the P65 beamline experimental station 79

Figure 41 Scheme of the ASTRA beamline experimental station [23] 79

Figure 42 View on the ASTRA beamline experimental station 80

Figure 43 ID26 experimental station 81

Figure 44 Example of the results of the registration of number of counts in function of the sample position 83

Figure 45 Cu K-edge XAS spectrum of copper foil, measured in laboratory, with marked 3 points used for calibration from number of pixel to energy of registered photon..... 85

Figure 46 Comparison of Cu K-edge XAS spectra of $Cu(phen)Cl_2$ pellet, obtained with taking signal transmitted through air (top) and cellulose (down) as I_0..... 87

Figure 47 Cu K-edge XAS spectra of $Cu(phen)Cl_2$ pellet in the number of pixel scale obtained after different total acquisition time..... 88

Figure 48 Cu K-edge XAS spectra of pellets with varying concentration of $Cu(phen)Cl_2$..... 89

Figure 49 Cu K-edge XAS spectra of pellets containing $Cu(phen)Cl_2$ in concentration 5 and 10 wt.%..... 89

Figure 50 Laboratory Cu K-edge XAS spectra of copper foil and pellets, containing 5 wt.% of copper compound 90

Figure 51 Laboratory Cu K-edge XAS spectrum of Cu foil (top), with the first (middle) and second derivative (down). With a vertical dashed line the energy of the maximum of the first derivative and the point crossing zero of the Y axis of the second derivative were marked. With horizontal dashed lines the value of the absorption totaling 1 and 0 respectively was marked..... 92

Figure 52 Laboratory Cu K-edge XAS spectrum of CuO pellet (top), with the first (middle) and second derivative (down). With a vertical dashed line the energy of the maximum of the first derivative and the point crossing zero of the Y axis of the second derivative were marked. With horizontal dashed lines the value of the absorption totaling 1 and 0 respectively was marked 92

Figure 53 Laboratory Cu K-edge XAS spectrum of $CuSO_4$ pellet (top), with the first (middle) and second derivative (down). With a vertical dashed line the energy of the maximum of the first derivative and the point crossing zero of the Y axis of the second derivative were marked. With horizontal dashed lines the value of the absorption totaling 1 and 0 respectively was marked 93

Figure 54 Laboratory Cu K-edge XAS spectrum of $Cu(phen)Cl_2$ pellet (top), with the first (middle) and second derivative (down). With a vertical dashed line the energy of the maximum of the first derivative and the point crossing zero of the Y axis of the second derivative were marked. With horizontal dashed lines the value of the absorption totaling 1 and 0 respectively was marked 93

Figure 55 Laboratory Cu K-edge XAS spectrum of the Cu foil. With red dashed lines regions of the chosen beginning and end of the rising edge were marked, and with blue one the determined its half of the height..... 95

Figure 56 Laboratory Cu K-edge XAS spectrum of the CuO pellet. With red dashed lines regions of the chosen beginning and end of the rising edge were marked, and with blue one the determined its half of the height 95

Figure 57 Laboratory Cu K-edge XAS spectrum of the $CuSO_4$ pellet. With red dashed lines regions of the chosen beginning and end of the rising edge were marked, and with blue one the determined its half of the height 96

Figure 58 Laboratory Cu K-edge XAS spectrum of the Cu(phen)Cl_2 pellet. With red dashed lines regions of the chosen beginning and end of the rising edge were marked, and with blue one the determined its half of the height.....96

Figure 59 View on the sample holder with attached pellet (marked with a yellow square) on the SuperXAS experimental table.....97

Figure 60 Holder for pellets from the P65 beamline.....98

Figure 61 Pellet attached to the holder from ASTRA beamline 99

Figure 62 Comparison of the results of interpolation, between the Cu K-edge XAS spectra of Cu(phen,triaz)Cl_2 pellet. With blue marked area indicating the region with disturbed data by monochromator issues.....100

Figure 63 Synchrotron Cu K-edge XAS spectra of copper foil and pellets, containing 5 wt.% of a given copper complex 101

Figure 64 Pre-edge region of the Cu K-edge XAS spectra of copper complexes.....102

Figure 65 Cu K-edge XAS spectra of copper samples obtained in synchrotron (red) and laboratory (black) conditions.....104

Figure 66 Comparison of the not smoothed and smoothed Cu K-edge XAS spectra of Cu(phen,triaz)Cl_2 5 wt.% pellet.....105

Figure 67 Cu K-edge XAS spectra of Cu foil, with marked with dashed line energy of the absorption edge 106

Figure 68 Cu K-edge XAS spectra of $CuSO_4$ pellet, with marked with dashed lines determined energy of the absorption edge for each spectrum.....106

Figure 69 Cu K-edge XAS spectra of CuO pellet, with marked with dashed lines determined energy of the absorption edge for each spectrum 107

Figure 70 Cu K-edge XAS spectra of Cu(phen)Cl_2 pellet, with marked with dashed lines determined energy of the absorption edge for each spectrum.....107

Figure 71 Cu K-edge XAS spectra of Cu(phen,triaz)Cl_2 pellet, with marked with dashed lines determined energy of the absorption edge for each spectrum.....107

Figure 72 Cu K-edge XAS spectra of chosen copper samples, that were obtained with SLS synchrotron radiation. With dashed lines of colours matching the corresponding spectra, the values of the determined energy of absorption edge were marked 109

Figure 73 Cu K-edge XAS spectra of chosen copper samples, that were obtained with DESY synchrotron radiation. With dashed lines of colours matching the corresponding spectra, the values of the determined energy of absorption edge were marked 109

Figure 74 Cu K-edge XAS spectra of chosen copper samples, that were obtained with ASTRA synchrotron radiation. With dashed lines of colours matching the corresponding spectra, the values of the determined energy of absorption edge were marked 110

Figure 75 Cu K-edge XAS spectra of chosen copper samples, that were obtained with radiation emitted by the X-ray tube. With dashed lines of colours matching the corresponding spectra, the values of the determined energy of absorption edge were marked.....110

Figure 76 Comparison of the values of energy of the absorption edge for different copper samples and used radiation sources. With the hatched area the region of the values for Cu^{2+} compounds was marked 111

Figure 77 Position of the center of pre-edge peaks in a function of their area under peak 112

Figure 78 Damaging processes of the DNA structure after irradiation [15] 122

Figure 79 Photography of the simple liquid delivery setup, that was tested before the experiment ... 124

Figure 80 Liquid delivery setup mounted on the experimental table of the ID26 ESRF beamline. With letters were marked: A- glass capillary, B- funnel, C- magnetic pump, D – connector with pipes..... 125

Figure 81 Created foam made from albumin as a result of the aerification 125

Figure 82 Liquid cell for experiments with the circulating sample..... 126

Figure 83 Liquid delivery setup mounted on the P65 beamline of DESY synchrotron 126

Figure 84 Part of the liquid delivery setup, with presented container from the part of syringe, and little peristaltic pump controlled by the microcontroler 127

Figure 85 Liquid delivery setup, which was mounted on the ASTRA beamline of SOLARIS 127

Figure 86 Synchrotron Cu K-edge XAS spectra of liquid and solid sample containing $Cu(phen)Cl_2$. With green circle the pre-edge region was marked, enlarged and inserted on the right bottom corner to show pre-edge peak..... 129

Figure 87 Synchrotron Cu K-edge XAS spectra of liquid and solid sample containing $Cu(phen,triaz)Cl_2$. With light blue circle the pre-edge region was marked, enlarged and inserted on the right bottom corner to show pre-edge peak..... 130

Figure 88 First derivative of Cu K-edge XAS spectra of $Cu(phen)Cl_2$ pellet and its 4 mM aqueous solution. With dashed lines maxima of both derivatives were marked, that determine the energy of the absorption edge..... 131

Figure 89 First derivative of Cu K-edge XAS spectra of $Cu(phen,triaz)Cl_2$ pellet and its 4 mM aqueous solution. With dashed lines maxima of both derivatives were marked, that determine the energy of the absorption edge..... 131

Figure 90 Cu K-edge XAS spectrum of $Cu(phen,triaz)Cl_2$ solution, with marked with dashed lines values of maxima of two peaks of the first derivative of spectrum within the XANES region 131

Figure 91 Experimental and calculated Cu K-edge XAS spectra of $Cu(phen)Cl_2$ solution 133

Figure 92 Experimental and calculated Cu K-edge XAS spectra of $Cu(phen,triaz)Cl_2$ solution 133

Figure 93 Experimental and calculated Cu K-edge XAS spectra of copper-phenanthroline complex solution, after substitution of two Cl atoms with two -OH groups..... 134

Figure 94 Experimental and calculated Cu K-edge XAS spectra of copper-phenanthroline-triazole complex solution, after substitution of two Cl atoms with two -OH groups..... 134

Figure 95 Experimental and calculated Cu K-edge XAS spectra of copper-phenanthroline complex solution, after substitution of two Cl atoms with one -OH and one $-OH_2$ group..... 134

Figure 96 Experimental and calculated Cu K-edge XAS spectra of copper-phenanthroline-triazole complex solution, after substitution of two Cl atoms with one -OH and one $-OH_2$ group 134

Figure 97 Cu K-edge XAS spectra of incubated 4 mM $Cu(phen)Cl_2$ solutions, with DNA (dark green) and alone (dark blue). Result of their subtraction was presented with a black line at the bottom. With dashed lines, in the same colours as the corresponding spectra, marked the values of the energy of the absorption edge and maxima of the white lines. Additionally, with the red dashed line on the bottom graph, the subtraction of the smoothed spectra is presented, to ease the analysis. 137

Figure 98 Cu K-edge XAS spectra of incubated 4 mM $Cu(phen,triaz)Cl_2$ solutions, with DNA (dark green) and alone (dark blue). Result of their subtraction was presented with a black line at the

bottom. With dashed lines, in the same colours as the corresponding spectra, marked the values of the energy of the absorption edge and maxima of the white lines. Additionally, with a red dashed line on the bottom graph, the subtraction of the smoothed spectra is presented, to ease the analysis .138

Figure 99 Experimental and calculated Cu K-edge XAS spectra of copper-phenanthroline complex solution with DNA, after substitution of two Cl atoms with two -OH groups.....139

Figure 100 Experimental and calculated Cu K-edge XAS spectra of copper-triazole complex solution with DNA, after substitution of two Cl atoms with two -OH groups.....139

Figure 101 Experimental and calculated Cu K-edge XAS spectra of copper-phenanthroline complex solution with DNA, after substitution of two Cl atoms with one -OH and one -OH_2 group .139

Figure 102 Experimental and calculated Cu K-edge XAS spectra of copper-triazole complex solution with DNA, after substitution of two Cl atoms with one -OH and one -OH_2 group.....139

Figure 103 Pre-edge region of the Cu K-edge XAS spectra of copper-phenanthroline solutions, that were incubated without and with DNA.....140

Figure 104 Pre-edge region of the Cu K-edge XAS spectra of copper-triazole solutions, that were incubated without and with DNA 140

Figure 105 Cu K-edge XAS spectra of incubated 4 mM copper-phenanthroline solutions, with BSA (dark green) and alone (dark blue). Result of their subtraction was presented with a red line at the bottom. 142

Figure 106 Cu K-edge XAS spectra of incubated 4 mM copper-triazole solutions, with BSA (dark green) and alone (dark blue). Result of their subtraction was presented with a red line at the bottom.142

Thesis hypothesis, goals, and structure

The hypothesis, that was the leading motivation of the whole doctoral project was: "The application of the X-ray Absorption Spectroscopy (XAS) gives the possibility to identify and describe interactions of two chosen copper-phenanthroline complexes with biomolecules". The proposed hypothesis was supported by the fact, that XAS spectra are sensitive to the changes in geometry around an analyzed element and its oxidation number, which can change when the complex interacts with the biomolecule.

There were also other goals formulated, that expanded the process of hypothesis verification:

1. Elaborating synthesis of copper-phenanthroline compound: dichloro-(1,10-phenanthroline)-(1H-1,2,4-triazol-1-yl)-copper(II) monohydrate, described in publication by Tabassum et al. (2012), with verification and optimization of this process.
2. Performing a series of measurements with the use of an XAS laboratory setup, to choose the parameters, which will enable efficient studies of solid copper-based samples, or which will provide information, that such samples cannot be examined in accessible conditions.
3. Comparing of the results obtained in laboratory and synchrotron conditions, which will provide information about the limitations, advantages, and disadvantages of selected conditions.
4. Comparing of the data obtained in synchrotron facilities, to identify the differences in XAS results, even if all of them were obtained with the application of intensive radiation source and with the same method of investigation.
5. Testing the liquid-delivery setups and developing the one, that will meet identified needs of the sample.
6. Conducting studies of copper-phenanthroline complexes solutions alone and with a chosen biomolecule.
7. Developing data analysis, that will enable answering the scientific question.

The thesis structure is composed as follows:

1) **Chapter 1** is focused on the explanation of the role of copper and its behavior in the human body. It presents the prospective use of copper-based drugs in chemotherapy and proposes two copper-phenanthroline-based complexes, that were an object of investigation. It also describes a process of synthesis of one of these

complexes and a method of verification if it went successfully. In this chapter meeting goal number 1 was described.

2) **Chapter 2** concentrates on the physical and experimental basics of X-ray Absorption Spectroscopy, including the presentation of sources of X-ray radiation and setups. It provides details about the laboratory XAS setup, including alignment of its elements, energetic calibration, and optimization of the signal measurements. Results of measurements of referential solid-state samples, performed at the laboratory and 3 synchrotron beamlines, are also provided in this chapter. Attempts to meet goals number 2-4 are described.
3) In **Chapter 3** the application of the XAS method to study biological samples is described and the identified dangers and difficulties are presented. A few tested setups for delivery of the liquids are presented, with their comparison and conclusions, which of them will be the most efficient for examined samples. It provides the results of investigation of the solutions of copper-phenanthroline compounds alone and with chosen biomolecule, that are bovine genetic DNA or bovine serum albumin (BSA). From the point of view of verification of thesis hypothesis, this is a crucial chapter, that provides the answer and describes attempts to achieve goals 5-7.
4) After Chapter 3, the **Final discussion was provided**, which sum obtained results and conclusions from all chapters.
5) The thesis ends with providing the **List of scientific achievements** of the thesis' author.

Additionally, at the end of each chapter, the discussion of the presented results and a list of used bibliography are provided, for more comfortable reading and easier searching for cited scientific sources.

Chapter 1

Copper and its complexes

1.1. Properties of copper and its behavior in the human body

Copper belongs to the transient metals and is located in the periodic table in the 11th group, between nickel and zinc, the 4th row, one above silver. It can be found mostly in the +1 and +2 oxidation states in nature. However, complexes with copper +3 or +4 state can be also found. For example, they appear in synthesized organometallic complexes, but their potential instability needs to be emphasized [1-3].

Copper belongs to the group of microelements, so elements that are needed for the human body for proper functioning. Basing on the scientific opinion published by the European Food Safety Authority (EFSA) in 2015 [4], the suggested copper intake for an adult man totals 1.6 mg per day, while for an adult unpregnant woman 1.3 mg per day. Pregnancy and breastfeeding increase the needed amount of copper by 0.2 mg per day. Copper accumulates mostly in the brain, liver, heart, kidney, and muscles (**Figure 1)** [5,6].

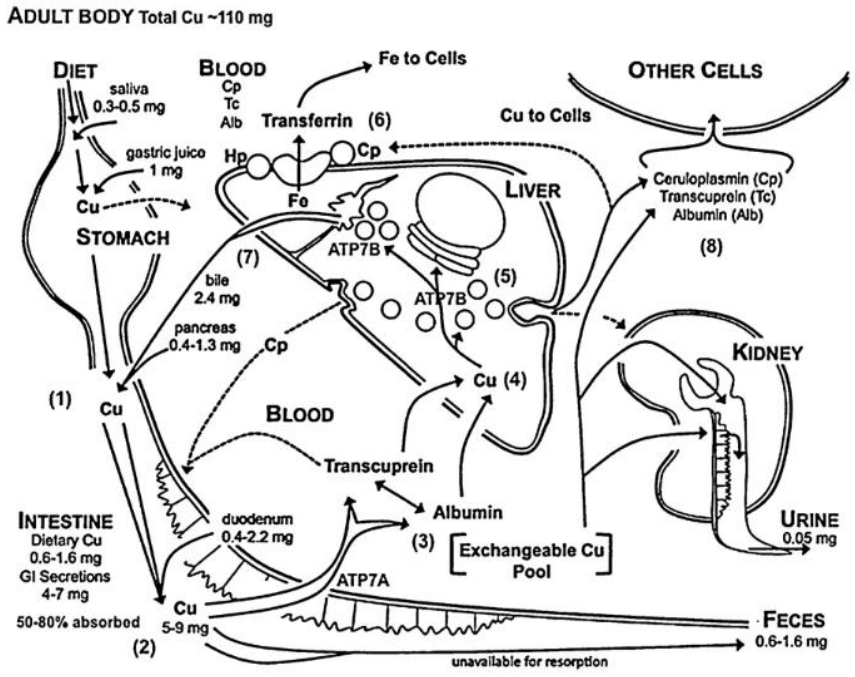

Figure 1 Cooper distribution inside a human body [6]

The electronic configuration for a copper metallic atom can be noted as [Ar] 3d^{10} 4s^{1}, while for Cu^{1+} [Ar] 3d^{10} and Cu^{2+} [Ar] 3d^{9}. The difference in the number of electrons bonded to the 3d orbital leads to observations of different magnetic properties – Cu^{1+} form exhibits diamagnetic properties, while Cu^{2+} is paramagnetic [7, 8]. The fact of the unfilled

d-orbital for Cu^{2+} will also have great importance in the analysis of X-ray Absorption Spectroscopy (XAS) spectra, which have been described in Chapter 2.

Copper is a micronutrient, which is redox-reactive, therefore its presence and concentration in cells and any tissue must be strictly controlled. In blood, copper ions are transported by dedicated proteins, mostly ceruloplasmin [9]. On the other hand, free copper ions in blood plasma attach easily to albumin or transcuprein [10]. Within cells, copper ions are prone to binding to cysteine-rich proteins [11]. Copper can be exported also from cells via an ATPase pump. Despite these mechanisms, sometimes the levels of copper can be abnormal, like in the case of the Wilson or Menkes diseases. Elevated levels of copper ions concentration can be observed where angiogenesis undergoes. This process occurs intensively in the growing, healthy organs, but also in the tumor progression. Indeed, raised concentrations of copper in cells are noticed in many types of cancer, where it is involved in the growth of the tumor and even metastasis [12].

What is important, copper is a redox-reactive element, that can undergo processes resulting in the production of free radicals (marked further with the "°" symbol). Changes between +2 and +1 states, observed during Fenton-like or Haber-Weiss-like redox reactions, and interactions of these two copper forms with biomolecules, like lipids or proteins, can lead to the production of hydroxyl radical or hydrogen peroxide, which are reactive oxygen species (ROS) (**Equations 1-6**) [6,7].

a) Fenton-like mechanism:

$$Cu^{2+} + O_2^- \rightarrow Cu^{1+} + O_2 \quad (1)$$

$$Cu^{1+} + H_2O_2 \rightarrow Cu^{2+} + OH^- + OH° \quad (2)$$

b) Haber-Weiss-like mechanism:

$$2Cu^{2+} + 2GSH \rightarrow 2Cu^{1+} + GSSG \quad (3)$$

Where: *GSH* – glutathione,

GSSG – glutathione disulfide

$$Cu^{1+} + O_2 \rightarrow Cu^{2+} + O_2^- \quad (4)$$

$$O_2^- + 2H^+ \rightarrow H_2O_2 \quad (5)$$

$$Cu^{1+} + H_2O_2 \rightarrow Cu^{2+} + OH^- + OH° \quad (6)$$

The generation of Cu^{3+} as a result of such redox processes was also noted in the literature, where copper also undergoes another reaction, leading to the production of new radicals (**Equations 7-8**) [13,14]:

$$Cu^{2+} + H_2O_2 \rightarrow Cu^{3+} + OH° + OH^- \quad (7)$$

$$Cu^{3+} \text{ (acidic solution)} \leftrightarrow Cu^{2+} + OH° + H^+ \quad (8)$$

The introduction of some reagents, like ascorbic acid, can lead to the promotion of the generation of oxidative stress in cells, since they can exert prooxidant, not antioxidant behavior, leading to the observation of the increased cytotoxicity of copper [15]. What is also interesting, is the fact that one of the proteins – glutathione, takes part in the binding of the free copper inside cells and acts as its chelator and antioxidant [16]. However, when Cu^{1+} was incorporated into some complexes, like 1,10-phenanthroline, it was found that glutathione started to become prooxidant and increased the DNA cleavage [17].

This redox reactivity of copper can be considered both an asset and a flaw, depending on the case. Firstly, when these kinds of reactions undergo within cancer cells, leading to death and therefore stopping cancer from progression, it would be a very promising effect. On the other hand, such behavior can generate radicals that will damage DNA and other important biomolecules [18], which can lead to cancerogenesis [19-21]. To stop this harmful situation and mentioned angiogenesis, there is a possibility to use chelating agents, that will bind to copper and therefore deprive it of such unwanted properties [22, 23]. As it was mentioned, in a healthy organism such a situation normally is prevented by the presence of some proteins, like albumins [10], that bind free copper ions, therefore hindering undergoing any redox reactions presented above.

However, such a behavior can be used to make the complexes naturally present in the human body catalyzers of some welcomed redox reactions. Copper ions can be found there in a Cu^{1+} or Cu^{2+} oxidation state, surrounded by sulfur or N-containing ligands [24]. One of the commonly known enzymes is copper-zinc dismutase, which possesses Cu^{2+} incorporated into its structure. It undergoes the redox reaction, which results in a disproportionation of O^{2-}, that comes from e.g., some immune responses [25]. Another enzyme is ceruloplasmin, which is rich in copper (6-8 atoms per molecule), and is the biggest transporter of copper in the blood, and takes part in the oxygenation of Fe^{2+} [9].

Another very important property of copper should be mentioned. It was found that copper tends to bind to DNA, both to the phosphate group or base [26]. Moreover, there are studies indicating that copper takes part in the folding of chromatin and keeping its

long-order structure [27]. Such interaction of copper with DNA can be taken into consideration while designing new drugs, like chemotherapeutics.

1.2. Copper in anticancer therapy

The importance and usage of copper have been known since prehistory, which led to the creation of the term “Copper Age”, for the time when this element was intensively used, preceding the widely known “Bronze Age” [28]. Also in ancient times, copper was already used for water purification and used to treat some diseases [29]. Even thousands of years later, copper seems to have not been that less important to be used for medical purposes. Especially, since there is a lot to be done for the development of more efficient chemotherapy, where it could be applied.

Still one of the most known and applied in oncology metal-based drugs is cisplatin, followed by other alternative platinum compounds, that are oxaliplatin or carboplatin. However, even if the application of cisplatin was found to be successful in many cases, some other problems remain to be solved. It was found that chemotherapy with cisplatin can lead to serious side effects, like nephrotoxicity, vomiting, and gastrointestinal toxicity, just to mention a few [30]. Therefore, other platinum-based complexes are being explored. Yet, platinum is not the cheapest element to obtain and is not included in the list of microelements. Also, this drug is fully inorganic, and its cytotoxicity probably mostly lies in the fact that it interacts with DNA, by the creation of intra- or inter-stand crosslinking binding [31]. Since some cancer cases exhibit resistance to the treatment with cisplatin, there is a possibility to develop new platin-based drugs, e.g., possessing some organic groups (like in the case of oxaliplatin and carboplatin) or by changing the metal.

The choice to study copper as an alternative metal to incorporate into future drug complexes was not so hard to make. As it was described in the previous subsection, copper is naturally present in the human body as a building block of some proteins and is involved in important processes, like angiogenesis. Its reactivity to undergo redox reactions, including Fenton- or Haber-Weiss-like ones, can make copper-based compounds cytotoxic. For example, it is widely known, that adding copper to alloys or using it in the coating, can make this kind of material antibacterial, and therefore they can be applied in environments that are exposed to contact with many types of bacteria, like hospitals [32, 33]. Other possible applications of copper can be also found, like for diagnostics in nuclear medicine or used as a part of anti-inflammatory complexes [34]. Also, some copper compounds have the potential for anticancer treatment.

One of the fast-growing studies branches where copper is under investigation is nanotechnology (**Figure 2**) [35]. From trying to reduce the dose of the applied drug, increase the proper targeting, to taking into account the copper redox reactivity, there are many undergoing studies performed on this topic [36, 37]. Yet, there are some obstacles to overcome, for example, it is very hard to keep the metallic nanoparticles unoxidized to Cu^{2+}, or one needs to consider the possible creation of the nanoparticle corona as a result of nanoparticles interactions with proteins [38, 39]. Nevertheless, nanoparticles used in chemotherapy are also one of the promising alternatives to be developed.

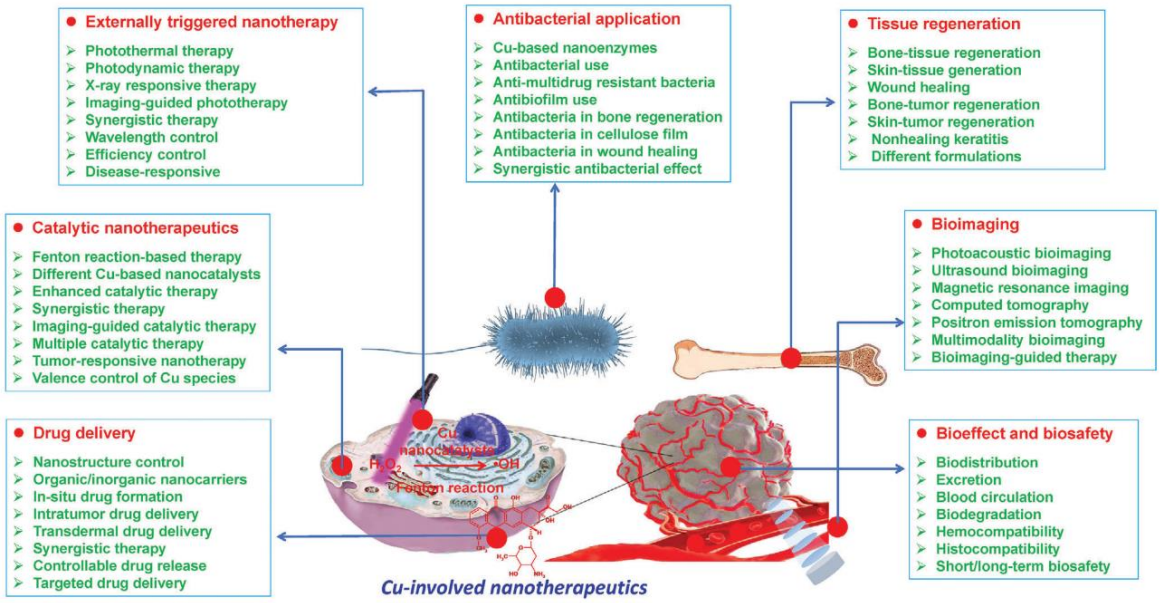

Figure 2 Application of copper nanoparticles in various fields of medicine [35]

Another group of copper-based drugs are patented Casiopeinas®, from which one complex went even to the 1st phase of a clinical trial. All of them are Cu^{2+}-containing complexes, that are chelated by different ligands, including a modified 1,10-phenanthroline group [40]. They were found to be antineoplastic for some resistant to cisplatin types of cancer. The difference with the cisplatin behavior is that other cytotoxic mechanisms are taken into consideration, like ROS generation or affecting mitochondrial pathways [41].

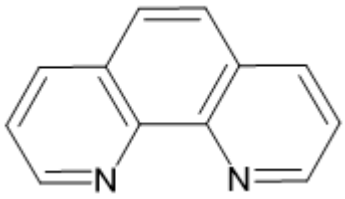

Figure 3 Chemical structure of 1,10-phenanthroline

The complex of Cu^{+1} with 1,10-phenanthroline was found to be the first synthetic nuclease that was studied. Nowadays, 1,10-phenanthroline and its derivatives, including those having metals, are widely synthesized and studied to use them as antibacterial [42] or antitumor compounds [43, 44]. Combination of the 1,10-

phenanthroline group with transient metal, like cooper, could result in obtaining two routes of cytotoxic action, cleavage of the DNA and generation of toxic free radicals, via Fenton/Haber-Weiss-like reactions, that were mentioned before [45].

The geometry of this organic group, making it a flat structure, enables the complex to fit between DNA strands **(Figure 3)** [46]. Then, in the presence of H_2O_2, copper-phenanthroline complexes can non-covalently bond to DNA and lead to the cleavage of the DNA [47]. There are also many studies on copper-phenanthroline complexes, which also show more than one atom of copper attached to phenanthroline. Such complexes can bind to the minor or major groove of the DNA strand and induce its scission [48]. Choosing the efficient anticancer compound to be cytotoxic for a given cancer line is one thing, however, problems can occur in its toxicity against normal cells and accumulation in healthy organs. For example, there are already undergoing studies to obtain a complex, that is only toxic for tumors, but not for healthy intestinal cells [49]. Another possibility is to try to lower the needed dose of a drug, for example, via adding to the chemical structure some additional groups, which can make the whole complex more cytotoxic, and therefore less amount of the drug itself would need to be provided to obtain a satisfactory effect. Such a group can be 1,2,4-triazole (**Figure 4**).

Triazole-containing compounds exhibit many antimicrobial properties. It was found that such complexes can be used against bacteria, fungi, and what is also very promising, against cancer cells [50, 51]. There are already some approved drugs to be used in medicine, that are derivatives of the 1,2,4-triazole, which are for example estazolam and trazodon, that act on the nervous system [52]. This moiety was found to inhibit various enzymes, including those active in cancer cells. A combination of both 1,10-phenanthroline and 1,2,4-triazole groups with copper seems to have the potential to develop some promising anticancer compounds, therefore in the presented study such one complex was taken for examination.

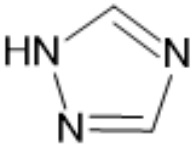

Figure 4 Chemical structure of 1,2,4-triazole

All mentioned by far complexes were characterized with the use of commonly known biochemistry laboratory methods, like UV-Vis spectroscopy or electrophoresis, to prove their cytotoxic behavior. Chosen method where X-rays were applied, was X-ray Diffraction (XRD), which is being widely used in crystallography and drug design. Specially designed tests to study ROS generation or general cytotoxicity with the presence of cells were also applied. However, there is at least one known method, which can probe the complex structure and changes in the oxidation number of a given element, including copper, in many types of environments, temperatures, etc. And this method – X-ray

Absorption Spectroscopy (XAS) was used in this study to examine copper-phenanthroline complexes, including one possessing a 1,2,4-triazole group, that was synthesized according to the reported procedure [53].

XAS studies are performed in energy ranges, that cover the needed energy of radiation, which will be absorbed by electrons from a given orbital of the element of interest. Therefore, this method is element-specific and will provide information on its oxidation number, type of neighborhood ligands, or length of bonds. Knowledge about complementary physical or chemical properties from different types of studies, performed on the same complex, can supplement the whole process of XAS examination. For this thesis, results of the X-ray diffractometry measurements of both copper-phenanthroline complexes were found and used during XAS analysis.

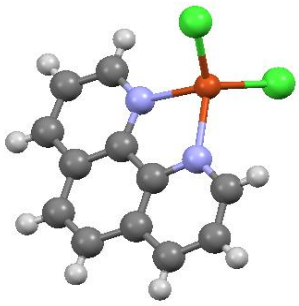

Figure 5 Spatial structure of $Cu(phen)Cl_2$

The first study covered the examination of Cu(1,10-phenanthroline)Cl_2 (*later:* ***Cu(phen)Cl$_2$***) [54]. This compound crystallizes to a monoclinic system and $P2_1/c$ space group. Copper atom was found to be coordinated by two chlorine atoms and two nitrogen atoms from 1,10-phenanthroline, in a distorted tetrahedral geometry (**Figure 5**). The length of the bonds between copper and nitrogen atoms totals 2.049 and 2.073 Å, while between copper and chlorine atoms 2.120 and 2.212 Å.

The second study involved an examination of Cu(1,10-phenanthroline)-(1H-1,2,4-triazol-1-yl)$Cl_2 \cdot H_2O$ (later: ***Cu(phen,triaz)Cl$_2$***) [53]. The complex was found to crystallize to a monoclinic system and $P2_1/n$ space group. Copper in this complex is coordinated by one nitrogen atom from 1,2,4-triazole, two nitrogen atoms from 1,10-phenanthroline, and two chlorine ones, resulting in obtaining a distorted square pyramid geometry around

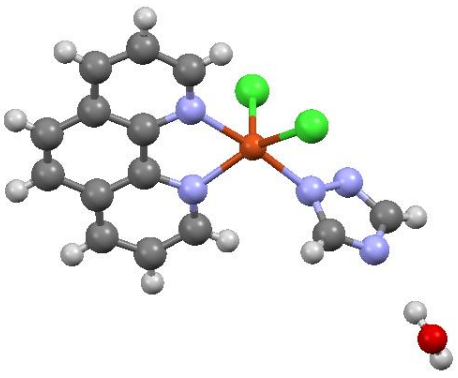

Figure 6 Spatial structure of $Cu(phen,triaz)Cl_2$

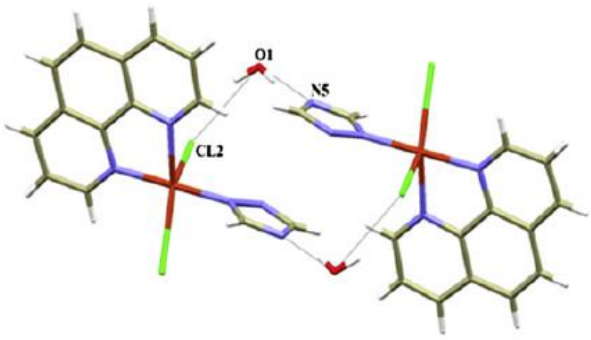

Figure 7 Dimeric structure of $Cu(phen,triaz)Cl_2$, created via hydrogen bondings with water molecule [53]

a metallic center (**Figure 6**). The length of the bonds between copper and 2 chlorine atoms totals 2.425 and 2.535 Å, while between copper and nitrogen atoms 2.010, 2.007 (from phenanthroline), and 1.974 Å (from triazole). Additionally, it was found, that the water molecule is involved in the creation of the hydrogen bonding, linking the chlorine atom of one molecule and nitrogen from the second molecule, what leads to obtaining a dimeric structure (**Figure 7**).

To verify the results of the synthesis of Cu(phen,triaz)Cl_2, the Fourier Transform Infrared Spectroscopy (FTIR) was used, with a setup based on the Attenuated Total Reflectance (ATR) technique of signal registration (**Figure 8**).

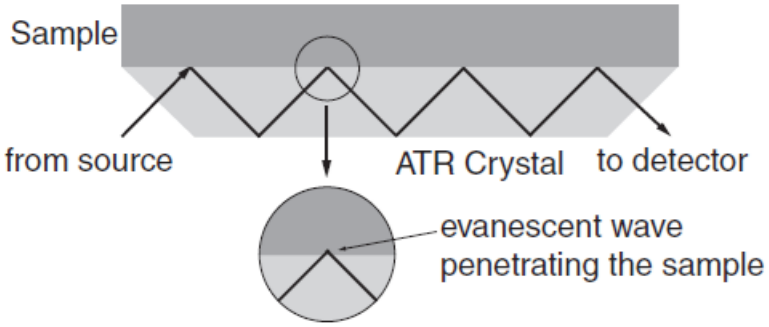

Figure 8 Scheme of the ATR-FTIR setup [55]

The infrared spectroscopy itself bases on the absorption of the infrared radiation (IR) by the sample, which results in promoting molecular vibrations, like stretching or bending of chemical bonds [56]. In the used geometry, radiation emitted by the source passes through a crystal, and then its part is absorbed by a thin layer of sample [57]. Not absorbed radiation passes again through the crystal and incidents on the detector. In ATR configuration, the incident angle is chosen to meet a condition for total internal reflection, which as a result, leads to many events of radiation passing the sample, that can be absorbed. Experimental data undergoes then Fourier transformation, which gives a spectrum consisting of bands, that correspond to given molecular vibrations of an examined compound.

Such a geometry enables measurements of pure complexes, without a need to prepare any mixture of compounds to register a strong signal [58]. Therefore, the powder obtained after synthesis can be transferred to the setup and analyzed with the use of the ATR-FTIR spectrometer, what was done in described project.

1.3. Synthesis of the copper-phenanthroline complex with triazole

Copper complex with 1,10-phenanthroline and 1,2,4-triazole was synthesized in the chemistry laboratory of the Department of Applied Spectroscopy, Institute of Nuclear Physics of Polish Academy of Sciences in Kraków, Poland, according to the description written by Tabassum et. al [53]. The undergoing reaction was written as follows (**Figure 9**):

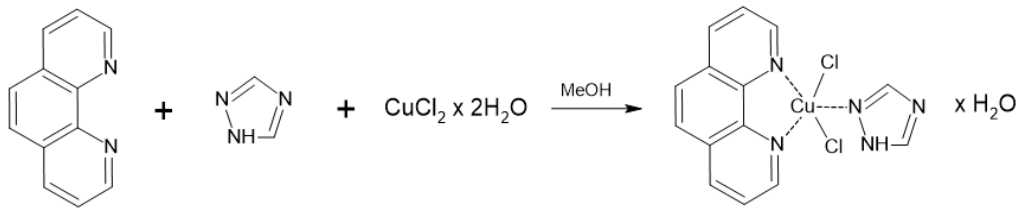

Figure 9 Chemical reaction scheme of Cu(phen,triaz)Cl_2 synthesis

After many attempts and observations, a complete procedure to obtain repetitive results was determined. The procedure involved below steps:

1. Weighting all the solid compounds with the use of the scale, in below proportions (**Table 1**):

Table 1 Proportions of reagents for Cu(phen.triaz)Cl_2 synthesis

Compound	**Weighted mass [g]**
1,10-phenanthroline	0.180
$CuCl_2 \cdot 2H_2O$	0.170
1,2,4-triazole	0.069

2. Dissolving in three flasks all of the above compounds separately in methanol: 1,10-phenanthroline and 1,2,4-triazole in 10 ml of the solvent, $CuCl_2 \cdot 2H_2O$ in 15 ml. Putting the flask with a solution of the latter compound into the preheated water bath, which was heated up to 25°C.

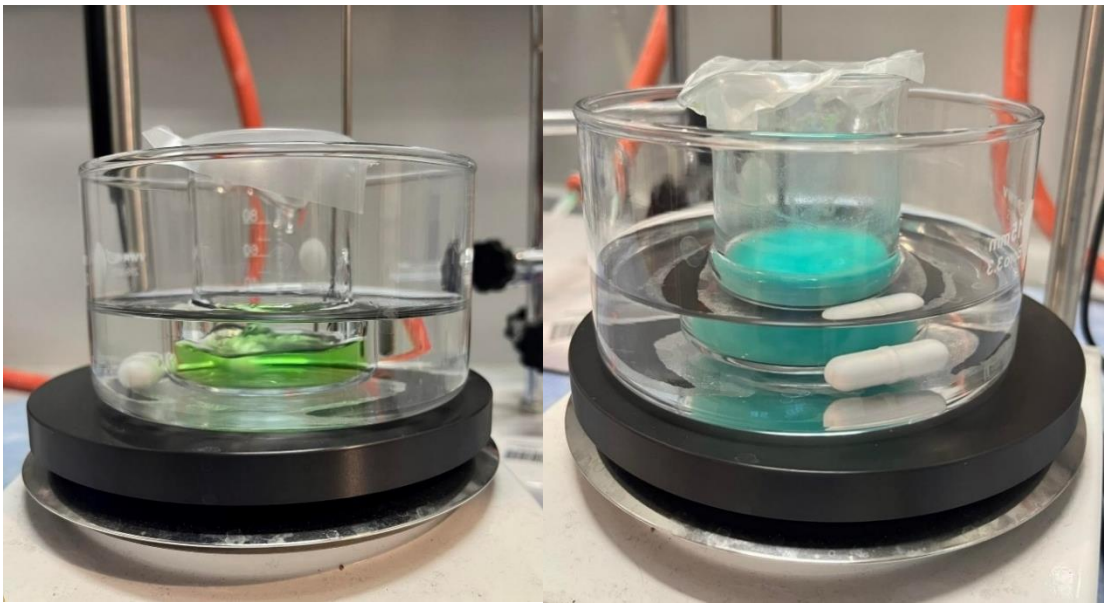

Figure 10 Reaction mixture before (left) and after (right) adding phenanthroline and triazole solutions

3. Adding separately both solutions into the flask with $CuCl_2$, drop by drop, with the use of a plastic dropping funnel. While adding, it can be seen that the whole solution changes its color from light and transparent green into a turquoise mixture with some sediment (**Figure 10**). The whole mixture needs to be left to be stirred by the magnetic stirrer for about 2 hours at a constant temperature.
4. After that time a setup for simple filtration needs to be prepared, which involves glassware and a water pump (**Figure 11**). First, the filter needs to be washed with methanol. Then the synthesis solution has to be filtered twice (including changing the filter).

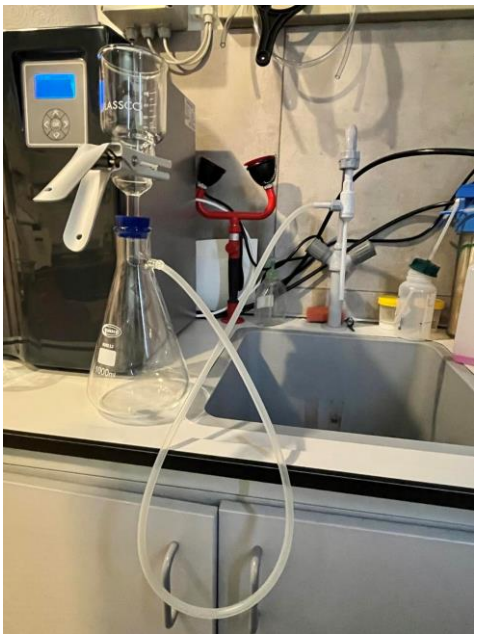

Figure 11 Filtration setup connected to the water pump

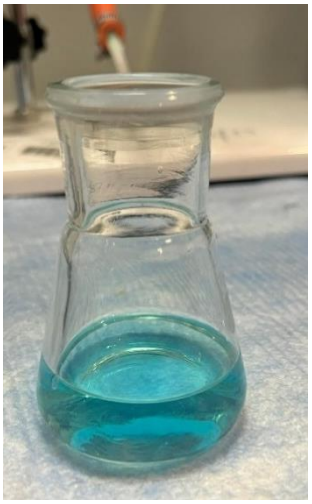

Figure 12 Filtrate of the performed synthesis

5. Transferring the light blue filtrate into the crystallizer (**Figure 12**). The whole sediment, which is green, should stick to the filter.
6. Leaving the solution in the crystallizer under the fume hood and waiting till all methanol evaporates. If after a few days, the product is still wet, the crystallizer needs to be transferred to the desiccator.
7. When the crystallized product is completely dry, it should be transferred to the Eppendorf tube and weighed.

After a few repetitions of the synthesis, some important parameters of the environment were found to have a significant influence on its result:

1) The temperature under the fume hood – there can be observed a difference in the temperature outside and inside the fume hood during cooler days. The temperature was measured once with the use of the thermocouple in January 2021, and below values were provided: 18.5°C in the laboratory room, and 15.4°C under the fume hood. Since the needed reaction temperature should total around 25°C, the difference between the fume hood and the expected for carrying a synthesis totalled 10 degrees. Therefore, there was a need to not only heat the water bath up to 25°C, but also to turn on the heating of the fume hood itself and closing it, to provide the highest stability of the temperature during undergoing reaction. On the other hand, on warmer days, which were in June, the temperature of the whole room was very close to the temperature of the water bath, so that to not overheat the reaction mixture, there was no need to heat the water bath anymore during the whole process.
2) The humidity of the air – during summer days it was found that the product of synthesis could not dry. Even after a few days from filtration, the product was still wet and when stripping it from the crystallizer surface, it started to form a paste instead of a dense material. Indeed, such a situation happened during warm days, not during the winter, when the humidity of the air was high. When the product could not dry, after most of the methanol evaporated, the crystallizer was transferred to the desiccator.
3) Choice of the filtration setup – there were two types of setups tested:
    a) Simple setup with glass funnel and filter
    b) Ordered filtration setup (Glassco, Chemland), containing a filter and which is connected to a water pump

After a comparison of the amount of obtained product after filtration, the second setup was found to be more efficient. There are two reasons for that – the first is that the filter in the first setup was significantly thicker and could absorb a portion of the liquid. Secondly, there were no pumps, the only source that was taking the solution down was gravity. Also, what should be mentioned, the second setup saved more time, because due to the application of the water pump, the whole mixture was filtered significantly faster, even if the filtration was done twice.

Additionally, attempts to modify the proposed parameters of the synthesis were undertaken, which were: increasing the temperature in the water bath up to 30°C, dissolving 1,10-phenanthroline and 1,2,4-triazole together in 10 ml of methanol, prolonging the time of the stirring of the mixture containing all of the reagents, or using different laboratory equipment to add phenanthroline and triazole dropwise to the flask with $CuCl_2$. All of these attempts seemed to not change the results of the synthesis, since every time the two products of the same color were obtained. Therefore, it was decided to study what are these two products of the synthesis.

1.4. Verification of the results of synthesis by performing ATR-FTIR measurements

To verify the success of the copper-triazole compound's synthesis, ATR-FTIR measurements of the powder samples were performed, which were: synthesized product

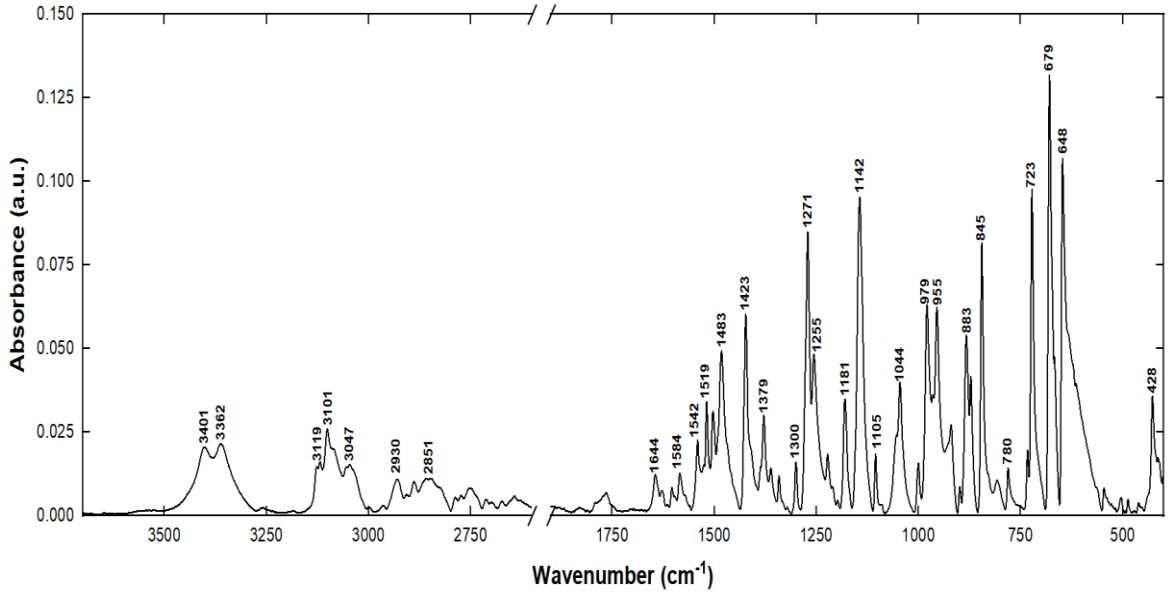

Figure 13 ATR-FTIR spectrum of the performed synthesis product

(expected Cu(phen,triaz)Cl_2), sediment from the synthesis, and Cu(phen)Cl_2. Spectra were measured by Nikolet iN10 FTIR spectrometer, which was equipped with a diamond ATR crystal and a deuterated triglycine sulfate (DTGS) detector. The number of scans per spectrum was 64, and the spectral resolution was 4 cm^{-1}. Spectra were collected in a spectral range from 4000 to 400 cm^{-1}. With the use of the OriginLab program, the baseline was manually defined and subtracted from the data, and the intensities of the most prominent absorption bands were marked. In **Figure 13** the ATR-FTIR spectrum of synthesized product was presented. On this spectrum, bands at 3401 and 3362 cm^{-1} can be observed, corresponding to the O-H stretching in the H_2O molecule [59]. In the region above 3000 cm^{-1} three bands correspond to C-H stretching [60].

Spectra for Cu(phen)Cl_2 and obtained sediment were also compared (**Figure 14**). From the colour of the sediment, which was characteristic light green, it was suspected, that this first compound is obtained parallel to the Cu(phen,triaz)Cl_2. Indeed, after correction of the baseline and comparing bands, it can be observed that these spectra are almost identical, except for one slight difference, which can be seen at 777 cm^{-1}, which does not indicate the different chemical structure.

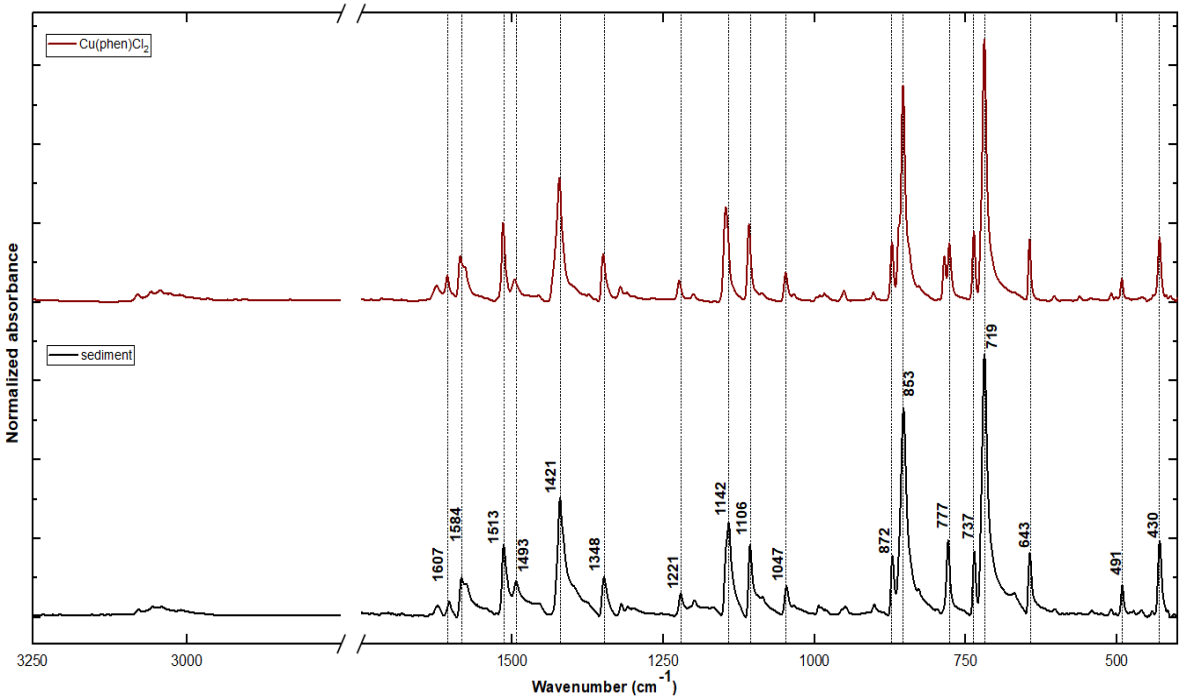

Figure 14 Comparison of ATR-FTIR spectra of Cu(phen)Cl_2 and sediment from performed synthesis

Comparing then fingerprint regions of spectra of all copper-complexes (**Figure 15**), there can be seen a band around 430 cm^{-1}, which might be attributed to the stretching vibrations of Cu-N [61]. Also, there can be found a band at 1584 cm^{-1}, which corresponds to the stretching vibrations of C=C from the 1,10-phenanthroline ring. There can be distinguished spectral features from the spectrum of synthesized product, that are not present in two other spectra, especially obtained sediment. These bands at 1255, 979, and 955 cm^{-1} correspond to stretching (1255 cm^{-1}) and deformation vibrations of the triazole ring [62]. Another very intense bands, which can be observed in the synthesized product spectrum, ascribed to the triazole ring, appear at around 1541 cm^{-1} (stretching N=N), 1483 cm^{-1} (stretching C-N), 1301 cm^{-1} (stretching C=N), 1271 cm^{-1} (deformation N-H), 883 cm^{-1} (wagging C-H) and 679 cm-1 (torsion of the triazole ring) [63-65]. Moreover, in all spectral profiles discussed. The spectral signal at ~1379 cm^{-1} (C-N stretching or C-H deformation vibrations), ~1144 cm^{-1} (NN/C=N stretching or C-H deformation oscillations) and band at ~720 cm^{-1} (C-H bending vibrations) can be distinguished [61, 64, 65].

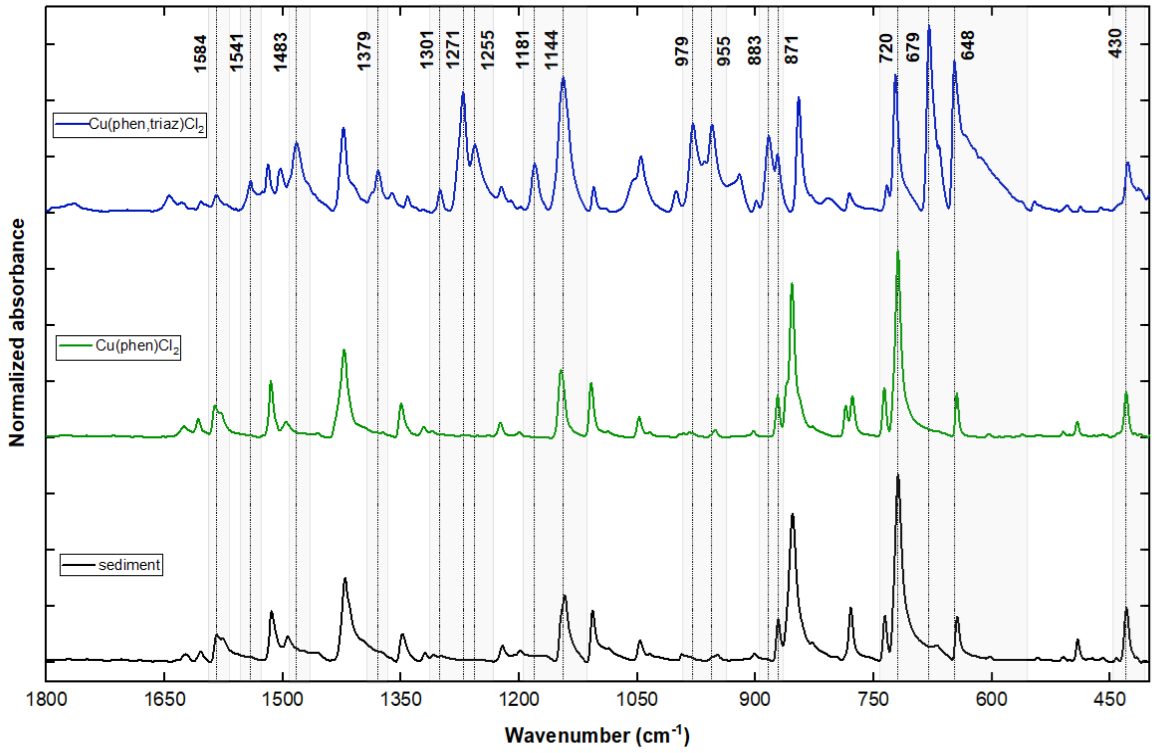

Figure 15 Comparison of fingerprint region of spectra of all studied samples

Taking into consideration all the above results, the proposed in literature synthesis reaction scheme was corrected as follows (**Figure 16**):

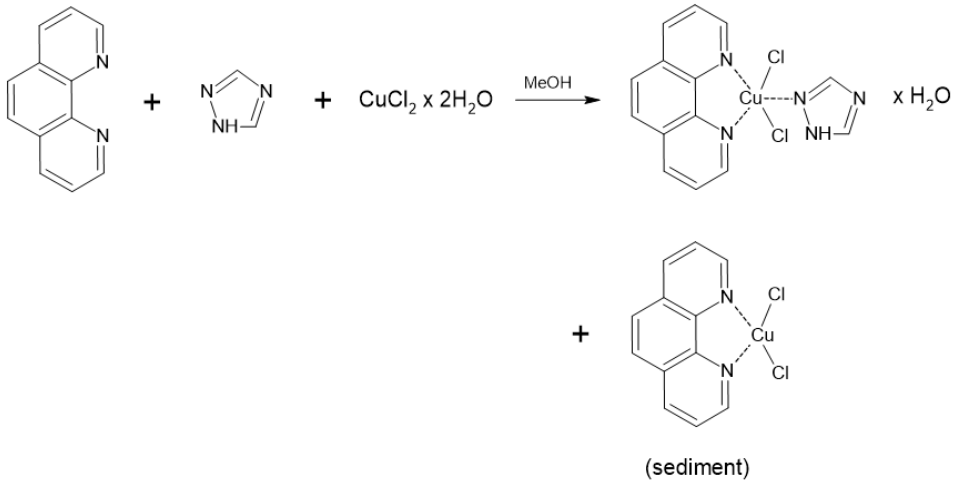

Figure 16 Proposed correction of the chemical reaction scheme of Cu(phen,triaz)Cl_2 synthesis

1.5. Discussion

Copper-phenanthroline complexes are believed to be good candidates for chemotherapeutic drugs. One of them was successfully synthesized and verified with ATR-FTIR measurements, basing on the report from the literature, therefore the first goal of the doctoral project was met.

What was found, is that during a synthesis of Cu(phen,triaz)Cl_2, competitive synthesis of the other complex of interest – Cu(phen)Cl_2 was undergoing, which was not reported in the cited publication. This second compound sedimented in the reaction mixture.

Cu(phen)Cl_2 compound can be easily separated from the Cu(phen,triaz)Cl_2, since it stays at the filter and has different colour by which can be identified – Cu(phen)Cl_2 has a light green colour, Cu(phen,triaz)Cl_2 a light blue.

A few parameters of synthesis were also optimized – the appropriate temperature of the reaction was provided by the usage of the water bath, which can be heated by the magnetic stirrer controller. During days of high humidity, partly evaporated filtrate should be transferred to the desiccator. The most efficient setup for filtration was a bought filtration glass setup, connected to the water pump.

Since both of the complexes were available for further measurements, to study their electronic structure and to verify their possible reactivity in the presence of some biomolecules, meeting the rest of the goals of the study was attempted.

1.6. Materials and laboratory

1) Chemicals used for synthesis:

a) 1,10 – phenanthroline - Merck, cat. nr: 8414910005, anhydrous for synthesis, CAS: 66-71-7

b) 1,2,4 – triazole - Sigma Aldrich, cat. nr: T46108-25G, 98%, CAS: 288-88-0

c) $CuCl_2 \cdot 2H_2O$ - Fluka™, Honeywell, cat. nr: 307483-100G, ACS reagent, ≥ 99.0%, CAS: 10125-13-0

d) Methanol (CH_3OH) - Sigma-Aldrich, cat. nr: 179337-1L, ACS reagent, ≥ 99.8%, CAS: 67-56-1

2) Laboratory equipment:

a) Scale: RADWAG, model: WPA 180/K, max. 180 g, min. 10 mg, d=0.1 mg

b) Magnetic stirrer: Heidolph Instruments GmbH & Co. KG, MR Hei-Tec, nr. 505-30000-00-4, voltage: 230 – 240 V, frequency: 50/60 Hz, power: 825 W, 100-1400 r.p.m.

c) Filtering setup: Glassco, Chemland, cat. nr: 01-261.202.01

d) Infrared imaging microscope: Nikolet iN10 FTIR spectrometer, Thermo Scientific™ (Madison, USA)

1.7. Bibliography

[1] Liu, He, and Qilong Shen. "Well-defined organometallic Copper (III) complexes: Preparation, characterization, and reactivity." *Coordination Chemistry Reviews* 442 (2021): 213923.

[2] Geoghegan, Blaise L., Yang Liu, Sergey Peredkov, Sebastian Dechert, Franc Meyer, Serena DeBeer, and George E. Cutsail III. "Combining Valence-to-Core X-ray Emission and Cu K-edge X-ray Absorption Spectroscopies to Experimentally Assess Oxidation State in Organometallic Cu (I)/(II)/(III) Complexes." *Journal of the American Chemical Society* 144, no. 6 (2022): 2520-2534.

[3] Popova, T. V., and N. V. Aksenova. "Complexes of copper in unstable oxidation states." *Russian Journal of Coordination Chemistry* 29.11 (2003): 743-765.

[4] EFSA Panel on Dietetic Products, Nutrition and Allergies (NDA). "Scientific opinion on dietary reference values for copper." *EFSA Journal* 13.10 (2015): 4253.

[5] Lech, T., and J. K. Sadlik. "Copper concentration in body tissues and fluids in normal subjects of southern Poland." *Biological Trace Element Research* 118 (2007): 10-15.

[6] Linder, Maria C. "The relationship of copper to DNA damage and damage prevention in humans." *Mutation Research/Fundamental and Molecular Mechanisms of Mutagenesis* 733, no. 1-2 (2012): 83-91.

[7] Valko, Marian, Klaudia Jomova, Christopher J. Rhodes, Kamil Kuča, and Kamil Musílek. "Redox-and non-redox-metal-induced formation of free radicals and their role in human disease." *Archives of Toxicology* 90, no. 1 (2016): 1-37.

[8] Gala, Lukas, Michael Lawson, Klaudia Jomova, Lubomir Zelenicky, Andrea Congradyova, Milan Mazur, and Marian Valko. "EPR spectroscopy of a clinically active (1: 2) copper (II) histidine complex used in the treatment of Menkes disease: a Fourier transform analysis of a fluid CW-EPR spectrum." *Molecules* 19, no. 1 (2014): 980-991.

[9] Wierzbicka, Diana, and Grażyna Gromadzka. "Ceruloplazmina, hefajstyna i cyklopen: trzy multimiedziowe oksydazy uczestniczące w metabolizmie żelaza u człowieka." *Advances in Hygiene & Experimental Medicine/Postepy Higieny i Medycyny Doswiadczalnej* 68 (2014).

[10] Linder, Maria C., and Maryam Hazegh-Azam. "Copper biochemistry and molecular biology." *The American Journal of Clinical Nutrition* 63, no. 5 (1996): 797S-811S.

[11] Dameron, Charles T., and Mark D. Harrison. "Mechanisms for protection against copper toxicity." *The American Journal of Clinical Nutrition* 67, no. 5 (1998): 1091S-1097S.

[12] Lelièvre, Pierre, et al. "The multifaceted roles of copper in cancer: a trace metal element with dysregulated metabolism, but also a target or a bullet for therapy." *Cancers* 12.12 (2020): 3594.

[13] Pham, A. Ninh, et al. "Fenton-like copper redox chemistry revisited: Hydrogen peroxide and superoxide mediation of copper-catalyzed oxidant production." *Journal of Catalysis* 301 (2013): 54-64.

[14] Theophanides, T., and J. Anastassopoulou. "Copper and carcinogenesis." *Critical Reviews in Oncology/Hematology* 42.1 (2002): 57-64.

[15] Marczewska, Jadwiga, Koziorowska, Jadwiga H., and Elżbieta L. Anuszewska. "Influence of ascorbic acid on cytotoxic activity of copper and iron ions in vitro." *Acta Poloniae Pharmaceutica* 57.6 (2000): 415-418.

[16] Freedman, Jonathan H., Maria Rosa Ciriolo, and Jack Peisach. "The role of glutathione in copper metabolism and toxicity." *Journal of Biological Chemistry* 264.10 (1989): 5598-5605.

[17] Milne, Lesley, et al. "Effects of glutathione and chelating agents on copper-mediated DNA oxidation: pro-oxidant and antioxidant properties of glutathione." *Archives of Biochemistry and Biophysics* 304.1 (1993): 102-109.

[18] Halliwell, Barry, and John MC Gutteridge. "[1] Role of free radicals and catalytic metal ions in human disease: an overview." *Methods in Enzymology* 186 (1990): 1-85.

[19] Obata, Hiroyuki, et al. "Abnormal accumulation of copper in LEC rat liver induces expression of p53 and nuclear matrix-bound p21waf 1/cip 1." *Carcinogenesis* 17.10 (1996): 2157-2161.

[20] Davis, Cindy D., and Samuel Newman. "Inadequate dietary copper increases tumorigenesis in the Min mouse." *Cancer Letters* 159.1 (2000): 57-62.

[21] Kasprzak, Kazimierz S. "Possible role of oxidative damage in metal-induced carcinogenesis." *Cancer Investigation* 13.4 (1995): 411-430.

[22] Baldari, Silvia, et al. "Effects of copper chelation on BRAFV600E positive colon carcinoma cells." *Cancers* 11.5 (2019): 659.

[23] Moriguchi, Michihisa, et al. "The copper chelator trientine has an antiangiogenic effect against hepatocellular carcinoma, possibly through inhibition of interleukin-8 production." *International Journal of Cancer* 102.5 (2002): 445-452.

[24] Andreini, Claudia, et al. "Metal ions in biological catalysis: from enzyme databases to general principles." *JBIC Journal of Biological Inorganic Chemistry* 13 (2008): 1205-1218.

[25] Hart, P. John, et al. "A structure-based mechanism for copper− zinc superoxide dismutase." *Biochemistry* 38.7 (1999): 2167-2178.

[26] Anastassopoulou, Jane. "Metal–DNA interactions." *Journal of Molecular Structure* 651 (2003): 19-26.

[27] Kruszewski, Marcin, et al. "Chelating of iron and copper alters properties of DNA in L5178Y cells, as revealed by the comet assay." *Mutation Research/DNA Repair* 434.1 (1999): 53-60.

[28] Pearce, Mark. "The 'Copper Age'—A history of the concept." *Journal of World Prehistory* 32, no. 3 (2019): 229-250.

[29] Borkow, Gadi, and Jeffrey Gabbay. "Copper, an ancient remedy returning to fight microbial, fungal and viral infections." *Current Chemical Biology* 3.3 (2009): 272-278.

[30] Piccart, M. J., H. Lamb, and Jan Baptist Vermorken. "Current and future potential roles of the platinum drugs in the treatment of ovarian cancer." *Annals of Oncology* 12.9 (2001): 1195-1203.

[31] Ghosh, Sumit. "Cisplatin: The first metal based anticancer drug." *Bioorganic Chemistry* 88 (2019): 102925.

[32] Mikolay, André, et al. "Survival of bacteria on metallic copper surfaces in a hospital trial." *Applied Microbiology and Biotechnology* 87 (2010): 1875-1879.

[33] Da Silva, F. S., et al. "Corrosion resistance and antibacterial properties of copper coating deposited by cold gas spray." *Surface and Coatings Technology* 361 (2019): 292-301.

[34] Szymański, Paweł, et al. "Development of copper based drugs, radiopharmaceuticals and medical materials." *Biometals* 25 (2012): 1089-1112.

[35] Dong, Caihong, et al. "The coppery age: Copper (Cu)-involved nanotheranostics." *Advanced Science* 7.21 (2020): 2001549.

[36] Jose, Gregor P., et al. "Singlet oxygen mediated DNA degradation by copper nanoparticles: potential towards cytotoxic effect on cancer cells." *Journal of Nanobiotechnology* 9 (2011): 1-8.

[37] Fahmy, Baher, and Stephania A. Cormier. "Copper oxide nanoparticles induce oxidative stress and cytotoxicity in airway epithelial cells." *Toxicology in Vitro* 23.7 (2009): 1365-1371.

[38] Midander, Klara, et al. "Surface characteristics, copper release, and toxicity of nano-and micrometer-sized copper and copper (II) oxide particles: a cross-disciplinary study." *Small* 5.3 (2009): 389-399.

[39] Cedervall, Tommy, et al. "Understanding the nanoparticle–protein corona using methods to quantify exchange rates and affinities of proteins for nanoparticles." *Proceedings of the National Academy of Sciences* 104.7 (2007): 2050-2055.

[40] Ruiz-Azuara, L., and M. E Bravo-Gomez. "Copper compounds in cancer chemotherapy." *Current Medicinal Chemistry* 17.31 (2010): 3606-3615.

[41] Bravo-Gómez, María Elena, et al. "DNA-binding mode of antitumoral copper compounds (Casiopeinas®) and analysis of its biological meaning." *Polyhedron* 102 (2015): 530-538.

[42] Ng, Neville S., Ming J. Wu, and Janice R. Aldrich-Wright. "The cytotoxicity of some phenanthroline-based antimicrobial copper (II) and ruthenium (II) complexes." *Journal of Inorganic Biochemistry* 180 (2018): 61-68.

[43] Heffeter, Petra, et al. "Anticancer activity of the lanthanum compound [tris (1, 10-phenanthroline) lanthanum (III)] trithiocyanate (KP772; FFC24)." *Biochemical Pharmacology* 71.4 (2006): 426-440.

[44] Thornton, Laura, et al. "Water-soluble and photo-stable silver (I) dicarboxylate complexes containing 1, 10-phenanthroline ligands: Antimicrobial and anticancer chemotherapeutic potential, DNA interactions and antioxidant activity." *Journal of Inorganic Biochemistry* 159 (2016): 120-132.

[45] Sigman, David S., et al. "Targeted chemical nucleases." *Accounts of Chemical Research* 26.3 (1993): 98-104.

[46] Bencini, Andrea, and Vito Lippolis. "1, 10-Phenanthroline: a versatile building block for the construction of ligands for various purposes." *Coordination Chemistry Reviews* 254.17-18 (2010): 2096-2180.

[47] Marshall, Laura E., et al. "Cleavage of deoxyribonucleic acid by the 1, 10-phenanthroline-cuprous complex. Hydrogen peroxide requirement and primary and secondary structure specificity." *Biochemistry* 20.2 (1981): 244-250.

[48] Arjmand, Farukh, et al. "Synthesis, characterization, biological studies (DNA binding, cleavage, antibacterial and topoisomerase I) and molecular docking of copper (II) benzimidazole complexes." *Journal of Photochemistry and Photobiology B: Biology* 114 (2012): 15-26.

[49] Roy, Sudeshna, et al. "Phenanthroline derivatives with improved selectivity as DNA-targeting anticancer or antimicrobial drugs." *ChemMedChem: Chemistry Enabling Drug Discovery* 3.9 (2008): 1427-1434.

[50] Bagihalli, Gangadhar B., et al. "Synthesis, spectral characterization, in vitro antibacterial, antifungal and cytotoxic activities of Co (II), Ni (II) and Cu (II) complexes with 1, 2, 4-triazole Schiff bases." *European Journal of Medicinal Chemistry* 43.12 (2008): 2639-2649.

[51] Kaur, Ramandeep, et al. "Recent developments on 1, 2, 4-triazole nucleus in anticancer compounds: a review." *Anti-Cancer Agents in Medicinal Chemistry (Formerly Current Medicinal Chemistry-Anti-Cancer Agents)* 16.4 (2016): 465-489.

[52] Sztanke, Krzysztof, et al. "Synthesis, determination of the lipophilicity, anticancer and antimicrobial properties of some fused 1, 2, 4-triazole derivatives." *European Journal of Medicinal Chemistry* 43.2 (2008): 404-419.

[53] Tabassum, Sartaj, et al. "Synthesis and characterization of copper (II) and zinc (II)-based potential chemotherapeutic compounds: their biological evaluation viz. DNA binding profile, cleavage and antimicrobial activity." *European Journal of Medicinal Chemistry* 58 (2012): 308-316.

[54] Liu, Y-Q. "Dichlorido (1, 10-phenanthroline) copper (II)." *Acta Crystallographica Section E: Structure Reports Online* 63.12 (2007): m2991-m2991.

[55] Blum, Marc-Michael, and Harald John. "Historical perspective and modern applications of attenuated total reflectance–Fourier transform infrared spectroscopy (ATR-FTIR)." *Drug Testing and Analysis* 4.3-4 (2012): 298-302.

[56] Ismail, Ashraf A., Frederick R. van de Voort, and Jacqueline Sedman. "Fourier transform infrared spectroscopy: principles and applications." *Techniques and Instrumentation in Analytical Chemistry*. Vol. 18. Elsevier, 1997. 93-139.

[57] https://www.bruker.com/en/products-and-solutions/infrared-and-raman/ft-ir-routine-spectrometer/what-is-ft-ir-spectroscopy/atr-attenuated-total-reflectance.html (accessed: October 2023)

[58] Kazarian, S. G., and K. L. A. Chan. "Applications of ATR-FTIR spectroscopic imaging to biomedical samples." *Biochimica et Biophysica Acta (BBA)-Biomembranes* 1758.7 (2006): 858-867.

[59] Palencia, Manuel. "Functional transformation of Fourier-transform mid-infrared spectrum for improving spectral specificity by simple algorithm based on wavelet-like functions." *Journal of Advanced Research* 14 (2018): 53-62.

[60] Socrates, George. Infrared and Raman characteristic group frequencies: tables and charts. John Wiley & Sons, 2004.

[61] Wang, Xiaoyan, et al. "A new homogeneous electrocatalyst for electrochemical carbonylation of methanol to dimethyl carbonate." *Química Nova* 38 (2015): 298-302.

[62] Grinshtein, V. Ya, A. A. Strazdin', and A. K. Grinvalde. "Infrared absorption spectra of some C-halogenated 1, 2, 4-triazole derivatives." *Chemistry of Heterocyclic Compounds* 6.2 (1970): 231-239.

[63] Trivedi, Mahendra Kumar, et al. "Characterization of physical, spectral and thermal properties of biofield treated 1, 2, 4-Triazole." *Journal of Molecular Pharmaceutics & Organic Process Research* 3.128 (2015): 2.

[64] Jbarah, Abdel Aziz, et al. "The electrosorption of 1, 2, 3-triazole on gold as studied with surface-enhanced Raman spectroscopy." *Journal of Raman Spectroscopy: An International Journal for Original Work in all Aspects of Raman Spectroscopy, Including Higher Order Processes, and also Brillouin and Rayleigh Scattering* 37.1-3 (2006): 123-131.

Chapter 2

X-ray Spectroscopy

2.1. X-ray interactions with matter

X-rays are electromagnetic radiation, which energy covers the range from around 0.1 keV up to 1 MeV. Discovered by W. Roentgen in 1895, quickly found their application in medicine in the diagnostic field. Since such radiation exerts both wave and particle behavior, one can observe its interactions with matter, which proves these both natures. To express the probability of the occurrence of such effects, a physical quantity called cross-section, in surface dimension [barn] was introduced, as seen in the below **Figure 17**. 1 barn equals 10^{-24} cm^2.

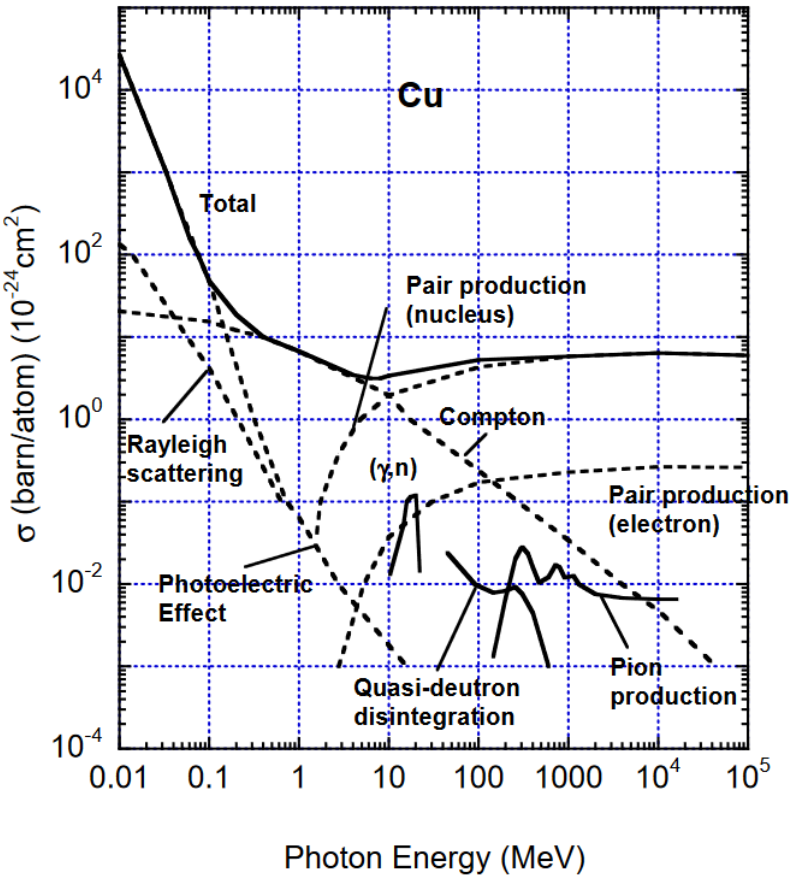

Figure 17 Cross sections for different interactions of photons with Cu atom [1]

The crucial parameter that determines which effect probably will be mostly observed (highest cross-section), is the energy of the X-rays, that undergo interaction with matter. For energies less than 1 MeV, which are usually used in typical studies of matter,

elastic (Rayleigh) and nonelastic (Compton) scattering with photoelectric effect predominate. Above 1 MeV the pair production starts to be more visible. Since in described research, photons with energies above 1 MeV were not used, only both types of scattering and photoelectric effect were taken into account.

In the method of the main interest, that is X-ray Absorption Spectroscopy, the process that predominates in the applied energetic range is a photo-electric effect. The cross-section for this effect determined per one atom $\boldsymbol{\tau_a}$ is defined as follows (**Equation 11**):

$$\tau_a = \tau_0 \frac{Z^5}{(h\nu_0)^3} \tag{11}$$

where:

τ_0 – constant factor of proportionality

Z – atomic number

h – Planck constant (6.626 x 10^{-24} [J/s])

ν_0 - frequency of the X-ray radiation

Since the examined sample consists of many atoms, therefore above equation can be corrected, which gives a parameter called mass photoelectric absorption coefficient $\boldsymbol{\mu_f}$ (**Equation 12**):

$$\mu_f = \tau_a \frac{N_A}{M_m} \tag{12}$$

where:

N_A – Avogadro number ($6.022 \cdot 10^{23}$ [1/mole])

M_m – molar mass (g/mole)

2.1.1. Elastic and non-elastic scattering

The first type of electromagnetic interaction, that proves the particle nature of X-rays, is elastic and non-elastic scattering. In the case where the incident photon has an energy smaller than the binding energy of the orbital electron, it interacts with the electron and is followed by the emission of the photon of the same energy as the incident one, but moving toward a changed direction (**Figure 18**). This effect is called elastic (Rayleigh) scattering.

During X-ray spectroscopy measurements, such scattered radiation can be registered by the detector and leads to the appearance of a so-called “elastic peak” on the spectrum.

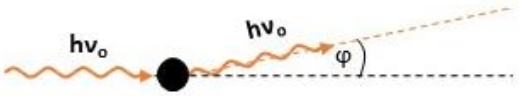

Figure 18 Scheme of the elastic scattering process

Another type of scattering is non-elastic scattering. Unlike in the case of elastic scattering, the incident photon transfers part of its energy to the electron and the emitted photon has smaller energy (**Figure 19**). As a result, the electron gains kinetic energy and recoils. In the case of the commonly used in spectroscopy range of energies of X-rays, we talk about the Compton effect, where such interaction of higher energy photons occurs with the quasi-free (valence) electrons.

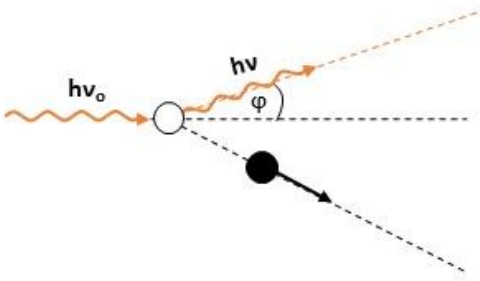

Figure 19 Scheme of the non-elastic scattering process

Apart from the interactions with electrons, high-energy X-rays can also scatter on the nucleus. A special case is the so-called Delbrück scattering, where the photons are scattered in the electric field of nuclei, during which the virtual electron-positron pair is produced. However, since such a phenomenon is not the subject of this thesis, it will not be discussed further.

2.1.2. Photoelectric effect

Since X-ray Absorption Spectroscopy relies on the photoelectric effect, there is a need to provide the physical basics of this effect. In comparison to non-elastic scattering, in this case, the whole energy of the photon is absorbed by the electron from the inner shell. The necessary condition is that the energy of the photon is higher than the binding energy of the electron to its orbital. Therefore, after absorption of the photon, the electron leaves it's orbital and is promoted to a higher, non-filled orbital or escapes the atom as

a photoelectron (**Figure 20**). The kinetic energy E_{kin} of such photoelectron can be determined as (**Equation 13**):

$$E_{kin} = E_{inc} - E_{bond} = h\nu_0 - E_{bond} \quad (13)$$

where:

E_{inc} – the energy of the incident photon

h - Planck constant

ν_0 - X-ray radiation frequency

E_{bond} - bonding energy of the given electron

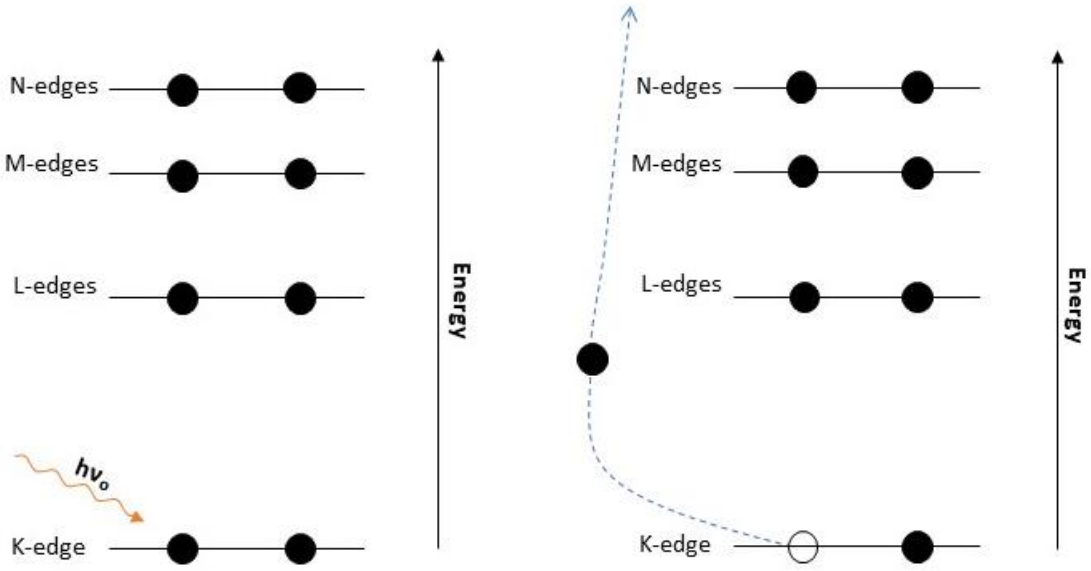

Figure 20 Scheme of the photoelectric effect, with irradiation followed by absorption of the radiation (left) and ejection of the electron (right). For clarity of these and following figures, the number of draw electrons bounded to edges was reduced and the ejected electron's path was marked on the side

As a result of this effect, a hole in the shell is created after the missing electron, the so-called corehole. It can be filled by an electron from a higher orbital. However, this situation can be followed by different effects, of which only one involves a radiative transition:

1) X-ray fluorescence

The first possibility is that the electron from the higher shell fills the vacancy created by the ejected electron after absorption of the photon, and its excess energy is emitted in the form of X-ray radiation (**Figure 21**). This effect is called X-ray fluorescence and gives rise to the radiation, that is measured in some X-ray spectroscopy methods, including one mode of X-ray Absorption Spectroscopy (XAS). What is important, is that the emitted radiation can be absorbed by the electron of the neighboring atom (if the energy is of course sufficiently high), therefore it will not be detected. Such an effect is called self-absorption, and sometimes registered data needs to be corrected over that disturbance.

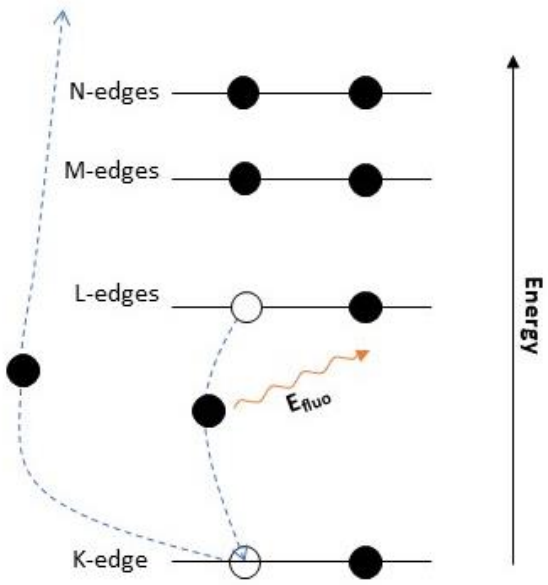

Figure 21 Scheme of the generation of the X-ray fluorescence radiation

2) Auger effect

The second option is that the excess energy emitted by the electron, that is going to fill the vacancy, is transferred to an electron from the same shell, and that electron is ejected, creating a new vacancy (**Figure 22**). This effect is called the Auger effect, and escaping electrons can be registered by the detector in so-called Auger Electron Spectroscopy (AES)

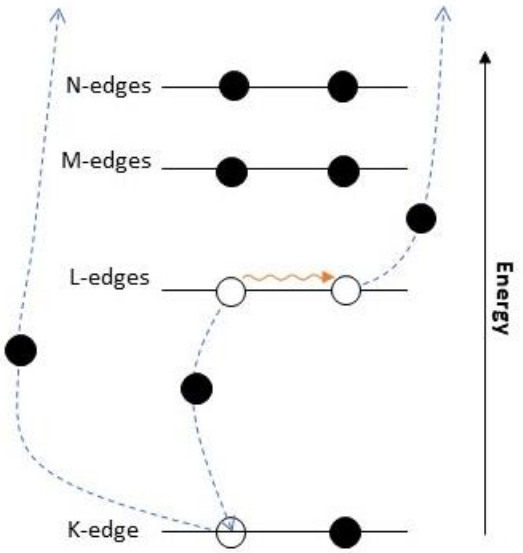

Figure 22 Scheme of the Auger effect

3) Coster-Kronig effect

The third option is very similar to the previous one. The difference lies in the fact that excess energy is transferred to electron from the higher shell (**Figure 23**). This process is called the Coster-Kronig effect.

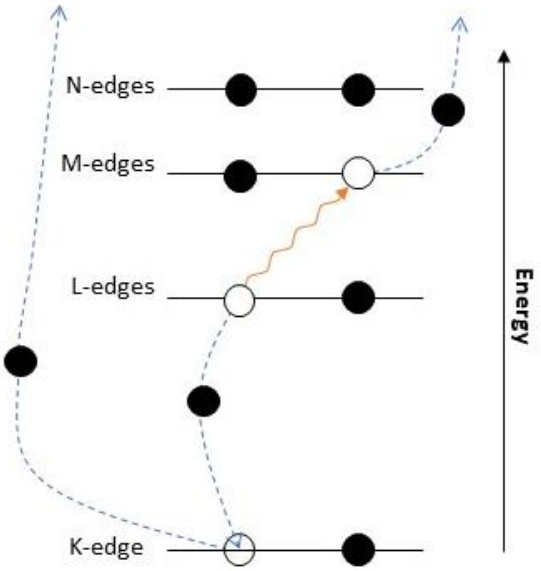

Figure 23 Scheme of the Coster-Kronig effect

All of those mentioned above processes can occur following the irradiation of the chosen sample by X-rays, which might result in the emission of scattered radiation, fluorescence radiation, electrons, and transmitted incident beam, however, attenuated by the occurring absorption process (**Figure 24**).

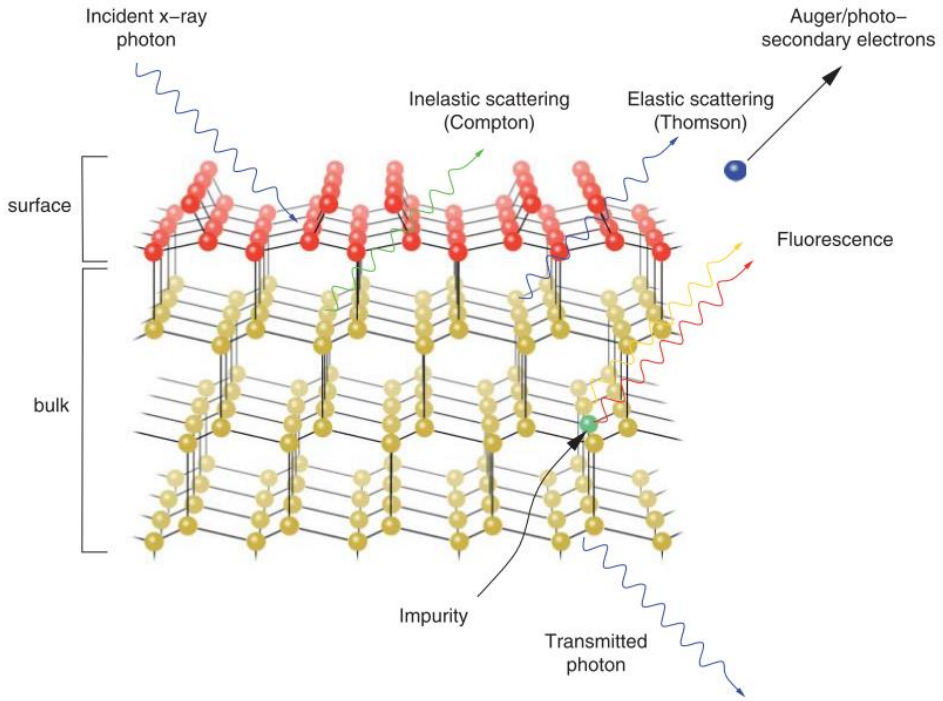

Figure 24 Scheme of possible processes, followed by the interactions of the incident X-rays with the matter in the given material [2]

2.1.3. Diffraction

Diffraction proves the wave nature of the X-rays, since for specific angles under which the radiation incidents on the sample, the interference or quenching of X-rays can be observed. On the other hand, looking into this effect as a result of the interaction of radiation with electrons of these atoms, the involved process is elastic scattering.

Diffraction was described by Bragg, who explained the relation between the angle of incident radiation, its wavelength, and the distance between the given crystallographic plane (**Figure 25, Equation 14**):

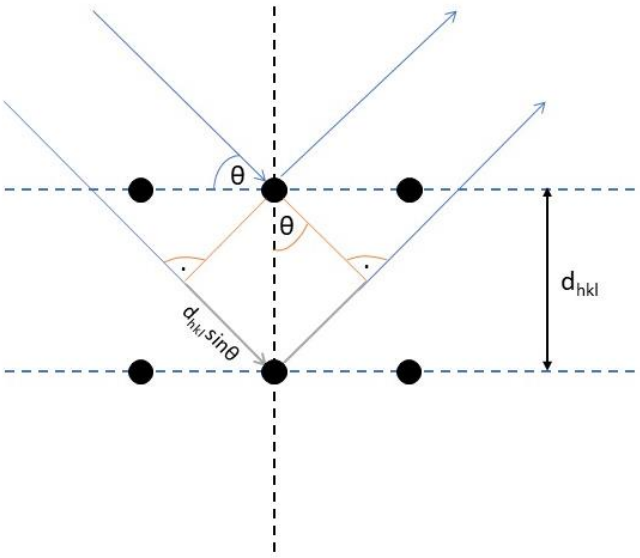

Figure 25 Scheme of the diffraction of X-rays on the crystallographic planes

$$n\lambda = 2d_{hkl}\sin\theta \quad (14)$$

where:

n – natural number

λ – wavelength of the radiation [nm]

d_{hkl} – the distance between the given crystallographic planes (lattice spacing)[nm]

θ – incidence angle [radians]

Since there is more than one possible family of planes, Bragg's law can be fulfilled for other parameters. What is needed to be emphasized, is the fact that the equation can also take into consideration the different energy of X-rays (**Equation 15**):

$$n\lambda = n\frac{hc}{E} = 2d_{hkl}\sin\theta \quad (15)$$

where,

h – Planck constant

c – speed of light (about $3 \cdot 10^8$ [m/s])

E – the energy of radiation [eV]

When fixing the parameters, which are d_{hkl} (by choosing only one type of crystal for measurement) and known constants, radiation of different energy will be diffracted with different, specific for each energy angle. This fact is used in the XAS, where crystals matching the specific equation's lattice spacing can be used for the separation of radiation that is registered further by a detector. Also thanks to this effect, crystals can be used as monochromators of the beam, since the radiation of different energies is being separated and with cutting residue wavelengths, only X-rays with a specific wavelength (energy) can be transmitted further.

2.2. Sources of X-rays

2.2.1. X-ray tube

An X-ray tube is probably the most available X-ray source to purchase by potential users. It is present not only in scientific units, but also in hospitals, dentists and veterinary clinics. The generation of radiation lies in the process where accelerated electrons ejected from the cathode hit the element called an anode and are halted due to the interactions with its atoms, especially repulsion by the positive charge of the nucleus. As a result of the deceleration process, the velocity of electrons is reduced along with the loss of the kinetic energy converted into energy of photons of generated radiation, called Bremsstrahlung. The electron's movement is induced by the applied voltage, from the cathode towards the anode in a vacuum environment.

Such a source is unfortunately not that efficient, because only 1% of the kinetic energy lost by electrons is passed on to X-rays and the biggest part is emitted as heat. Emitted radiation can be of different energies, because the deceleration paths of electrons can differ from each other, therefore the spectrum of the source is continuous. Intensive warming up of the anode can lead to its damage. Therefore some setups provide the rotation of the anode, for better heat distribution in the material.

The material of the anode has an important impact on the energetic distribution of the produced X-rays, since part of the energy can be absorbed by the element that builds the anode, resulting in the excitation of its electrons and emission of the fluorescence radiation, which escapes the tube. As a result, on the spectrum of the radiation emitted by the source, there are also visible emission lines characteristic for the material of the anode, that relate to the emitted X-ray fluorescence radiation.

Using an X-ray tube as an X-rays source has the advantage of being the cheapest, smallest, and most accessible for scientists source from these, that were discussed in this chapter.

2.2.2. Synchrotron

In the beginning, synchrotron radiation was treated as parasite radiation, that was emitted during the acceleration of charged particles. Nowadays this situation is reversed and the acceleration of such particles, usually electrons, is only a necessary process to produce expected synchrotron light for many important scientific studies. Because electrons are lighter than protons, to acquire the same value of kinetic energy, the velocity of an electron needs to be higher than needed by a proton. To reach the energies of the particles whose hampering will generate the radiation in the used energetic range of X-rays, electrons need to be accelerated nearly to the speed of light. Therefore relativistic physics starts to be in operation.

Synchrotron light is being produced as a result of the controlled changes in the trajectory of the electron, forced by the applied magnetic field, without the collision with synchrotron elements or electrons themselves. To achieve that, there is a need to remove any compounds or atoms from the interior of the synchrotron elements, that could collide with electrons, therefore a vacuum environment is provided. Secondly, a magnetic field needs to be implemented, to generate a Lorentz force $\mathbf{F_L}$ that acts on each electron and keeps them on a determined circular path of acceleration closed in a synchrotron's ring, which can be defined as (**Equation 16**):

$$\mathbf{F_L} = q_e \mathbf{v} \times \mathbf{B} \qquad (16)$$

where:

q_e – charge of the electron ($1.6 \cdot 10^{-19}$ [C])

$\mathbf{v}$ – electron's velocity [m/s]

$\mathbf{B}$ – magnetic induction [T]

Lorentz force is directed perpendicularly to the electron path, therefore (**Equation 17**):

$$F_L = q_e v B \sin(90°) = q_e v B \quad (17)$$

Since the electrons are moving in the circular path, Lorentz force acts as a centripetal force (**Equation 18**):

$$F_L = \frac{m_e v^2}{R} \quad (18)$$

where:

R - radius of the arc [m]

What is important, is the fact that the electron's velocity is close to the speed of light (ultra-relativistic), therefore one needs to take into consideration the relativistic effects. Because of that above equations should be corrected as follows (**Equations 19-20**):

$$F_L = q_e c B = \frac{m_{eR} c^2}{R} = \frac{\mathcal{E}}{R} \quad (19)$$

where:

$\mathcal{E}$ - total energy of the electron [GeV]

m_{eR} – the relativistic mass of the electron, defined as:

$$m_{eR} = \gamma m_e \quad (20)$$

(where: γ – Lorentz factor)

If one would like to estimate the needed radius of the storage ring, that will enable acceleration of the electrons to the needed speed and its maintenance, therefore usual operating magnetic-field strength is in the range of a few [T] and energies in the range of [GeV] (**Equation 21**):

$$R = \frac{m_{eR} c^2}{q_e c B} = \frac{\mathcal{E}}{q_e c B} \quad (21)$$

what will give the range of a few meters.

With the application of the sources of the magnetic field, which are bending magnets and insertion devices, electrons accelerated to the ultra-relativistic speed rapidly change their direction, therefore emitted electric field lines also change direction, resulting in the generation of electromagnetic radiation. If the speed was significantly lower, the angular distribution of such radiation would be like this emitted by the dipole, however, since the speed is ultra-relativistic, this distribution significantly changes and narrows to the cone (**Figure 26**).

Figure 26 Schemes of the angular distribution of emitted radiation by the accelerated electron

Such emitted synchrotron radiation can be later described with a few important parameters:

a) **Flux** – which is a number of emitted photons by the source during 1 second and within 0.1% bandwidth

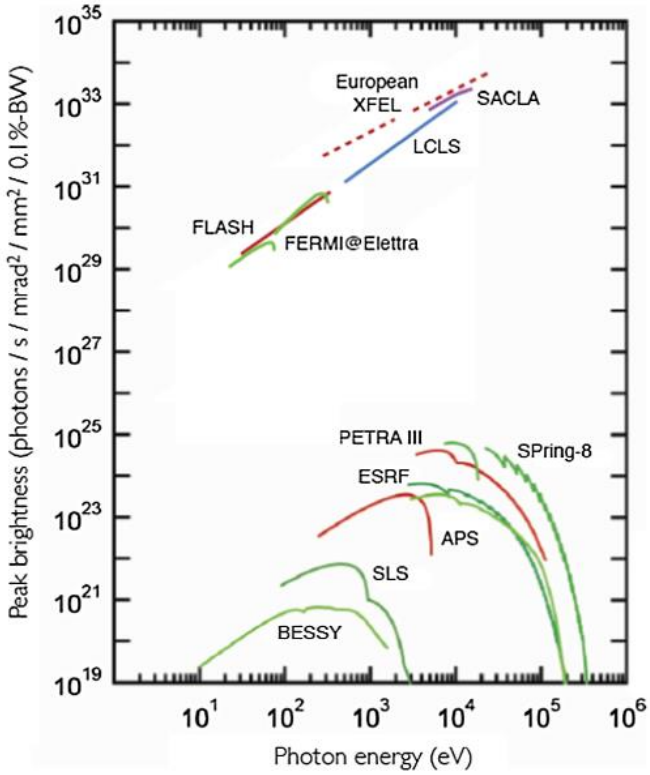

Figure 27 Comparison of the synchrotron radiation brightness generated by different X-ray sources [2]

b) **Brilliance** – that is a flux distributed within the given space and angular range

c) **Brightness** – a brilliance per 1 mm^2 of the beam

As a result of the application of different construction elements, sources of synchrotron radiation differ in these parameters (**Figure 27).**

The road to obtaining X-rays in a given energetic range involves a few steps. First, the thermionic ejection of electrons undergoes from the heated filament placed in an electron gun. Emitted electrons in packs, called bunches, are gradually accelerated in the linear compartment called **LINAC** to obtain energy around 100 MeV [3]. Then they are usually inserted into the smaller circular accelerator, called **booster**, where they are accelerated to obtain the destined or smaller energy than expected in the storage ring. After that, they are injected into the latter ring, where they circulate for hours. Since the electrons can interact with any minor impurities in the vacuum, they lose track and energy, for example in the form of Bremsstrahlung. As a result, there is a need to refill the storage ring with new packs of electrons. This process can occur in regular lags during the synchrotron operation, or during a scheduled time, when there is a break in the operation dedicated to the injection process. Because electrons are losing their energy by emitting synchrotron radiation, there is a need to top their energy up with the application of radiofrequency cavities. The scheme of all of the synchrotron elements was presented in **Figure 28**.

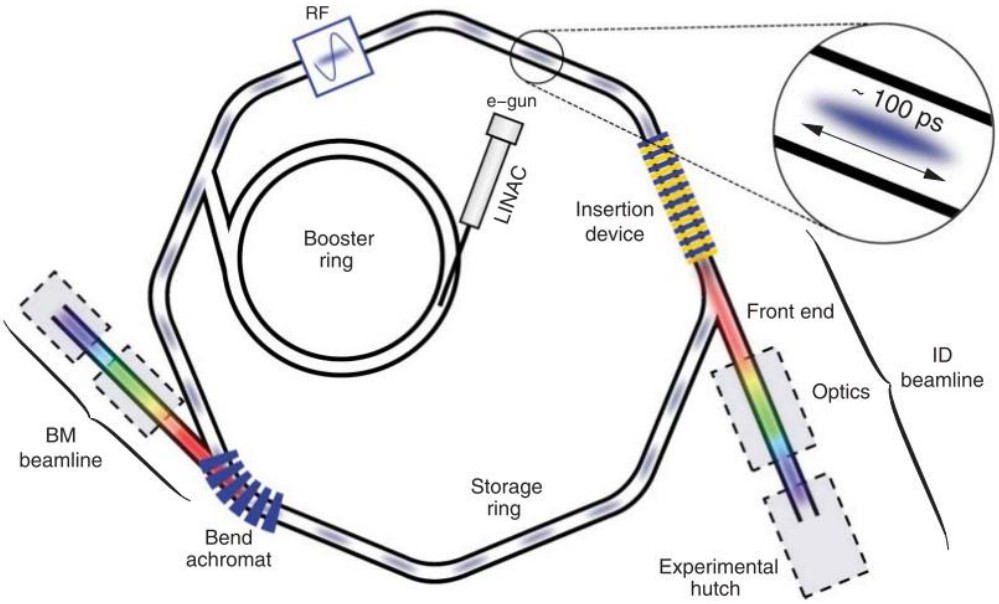

Figure 28 Example of synchrotron machine scheme [3**]**

Beamlines are placed tangentially to the storage ring, to which the radiation can be provided from the **insertion devices (ID)**, like **undulators** or **wigglers**, or from bending magnets. In this case, the application of the sources of the magnetic field is not only used

to maintain the path of the accelerated electrons, but also to increase the synchrotron radiation flux and brilliance that will be derived to the examination setup. The advantage of the insertion devices over bending magnets is that they produce significantly higher flux, as a result of the slalom path along which the electrons are driven (**Figure 29**). This kind of path is obtained by more than one change in electron direction which happens in the bending magnet.

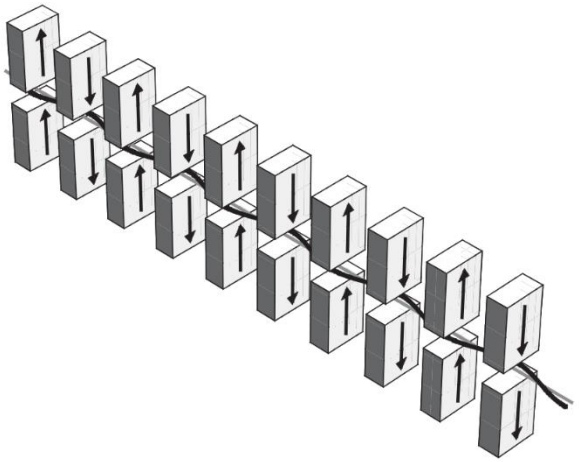

Figure 29 Scheme of the magnets setup in an insertion device [4]

To construct the insertion device, a series of pairs of magnets with changing in the row orientations of the magnetic field are used. As a result, the direction of the electrons is systematically changed, leading to a sinus-like trajectory. With every bend of the electron path, radiation is emitted. In wigglers, the resultant emitted radiation looks as if it was obtained from the train of bending magnets. In contrast, the undulators provide a more intensive beam, as a result of the smaller excursion of electrons from their trajectory (than this in bending magnet or undulator) and enabled by this fact interference of the radiation emitted from different regions of the undulator. It is possible by reducing the distance between the opposite magnetic poles. The emitted radiation cone is very narrow and is called a “pencil beam”.

As a parameter that will easily distinguish the type of the ID, the K parameter indicating the deflection induced by the magnetic field is used, which is defined as (**Equations 22-24**):

$$K = \phi_{max} \cdot (1/\gamma)^{-1} \qquad (22)$$

where:

ϕ_{max} – a maximum angular deviation that the electron path undergoes

$1/\gamma$ – natural opening angle

or:

$$K = \frac{B_0 e}{m_e c k_{ID}} \quad (23)$$

where:

$$k_{ID} = \frac{2\pi}{\lambda_{ID}} \quad (24)$$

λ_{ID} – spatial period, which is the distance between the two same poles in the one row in the given ID

For wigglers, the K value usually varies between 10 - 50, and for undulators reaches nearly 1. In the presented further beamlines, only bending magnets or undulators are applied to reach the expected energetic range.

Taking into consideration all the mentioned sources of X-rays, the decision on which one to choose in the X-ray spectroscopy experiment will be based on a few critical factors, like:

a) type of the sample: e.g. chosen element/s of interest, state of the matter, concentration, sensitivity to radiation damage
b) information about the given material to study: e.g. type and rate of the monitored reaction and/or determination of the electronic structure and/or study of the oxidation state
c) chosen X-ray spectroscopy method, which results in expecting a dedicated to it set of an advanced equipment, like specific detector or spectrometer, that is accessible only on a few beamlines
d) economic situation: e.g. available money to fund a few days of stay abroad, cost of the materials (not only sample itself but also elements of setups, that are dedicated to the sample, and sometimes their delivery)
e) access to the scientific unit: e.g. big number of applicants for beamtime, distance from the workplace
f) available X-ray sources in the workplace or nearby

The line of thinking, which source and beamline to choose, in the case of the described in this work copper-phenanthroline complexes, was carried as follows. First of all, there were no found reports at the beginning of the project about the X-ray absorption spectroscopy study of both complexes of interest. Therefore, as a first attempt to have

a look at the spectra, a laboratory study was performed with the use of referential compounds, where samples were in the form of pellets (solid samples) and different concentrations. Only one copper-phenanthroline compound was studied at that time – Cu(1,10-phenanthroline)Cl_2. Results completed with the theoretical calculations in the FEFF program were a part of the Master Thesis prepared by the author of this work, and have been already published (during the first year of the doctoral school) [5]. It was found that there is a possibility to distinguish an oxidation state of the copper in all studied complexes, however, any more detailed analysis of the spectra will need a more intensive source to get rid of the visible noise, that occurs with the application of the X-ray tube, which handicaps it. Since there was a need to analyze the XAS spectra for a better understanding of the electronic structure of the mentioned complex, a more precise examination was moved to the synchrotron facilities. Further, there was a need to design and perform studies of the solution of the copper-phenanthroline complex, since any detection of interactions between this complex and biomolecules needs to be performed in a liquid environment (as it was explained in Chapter 1). Also, the copper-phenanthroline complex with triazole was finally synthesized in the chemistry laboratory and could be moved to the XAS study. Since the synthesized product had to be checked with complementary methods to evaluate the result of the synthesis and compared to the similar purchased one, liquid solutions in water were prepared. It was found that both complexes are not well-soluble, and the maximum concentration, for which both of them were dissolved, was 25 mM. This concentration was expected to be unfortunately too low to be applied in the laboratory XAS study, nevertheless, studies were performed to prove that suspicion. The decision to focus on the use of the synchrotron source was motivated firstly by the results from the studies performed on the very similar laboratory XAS setup present in Warsaw, where the minimum detectable concentration of the material in solution was established to around 200 mM, so nearly 10 times higher [6]. Parallelly, since even for the solid samples the noise was too high to perform an accurate determination of the electronic structure with the use of the X-ray tube, such a decision was favored.

After a comparison of the available beamlines dedicated to XAS studies, the SuperXAS beamline of Swiss Light Source in Switzerland, the P65 beamline of DESY in Germany, and the nearest one – the ASTRA beamline of SOLARIS in Poland were chosen. All these beamlines operate in destined energy ranges and enable measurements of both solid and liquid samples in expected experimental conditions.

2.3. X-ray Absorption Spectroscopy (XAS)

2.3.1. Introduction to the method

X-ray Absorption Spectroscopy founds its applications in many fields of study, from medicine to electrochemistry up to the art. The reason is that there is no demand for the type of samples or measurement environments, therefore there are possible studies of both crystalline and non-crystalline samples, in low and high temperatures, at different pressures and times. Such a variety of possibilities leads to many types of measurement setups, including liquid delivery systems or vacuum chambers. Nevertheless, even if measurements with the same method but in different sample environments seem to be different studies, all of them provide as a result an XAS spectrum thanks to the same physical phenomenon.

XAS is an element-oriented method, therefore during one measurement, there is a possibility to detect the absorption process by the electrons of the chosen element. Some setups enable choosing more than one element, however, it is normally not that common, but can be realized with the application of a polychromator or more than one crystal dispersing the beam [7]. This method is based on the photoelectric effect, and via tuning the energy of the X-ray incident radiation, one can focus on a concrete excitation, e.g. absorption by the electrons from the K-shell. What is exactly determined is the difference in the value of the so-called absorption coefficient μ(E) in the function of the energy of the incident radiation, which indicates the absorption process.

Taking into consideration different elements that can be studied, the absorption coefficient is inversely proportional to the atomic mass and incident energy (**Equation 25**):

$$\mu(E) \approx \frac{\rho Z^4}{AE^3} \tag{25}$$

where:

ρ – density of the sample [g/cm^3]

Z – atomic number

A – atomic mass

E – incident energy [eV]

The higher μ(E) means, that the more intensive absorption undergoes. After choosing the energy range and irradiating the given sample containing an element of interest, three types of signals can be registered, giving rise to the three modes of XAS examination:

1) Transmission mode

In the transmission mode, the difference between the incident radiation I_0 and the transmitted one I_{trans} can be determined, which gives insight about the amount of radiation absorbed in the sample.

To estimate the changes in the absorption coefficient, both the incident and transmitted radiation need to be registered and put into the equation (**Equation 26**):

$$\mu(E) \approx -\ln(I_0/I_{trans}) \quad (26)$$

As presented in **Figure 30**, the linear position of the source, sample, and detector enables efficient registration of the X-rays. In synchrotron centers, it is possible to register both I_0 and I_{trans} at the same time, while in laboratories it is mostly detected during separate measurements.

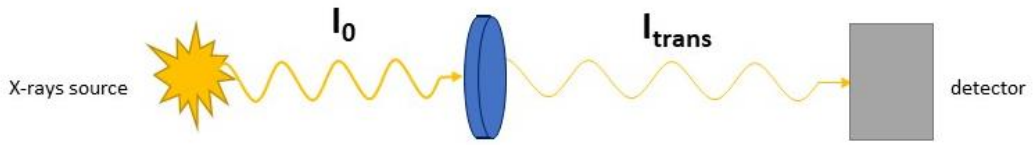

Figure 30 Configuration of the XAS setup, operating in the transmission mode

2) Fluorescence mode

As the name indicates, this mode is based on the detection of the emitted fluorescence X-ray radiation I_{fluo} from the sample (**Equation 27**):

$$\mu(E) \approx I_0/I_{fluo} \quad (27)$$

In this case, the absorption process is being registered non-directly, but via the secondary phenomena. The sample is rotated 45 degrees to the beam trajectory, and the detector is placed perpendicular to this trajectory [8] (**Figure 31**). The reason for such configuration is to get rid of the scattering radiation, since the fluorescence radiation is emitted isotropically from the sample, but the scattered one is not. In the case of the synchrotron, the radiation is polarized in the stored electrons' plane, therefore it won't be emitted isotropically and in the direction towards the position of the detector, so that the amount of incoming elastically scattered radiation will be significantly suppressed [4, 9].

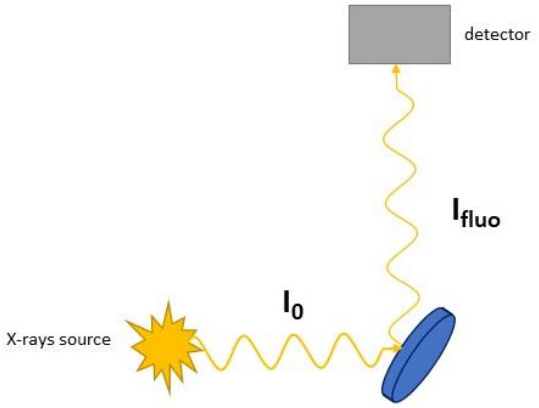

Figure 31 Configuration of the XAS setup operating in the fluorescence mode

3) Electron-yield mode

Similarly to the previous mode, the electron-yield mode concentrates on the effect following the absorption process. The ejected photoelectrons can be driven as a current and registered as the XAS signal $I_{current}$ (**Equation 28, Figure 32**).

$$\mu(E) = I_{current}/ I_0 d \tag{28}$$

where: d - X-ray penetration depth [nm]

The bigger the amperage, the more electrons were ejected from the sample, suggesting more absorption processes. This process undergoes within the surface of the sample, which needs to be placed inside the detector, to be able to register generated current. To prevent the situation, that the electrons would undergo interactions with air and recombine, leading to their loss from the signal, the sample and the detector are placed in the vacuum chamber. This mode is the most useful for well-conductive samples because in the case of insulators or other less-conductive samples, the charge would not be

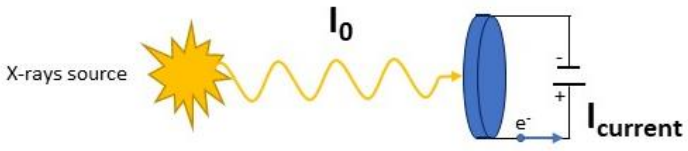

Figure 32 Configuration of the XAS setup operating in the electron yield mode

appropriately channelled from the sample and one can observe charging of the material, resulting in an altered XAS signal [4]. Therefore this mode works best for specific (conductive) types of materials.

The crucial parameters, that need to be identified before conducting an XAS experiment, are the concentration of the chosen element, the thickness of the sample, its composition, and homogeneity. In transmission mode, the bigger the concentration of the element of interest, the more attenuated beam that is registered. Similarly, the thicker the sample, the more attenuation can be observed. Such effect, which can be attributed to higher attenuation when increasing the concentration of the element in samples of the same thickness, or with the same concentration but growing thickness, is described as the "thickness effect" and should be taken into consideration in planning the experiment in the transmission mode [10]. While this effect is mostly explained as the limitations of the detector, thickness is indeed a parameter that influences strongly the intensity of the transmitted beam. **Equation 29** can be complemented with the value of thickness **x**, which is a commonly known Lambert-Beer law:

$$I_{trans} = I_0 e^{-\mu x} \tag{29}$$

For fluorescence mode, increasing concentration results in more intensive fluorescence radiation, however, parallelly intensified self-absorption process. Therefore in that case, the increase in the concentration of the element could not be the best way to improve the intensity of the signal, since it can be more altered and need appropriate correction (e.g. [11, 12]).

Nevertheless, sometimes the concentration is dictated by the available amount of the sample, like the limit of solubility or small amounts that could be purchased or synthesized. Therefore the choice of the mode should be made by taking into account the probable intensity of the detected radiation. When samples are highly concentrated (e.g. metallic foils, pure powders), the best choice is to measure spectra in transmission mode, since in fluorescence mode the self-absorption effect will be intensively observed. For diluted samples or less concentrated (e.g. few mM aqueous solution of the compound, tens of ppm of the element in the sample), the best choice is a fluorescence mode, since only emitted by the sample radiation will be detected, while in the transmission mode, the transmitted beam will be only slightly attenuated, what could not be registered with an expected resolution by the detector.

Another important aspect is the composition of the studied samples. In the case of solid samples, it is common to study powder compounds, mixed with some matrix

compound to obtain a cohesive pellet. The chosen compound should not consist element of interest nor interact chemically with the studied complex. Such compounds are e.g. cellulose or KBr. For liquid samples, it is important to choose the appropriate solvent. The best choice is a solvent in which the compound could be dissolved *in situ*. In the case of the drugs, naturally one thinks about the water or aqueous buffers (since blood or cytosol are this kind of environment) not any organic solvent, like toluene.

The importance of the proper preparation of the samples is even greater for laboratory XAS setup with an X-ray tube, where the beam is polychromatic and significantly less intensive than a synchrotron, therefore it is not possible to obtain one satisfactory XAS spectrum in minutes. The wrong position of the beam on the sample, for example, when the compound is not spreaded evenly in the whole sample and the chosen point has significantly fewer/more amount of the element than it should have, can cost a loss of even a day of examination.

2.3.2. XAS spectrum

Results of the measurements in the above modes lead to the generation of the XAS spectrum, by putting the registered values into one of the equations dedicated to each mode (**Equations 26-28**). Raw data is then normalized, which can be done manually or via using available codes, like XAS Viewer from the Larch package. Detailed procedures that were applied in the presented project are described in the posterior subsections.

Within XAS spectra, one can distinguish two regions – **XANES**, which stands for X-ray Absorption Near-Edge Structure, and **EXAFS**, from Extended X-ray Absorption Fine Structure (**Figure 33**). The first one covers the region +/- 30eV around the absorption edge, and the latter is the region above XANES. Both regions provide different information about the chosen element and its neighborhood, and possess characteristic features. XANES analysis can give information about the oxidation state, mainly by determination of the position of the absorption edge on the energy scale. With an increasing oxidation state, the position shifts towards higher energies, what is called a “chemical shift”.

For some oxidation states, in the region before the rising edge, a pre-edge structure can occur. This kind of structure can be a single peak or more complex, like a combination of peaks. The position of this structure on the energetic scale and its intensity can provide information about the geometry around the atom of interest.

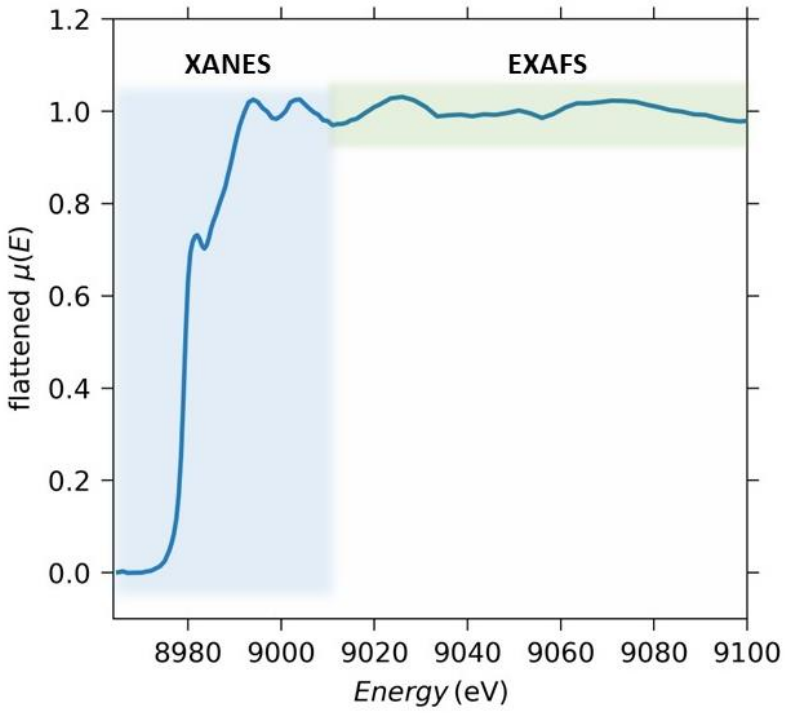

Figure 33 Cu K-edge XAS spectrum of the copper foil, with marked XANES and EXAFS regions

For example, in the case of Cu^{2+} centrosymmetric compounds, only quadrupole transition from 1s to 3d orbital can be noted [13]. Such transition is possible because the 3d orbital has 9 electrons, not 10, therefore there is an empty position for the excited electron. For Cu^{1+} 3d orbital is full (10 electrons), therefore such transition cannot occur. As a result, by verifying the presence of a pre-edge structure, one-can distinguish whether the Cu has a 2+ (present) or 1+ (not present) oxidation state in the given complex. Moreover, when the inversion symmetry is broken, mixing of the 3d metal orbital and 4p ligand orbital undergoes, enabling normally forbidden dipole transition from 1s to hybridized 3d orbital, due to the passing of the p-character, contributing to the significant increase of the pre-edge structure intensity [13].

The maximum of the peak covering the absorption edge can be one prominent peak, called a “white line”, or more peaks. With a decreasing oxidation state, its intensity decreases. For metallic forms, like metallic foils (Cu^0), a double shoulder (double peak) can be observed (like in **Figure 33**), while in complexes only one prominent peak starts to be visible.

Taking into consideration, that for different oxidation states, the mentioned features significantly change, like are present/absent or have other intensity, their changes while conducting experiments suggest undergoing redox reactions. Also, changes in the position of the absorption edge in the energetic scale (chemical shift) suggest increasing or decreasing valence. Therefore, when gathering many spectra over time and comparing

them together, one could obtain information on which reactions undergo in the sample. This property of XAS is widely used in monitoring any redox reactions, that are undergoing during experiments. For example, one can add some reducer or oxidizer after gathering the data of the primary sample, and with XAS can monitor redox reaction over time.

Summing all this information up, XANES provides information about the oxidation state of the atom of interest, the geometry of its complexes, and some undergoing changes in the samples.

The other region of the XAS spectrum – EXAFS, involves the effect following the ejection of the photoelectrons after absorption. Since studies are not carried out on single atoms but many, the photoelectrons interact with their surroundings. To be more precise, the photoelectron wave scatters on the neighboring atoms, and then the scattered part of the wavefunction interferes with the outgoing part. As a result, there are visible modulations of the absorption coefficient on the XAS spectra above the absorption edge. Since this scattering undergoes on the neighboring atoms, the parameters that will affect these modulations are the distance from the atom of interest to the nearest neighboring atoms, their type, and number. Therefore, from this region, one can determine the coordination number and mentioned distances to the surrounding atoms.

2.3.3. XAS laboratory setup

From the very beginning, the first X-ray absorption spectroscopy setups were developed in laboratory conditions. Yet, since significantly more intensive X-ray sources, which are synchrotrons, enabled detection of the signal with the high signal-to-noise ratio and shortened the measurement time, their growth was further noticed in synchrotron centers. Nevertheless, because more efficient setups attract more scientists, who would like to work on them, and the number of synchrotrons is greatly smaller than willing prospective users, access to these setups is still quite limited. That is why the development of new laboratory XAS setups is not and probably will not be out of date.

There are already many examples of contemporary laboratory X-ray absorption spectroscopy setups, that work in different conditions and are built in different geometries. For example, at the University of Helsinki, there is an XAS setup designed in the Johann geometry [14]. The source of X-rays is an X-ray tube with an Ag anode, providing the radiation for measurements in the energy range 4 - 20 keV, covering the transition metals 3d K-edge and 5d L-edge energy regions. Setup operates in transmission or fluorescence modes and is encased in a chamber filled with helium, to decrease absorption and

scattering processes undergoing in air. Another example is a laboratory XAS setup placed in the Wigner Research Centre for Physics in Budapest [15]. It was designed in the von Hámos geometry and consists of an X-ray tube with a copper anode, a cylindrically bent analyzer with Si(111) crystal wafers, and a Mythen detector. It can be successfully used for measurements around the transition metals' absorption K-edge's energy range. The source and detector are separated by the shielding wall. Elements of the setup can be easily rearranged to perform X-ray emission spectroscopy (XES) measurements.

X-ray absorption spectroscopy laboratory setup, which was used to analyze chosen copper(II) samples, is present in the Institute of Nuclear Physics PAN in Kraków, Poland, and is very similar to the laboratory setup from Budapest. However, in this case, it was built together with an X-ray emission spectroscopy setup, which allows measuring samples in both modes (XAS and XES) at the same time. The experimental table with all XAS/XES setup elements is closed in the hutch, and doors are connected to the interlock system to provide safe conditions for experimenters to perform their studies.

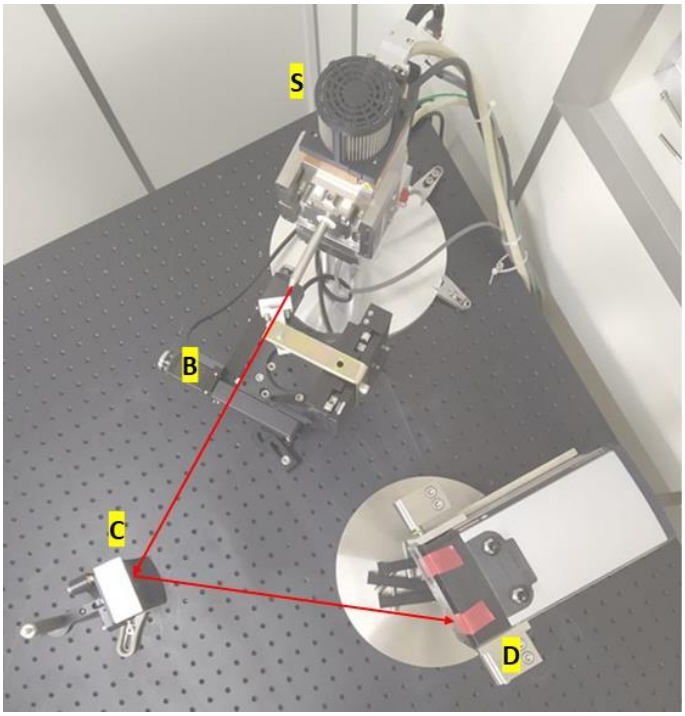

Figure 34 Configuration of the XAS laboratory setup. With letters: S - X-ray tube, B - sample holder station, C – crystal analyser, D – detector were marked. The red line shows the possible propagation pathway of the emitted X-rays from the X-ray source

This setup has been built analogously to the setup widely described in [6], which is placed in the Institute of Physical Chemistry PAN in Warszawa, Poland. The difference between these two is that in the second case, both XAS and XES setups are hidden in the shielding box. Elements of the setup are placed in agreement with the van Hamos geometry (**Figures 34-35)**.

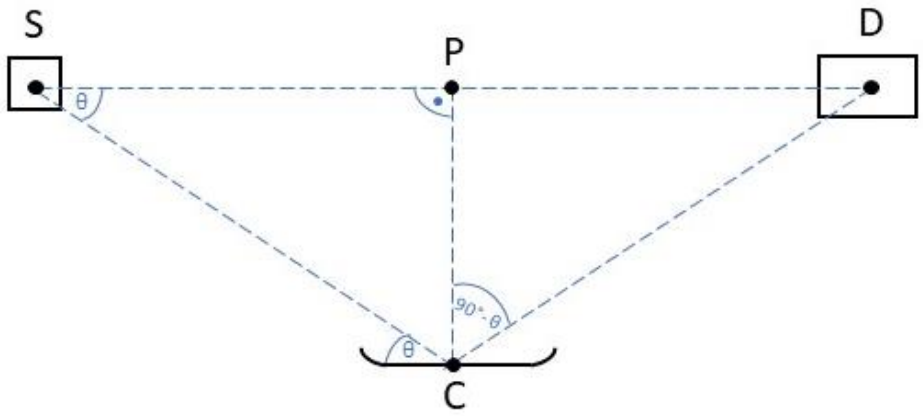

Figure 35 Scheme of the position of the elements of laboratory XAS setup

where:

S – a center of the sample

D – a center of the detector

C – a center of the crystal analyzer

|PC| = crystal analyser curvature = 25 cm = 0.25 m

$$|SP| = ½\ |SD| \tag{30}$$

$$|SC| = |CD| \tag{31}$$

The type of crystal in the analyzer for a given element of interest is chosen after first solving **Equation 14** provided in Subchapter 2.1.3., where the incident angle is set as an unknown value to be found. Let's consider the case, where the chosen element will be copper, with the value of the K - absorption edge energy 8979 eV. The transferred equation in this case looks as follows:

$$\arcsin\left(\frac{n\lambda}{2d_{hkl}}\right) = \theta \tag{32}$$

In the first step, the energy value (8979 eV ≈ 1.44 · 10^{-15} J) must be converted to wavelength λ. To obtain this value, the commonly known Planck's equation is used:

$$E = h\nu = h\frac{c}{\lambda} \tag{33}$$

From which:

$$\lambda = h\frac{c}{E} = \frac{6.63 \cdot 10^{-34} \cdot 3 \cdot 10^{8}}{1.44 \cdot 10^{-15}} = 13.81 \cdot 10^{-11}\,[m] = 1.381\ \text{Å}$$

Values of d_{hkl} are commonly known, and vary between crystals. For the presentation of the line of thinking and clarity of this part, the rest of the calculations will be obtained for two crystal types: Si(111) and Si(440).

a) **Si(111)** :

d_{hkl} = 3,1355 Å

considering 1st order of diffraction (n = 1)

$\arcsin\left(\frac{\lambda}{2d_{hkl}}\right) = \arcsin\left(\frac{1.381}{2 \cdot 3.1355}\right)$ = 12.72 degrees

b) **Si(440)** :

d_{hkl} = 0.96 Å

n = 1

$\arcsin\left(\frac{\lambda}{2d_{hkl}}\right) = \arcsin\left(\frac{1.381}{2 \cdot 0.96}\right)$ = 45.99 degrees

The next part is to find the distances between the sample and detector |SD| and between the sample/detector and crystal analyzer: |SC| or |DC|. Since the positions are set manually, these distances will be used to move all the elements to the expected positions on the experimental table.

From the **Figure 35**, it can be found that:

$$\frac{|PC|}{|SC|} = \sin(\theta) \tag{34}$$

To obtain |SC| above can be transferred to:

$$|SC| = \frac{|PC|}{\sin(\theta)} \tag{35}$$

Additionally, from the Pitagoras equation :

$$|PC|^2 + |SP|^2 = |SC|^2 \tag{36}$$

from which the unknown |SP| :

$$|\mathrm{SP}| = \sqrt{(|SC|^2 - |PC|^2} \tag{37}$$

Therefore for:

a) **Si(111)**:

$|SC| = \frac{0.25}{\sin(12.72)} = 1.1354$ [m] = 113.54 [cm]

$|SP| = \sqrt{(1.1354)^2 - (0.25)^2 =}$ 1.1075 [m] = 110.75 [cm]

|SD| = 2|SP| = 221.50 [cm]

b) **Si(440)**:

$|SC| = \frac{0.25}{\sin(45.99)} = 0.3476$ [m] = 34.76 [cm]

$|SP| = \sqrt{(0.3476)^2 - (0.25)^2 =}$ 0.2415 [m] = 24.15 [cm]

|SD| = 2|SP| = 48.30 [cm]

Taking into account the above results, it seems reasonable to choose the Si(440) crystal, because the calculated distances can be set on the experimental table. For Si(111), the distances reach more than 100 centimeters which are quite long, and setting the elements to the destined position is impossible, since in the hutch the experimental table is shorter. Therefore, for experiments with copper, the Si(440) crystal-based analyzer is applied, and distances are set as calculated. Next, a small flashlight is put onto the closed X-ray tube, and by following the diffracted light that incident on the detector, the position of the crystal analyzer and detector are tuned to obtain the best signal from the sample.

The source of the X-rays is an X-ray tube - XOS X-beam Superflux PF with Mo anode. It provides measurements around transition metals K-edges in the energy range 5-10 keV [16]. With the application of the poly-capillary, the spot on the sample reaches the diameter 100 x 100 μm^2 [6]. Maximum parameters that could be set are 50 V voltage and 1 mA current. When running at full power, the radiation flux totals 5 x 10^8 photons/second [6]. CCD two-dimensional camera - Andor Newton DO920P is being used as a detector. It consists of 1024 x 256 pixels, where each pixel has a size of 26 μm. The positions of the XAS setup elements enable measurements in a transmission mode, in ambient atmosphere and room temperature. Between the X-ray tube and crystal analyzer, there is a holder for sample attachment. Since the X-ray beam is being focused to the spot at a distance 2 cm from the X-ray tube poly-capillary, the sample needs to be put at this exact distance from

the X-ray tube to have a focused beam incident on the sample. The holder is dedicated to solid samples, but can be removed to install the liquid delivery setup or others.

Since in this setup polychromatic source of X-rays is being used, one can differentiate the photons of different energies that were transmitted since each wavelength meets the Bragg law with a different angle (as it was mentioned in the Subchapter 2.1.3.). Therefore photons of various energies are registered by other pixels of the camera. Also because it is not possible to operate with a monochromatic beam, conducting XAS experiments in the fluorescence mode is disabled.

2.3.4. XAS synchrotron setup

Nowadays, it is still more popular to perform XAS measurements with the use of synchrotron sources, than in laboratories. The beam's high brilliance, advanced machinery of the beamlines, and complementary methods present nearby, enable users complex examination of many types of samples and monitoring changes undergoing over time during experiments. The first significant difference to the laboratory setups is (of course) the used source of X-rays, that is synchrotron. The photon flux emitted by this kind of source is a few orders of magnitudes higher than the X-ray tube. E.g. for the European Synchrotron Radiation Facility ID26 beamline, the flux totals around 10^{13} photons/sec, while X-ray tube, that was chosen in the described examination, reaches the flux of $5 \cdot 10^{8}$ photons/sec, so it is 5 orders of magnitude more intensive [17, 6].

To study copper-phenanthroline-based compounds and references, three synchrotron sources were used: Swiss Light Source (SLS), at SuperXAS beamline, Villigen, Switzerland; Deutsches Elektronen-Synchrotron (DESY), at P65 beamline, Hamburg, Germany, and SOLARIS, at ASTRA beamline, Kraków, Poland. Additionally, one setup dedicated to the delivery of liquid samples was tested at the ID26 beamline of the European Synchrotron Radiation Facility (ESRF).

The first attended beamline was SuperXAS at the SLS synchrotron, being a part of the Paul Scherrer Institut (PSI) (**Figure 36**). SLS opened to users in 2001 and it is the 3rd generation synchrotron. Nowadays, it is closed for upgrading to SLS 2.0. It operated with the electron energy 2.4 GeV and 400 mA beam current. For researchers, 16 beamlines were accessible to perform studies.

Figure 36 View on the SLS and SwissFEL facilities [18]

The radiation derived to the SuperXAS station, presented in **Figures 37-38**, comes from the superbending magnet, operating with a magnetic-field strength of 2.9 T, however, the planned upgrade will increase this parameter up to 3.5 T or even 5 T [20]. The accessible energy range varies from 4.5 to 35 keV. The chosen wavelength of the radiation is obtained with the use of a Double Crystal Monochromator (DCM) or Quick EXAFS monochromator (QEXAFS). The beam size is adjusted by the slits while focusing and collimation are realized by mirrors. Flux on the sample for 12 keV photons totals $1 \cdot 10^{12}$ photons/second. There are two access modes for measurements: transmission and fluorescence (both total and partial).

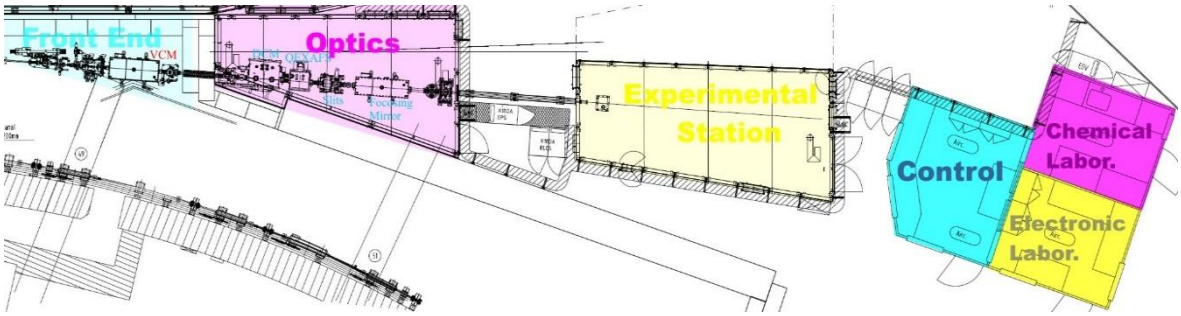

Figure 37 Scheme of the SuperXAS beamline [19]

Figure 38 View on the experimental table of the SuperXAS beamline

The second beamline was P65 at DESY, which is dedicated to the Applied XAFS. The exact name of the DESY synchrotron is PETRA III, 3rd generation synchrotron source, which is planned to be upgraded to PETRA IV in the near future [21] (**Figure 39**). PETRA III operates with the 6 GeV electron energy and 100 mA of the beam current.

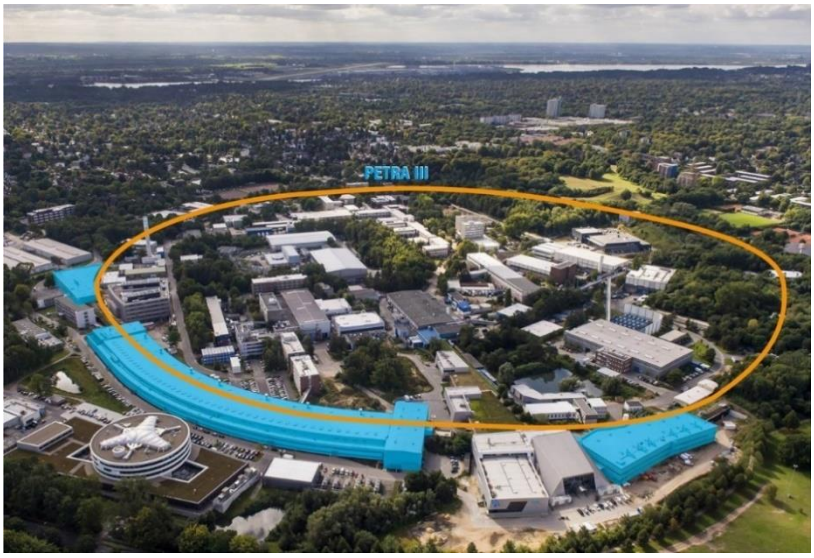

Figure 39 View on the DESY facility with PETRA III synchrotron [22]

P65 operates in the energy range from 4 to 44 keV (**Figure 40**). Incident flux on the sample totals around $2 \cdot 10^{12}$ photons/second, determined for an energy of 8.9 keV. The beam is derived from the undulator, monochromatized by water-cooled DCM, and two mirrors are used to cut the higher wavelength harmonics. There are two modes of data acquisition available transmission and fluorescence.

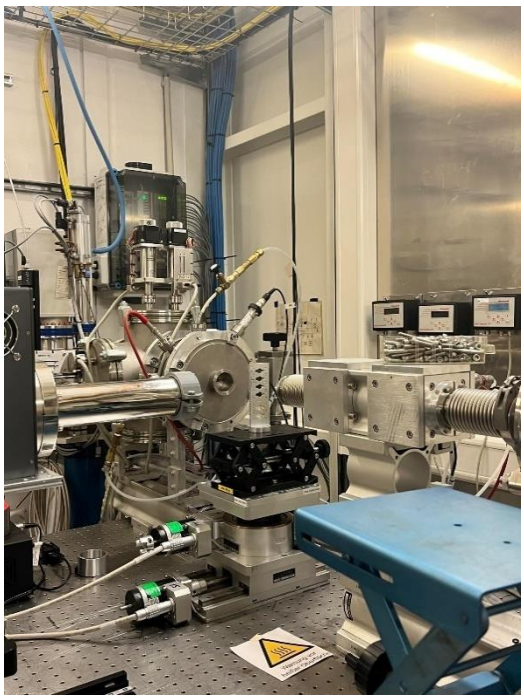

Figure 40 View on the P65 beamline experimental station

The third and the youngest synchrotron source used for the described research was the Polish SOLARIS synchrotron. Opened in 2015, has 5 operating beamlines, including 2 dedicated to XAS measurements - PIRX and ASTRA. SOLARIS synchrotron possesses only one ring, which plays the role of a booster and storage ring at the same time. Therefore, there are two breaks in operation for electron injections. Electron energy reaches 1.5 GeV, which gives a current of around 400 mA decreasing in time. ASTRA beamline operates in the energy range from 1 up to 15 keV. Radiation is derived from a bending magnet.

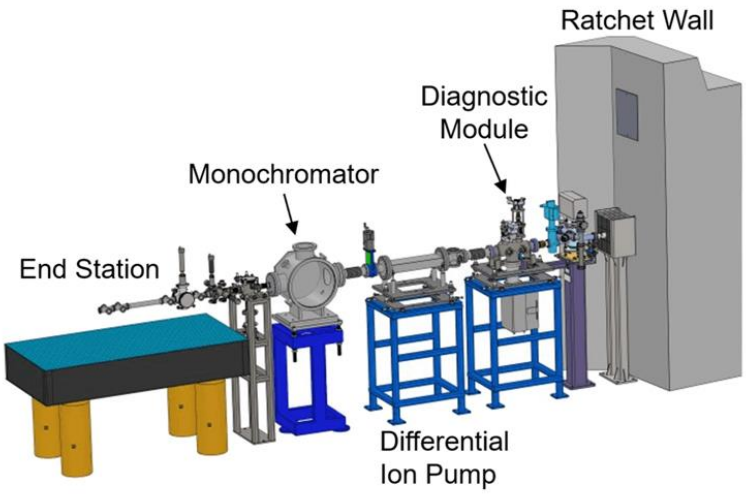

Figure 41 Scheme of the ASTRA beamline experimental station [23]

Both transmission and fluorescence modes are accessible, however, the obstacles come from the fact that all samples need to be put inside the chamber (**Figures 41-42**). Therefore, while solid samples are nearly always easy to transfer, the setup where the liquids need to be in a constant flow has to be specially designed.

Figure 42 View on the ASTRA beamline experimental station

Lastly, the ID26 beamline of the ESRF synchrotron was visited to perform tests of liquid delivery setup (**Figure 43**). This beamline is dedicated to studies of very diluted samples [24]. The minimum detectable concentration of the element in the sample is a few ppm, in the fluorescence mode. The applied energy range can vary between 2.4 to 27 keV. The chosen energy is adjusted with the use of three undulators dedicated to the beamline. Incident flux on the sample can reach even 10^{13} photons/second. Since, the beamline is dedicated to study liquids, there was already a setup dedicated to its delivery for measurements. Therefore, it was tested, whether it could be used effectively to study solutions of copper-phenanthroline complexes.

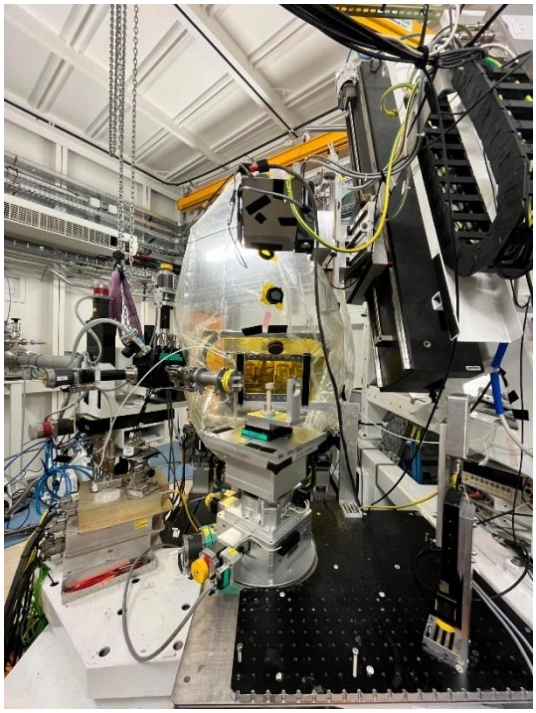

Figure 43 ID26 experimental station

2.4. XAS measurements of copper referential samples in laboratory conditions

Before measurements of the compounds of the main interest, there is a common practice to measure some referential materials first. The reason is that for newly synthesized compounds, the registered XAS spectrum is the first ever measured, and therefore there is yet no standard to refer to the results. Therefore, also in this research, a few referential materials were chosen: copper foil (Cu^0), CuO (Cu^{2+}), and Cu(1,10-phenanthroline)Cl_2 (Cu^{2+}). The chemical structure and some physicochemical properties of the latter are known, however, to our best knowledge, no other scientific group has measured the XAS spectra of this compound. This complex was treated as a referential for the triazole-containing compound, since the chemical structure of this purchased complex is very similar to the synthesized one. At the same time, it was treated as the second copper-phenanthroline compound with potential cytotoxic activity to be studied with XAS, to evaluate its possible interactions with chosen biomolecules.

2.4.1. Sample preparation

As it was mentioned, 4 referential materials, which were: Cu foil, $CuSO_4$, CuO, and Cu(1,10-phenanthroline)Cl_2 (*Cu(phen)Cl_2*) were chosen. To prepare a sample in the form

of a pellet (13 mm in diameter), one of the compounds at a time was mixed with cellulose. The reason for this is that the pellet consisting of only the chosen compound is very fragile, easily breaks, and is hard to transfer. Therefore, there is a need to add the matrix compound, that will enable obtaining a firm pellet. Cellulose is also an inert compound, which does not interact chemically with copper compounds, which prevents any structural or oxidation reactions in the sample, and does not alter the results from XAS measurements. Another reason is to decrease the amount of the analyzed compound in the sample – for transmission mode, it leads to increasing of the XAS signal and obtaining more detailed spectra, while for fluorescence mode, it lowers the self-absorption.

To prepare pellets, the needed weight of the compounds to obtain different concentrations in samples was calculated and presented in (**Table 2**). The total weight of the pellet was 150 mg. Additionally, a pellet containing only cellulose was prepared for background measurements.

Table 2 Mass ratios of the used compounds to create a pellet sample

	Concentration [wt.%]			
	1	**3**	**5**	**10**
Mass of the copper compound [mg]	1.5	4.5	7.5	15.0
Mass of cellulose [mg]	148.5	145.5	142.5	135.0

All the pellets were prepared according to the following procedure:

1. With the use of the scale, copper(II) compound and cellulose were weighted, according to the chosen ratio.
2. Powders were transferred into the agate mortar and both compounds were milled accurately.
3. The mixture was transferred to the pellet pressing mold and put into the hydraulic press. A pressure of around 20 tonnes was applied.
4. The pellet was pressed for around half a minute, and then the pellet pressing mold was removed from the hydraulic press and opened to take off the pellet.
5. The pellet was covered with the Kapton foil and transferred to the hutch for measurements, where the pellet was attached to the holder.

2.4.2. Data acquisition

1) Setting the parameters on the apparatus

Before starting the measurements, the experimenter needs to close the hutch to actuate the interlock system (for safety reasons), that is linked to the X-ray tube. This system operates in such a manner, that any rapid opening of the doors of the hutch immediately turns off the X-ray tube, which results in a rapid change in the applied voltage. Such improper usage might damage the X-ray tube.

Following the closure of the hutch, the X-ray tube can be set progressively to the destined values. In the case of the reported data, the chosen parameters were 50 kV and 0.9 mA. Also, the detector is being cooled down to -40°C. In the program operating the detector, firstly the measurements of the background and unattenuated beam from the source are checked to choose the best region of interest (ROI) on the area of the CCD camera.

2) Choosing the optimal position of the sample

To find the center of the sample, which will be the appropriate spot for measurements, the scans along the *X* and *Y* axes with the use of motors are performed. The *Z* position is fixed to the position of the focus of the beam. The example of the results of the scans across the whole pellet, along the *X*-axis and fixed *Y* position, are presented below in **Figure 44**.

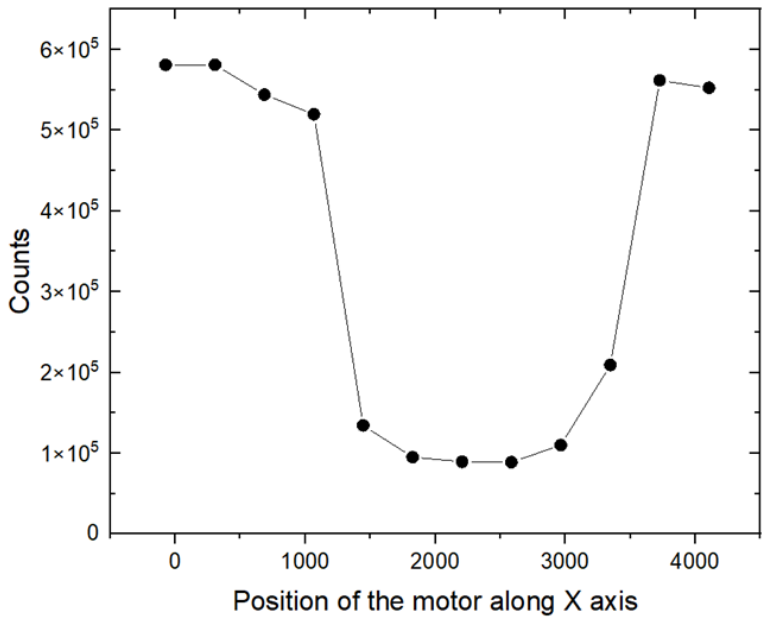

Figure 44 Example of the results of the registration of number of counts in function of the sample position for choosing the best spot for measurements

The position is chosen by the identification of the coordinates for which the absorption is the most intensive, and then the coordinates around the middle of the distance between two extreme positions with high absorption are found (in here the points around 1000 and 3500 position of the motor). After the positioning procedure, one can run the measurements.

3) Running the macro and starting measurements

At this point, also the other parameters of the data acquisition are chosen. For reported data, it was 1 second of exposure time per frame, 3 cycles with 30 frames per cycle. A frame is in this case a single registration of counts performed by the detector, that underwent according to the set parameters, like acquisition time or chosen ROI. Counts are added collectively and only manual stop of the measurements aborts the data acquisition.

2.4.3. Energetic calibration and data analysis procedure

Results of measurements with the use of laboratory XAS setup are in the form of a .txt data file, containing two columns: first with the detector's pixel number, and second with the number of registered counts. To normalize data to obtain the value of counts per second, the number of counts was divided by the number of collected one-second-long frames. Furthermore, because the number of counts registered by each pixel will give the value of energy step higher than the resolving power of the setup, there is a need to bin the values obtained from neighboring pixels, and in presented results summed the counts from 5 pixels. All of these procedures were applied for gathered data for references and samples containing copper-phenanthroline complexes. A choice of I_0 signal, that is a detected incident beam, was described in the following subchapter. XAS data obtained for the given copper sample and I_0 was put into **Equation 26**, to obtain the numerical value of absorption.

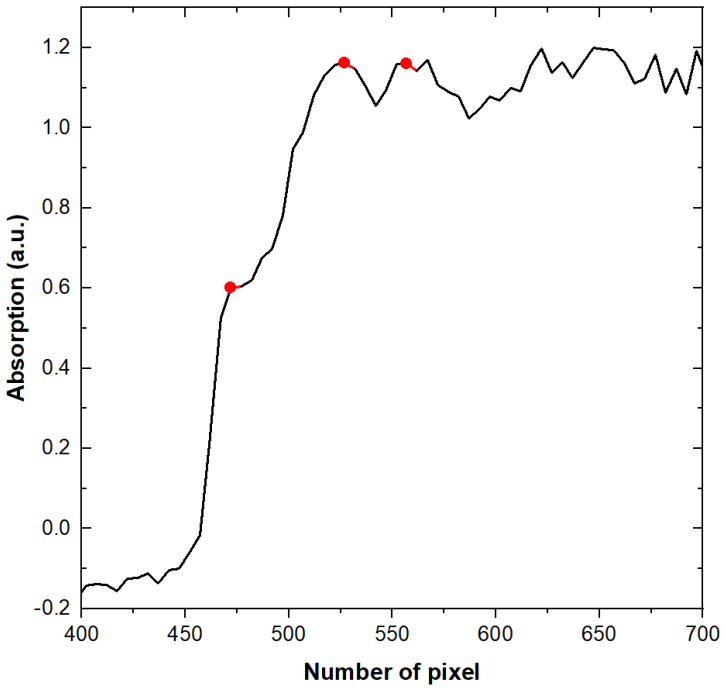

Figure 45 Cu K-edge XAS spectrum of copper foil, measured in laboratory, with marked 3 points used for calibration from number of pixel to energy of registered photon

The result of the above operations gives an XAS spectrum in the number of pixel scale. To convert the number of pixels to the energy of detected photons scale, one needs to use the data obtained for reference material, such as Cu foil. To obtain further presented results, firstly, 3 characteristic points from the laboratory spectrum were chosen (**Figure 45**), which were the maximum of the inflection within the absorption edge region, and the maximum of the first and second shoulder above the edge. The next step was to use the spectra of Cu foil from the available libraries with XAS spectra data. Two datasets from the [25] library were chosen, since with two references it was already possible to perform efficient linear interpolation of pixels' number to values of the energy of registered photons. The same three points at the referential spectra were identified, as in laboratory one, and the values of the energy of the same point for two spectra were averaged. Then the number of pixel with the averaged value from the referential spectra were compared, and linear interpolation to convert the number of pixels to the energy scale was performed. All the above procedures were performed with the use of the OriginLab code. For further analysis, separate .txt files were created for each sample's data, to open them in the XAS Viewer program for more detailed analysis.

Once the data were opened in the XAS Viewer program, the first step was a rebinning of the data for easier further comparison with the synchrotron results, where the step varied between the regions of the XAS spectra, what is impossible to be done with the laboratory setup. The chosen rebbining manner was as follows:

a) In pre-edge region: E0 - 60 [eV]: E0 – 15 [eV], set a 2 eV step,
b) In the edge-region: E0 - 15 [eV]: E0 + 15 [eV], set a 0.35 eV step,
c) In the post edge region: 0.05 [1/ λ] step.

E0 value was obtained by taking the maximum of the first derivative, provided by the program, and corrected manually if needed.

The rebinning resulted in obtaining a less noisy first derivative, which eased the determination of its maximum. After that, the data was deconvoluted with the use of the Gaussian function. To normalize the spectra, the polynomial function to the pre-edge and post-edge regions was fitted, by applying manually the appropriate energy ranges. Since the noise was changing between samples and normalization parameters differed, the flattening function was used to present all XAS spectra in one figure.

After that, the value obtained for the spectrum of the copper foil was checked. For the laboratory spectrum, the value was higher than it is reported in the model tables, that is 8979 eV, therefore this data and for all references, were shifted 1.5 eV toward lower energies, to calibrate the energetic range and meet that value. After that, values of the maximum of the first derivative for all spectra were re-checked and normalization was corrected when needed. Data were then exported to a .csv file to prepare graphs in the OriginLab program.

2.4.4. Results

1) Choosing the source of the I_0 signal

For measurements of pellets, two aspects need to be taken into account: first - the scattering processes and absorption by the air, second – the presence of cellulose in the pellets, which also attenuates transmitted radiation. Therefore, to improve the I_0 signal, two attempts were implemented: registration of the X-rays passing only through the air ($I0_{air}$), and secondly, registration of the radiation that passed through the pellet, consisting of the cellulose only ($I0_{cellulose}$). The cellulose pellet had a thickness and mass the same as each of all examined further pellets with copper. As a copper compound sample, a $Cu(phen)Cl_2$-containing pellet was prepared, that had a concentration of 6 wt.% of this compound in the sample. All measured signals were substituted into the **Equation 26**, to determine the absorption, and obtained spectra were normalized in the OriginLab program, by setting the minimum value of the absorption as 0, and the maximum as 1. Since the quality of the spectra was an aspect that was compared, the calibration to the energetic scale was not performed at that time, and the presented spectra are in the scale of the number of pixel.

Additionally, both spectra were smoothed with the Savitzky-Golay function, to favor the comparison.

By comparing the spectra after taking a different type of I_0 signal (**Figure 46**), there is observed one significant difference. With taking the I_0 signal, that was transmitted radiation through the air, the white line is not visible, which is a characteristic feature for spectra of Cu^{2+} samples. By taking the signal, which was radiation transmitted through the cellulose pellet, there can be seen an origin of this feature. Within this energetic region, the energy of the absorption edge is determined, therefore it is crucial to optimize the quality of this part of the spectrum. Therefore, the second type of I_0 signal was chosen to be used to obtain laboratory XAS spectra.

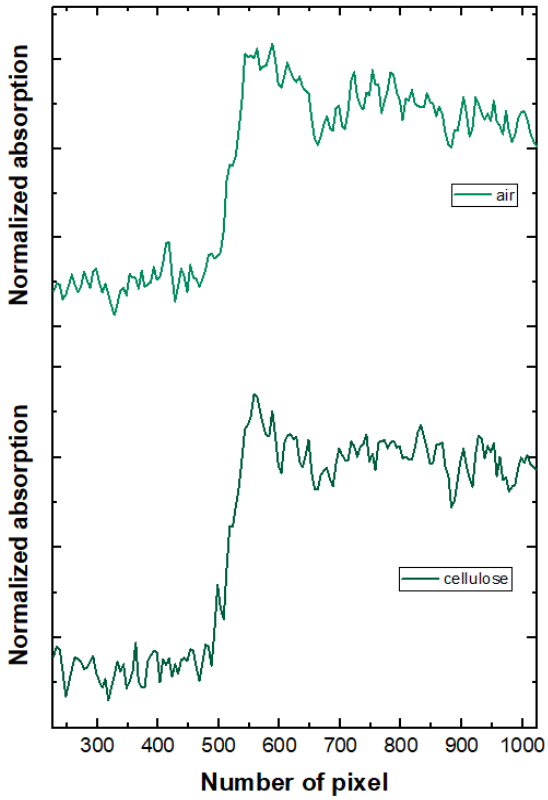

Figure 46 Comparison of Cu K-edge XAS spectra of $Cu(phen)Cl_2$ pellet, obtained with taking signal transmitted through air (top) and cellulose (down) as I_0

2) Acquisition time optimization

Before measuring all the prepared pellets with changing concentration, there was a need to decide on the optimal measurement time in terms of reasonable time to spend only for one sample, and equally to collect enough data to obtain a spectrum of good quality. For this aim, 24-hour measurements series of the 3 wt.% pellet with $Cu(phen)Cl_2$ were performed, taking data after 1, 2, 4, 6, 8, 12, and 24 hours of acquisition for comparison. The results are presented in **Figure 47**.

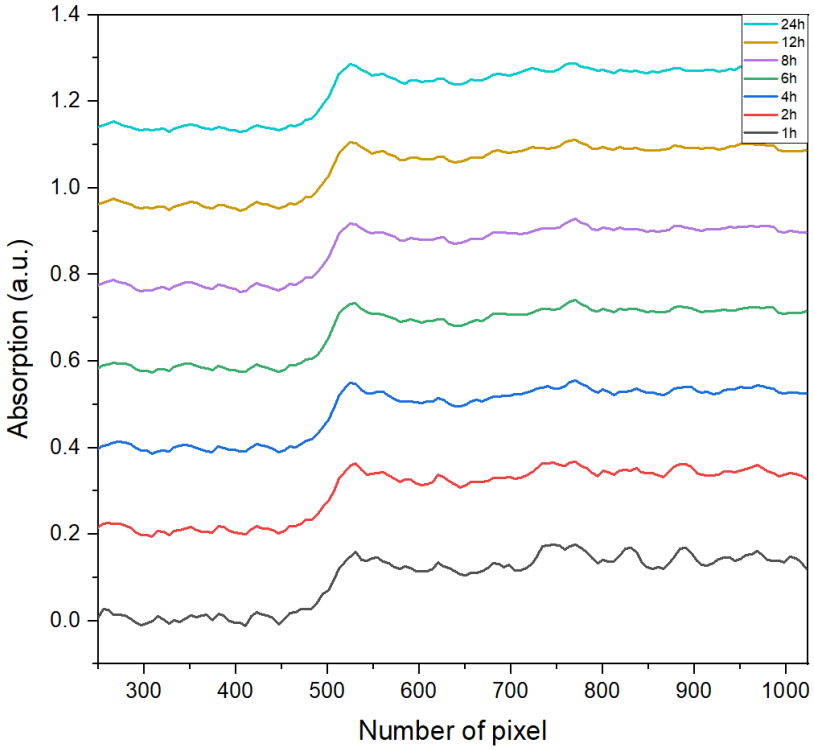

Figure 47 Cu K-edge XAS spectra of $Cu(phen)Cl_2$ pellet in the number of pixel scale obtained after different total acquisition time

Since the counts after each completed cycle are being summed, the prolonged timespan of the measurement should result in the improvement of the signal-to-noise ratio. Looking at the results, this improvement can be observed till the 6 hours of the measurement. After that time, there are no visible differences in the level of the noise. Hence, to include some spare time if anything happened during this cumulative mode of data acquisition, 8 hours were chosen as the optimal time for examination per one sample.

3) Comparing the XAS spectra of samples with different concentrations of the copper(II) compound

Because even small changes in the concentration of the copper in the sample have a visible impact on the registered number of counts, there was a need to measure samples containing various concentrations of Cu(II) compounds, to determine the most appropriate ratio for further comparison and analysis. As a model compound, $Cu(phen)Cl_2$ was chosen.

Four pellets were prepared, in a mass ratio of the compound: 1, 3, 5, 10 wt.% in a pellet, mixed with cellulose. Obtained XAS spectra are presented in **Figure 48**. At first sight, it is visible clearly, that the XAS spectrum for a pellet with 1 wt.% of the compound is significantly altered by the noise and even normalization did not reveal any shape or expected details for further analysis. The less disrupted by noise spectrum seems to be for a sample with 5 and 10 wt.% of $Cu(phen)Cl_2$ (**Figure 49**). However, with the decrease of the noise, also the intensity of the spectrum drops, according to the well-known "thickness effect" [26].

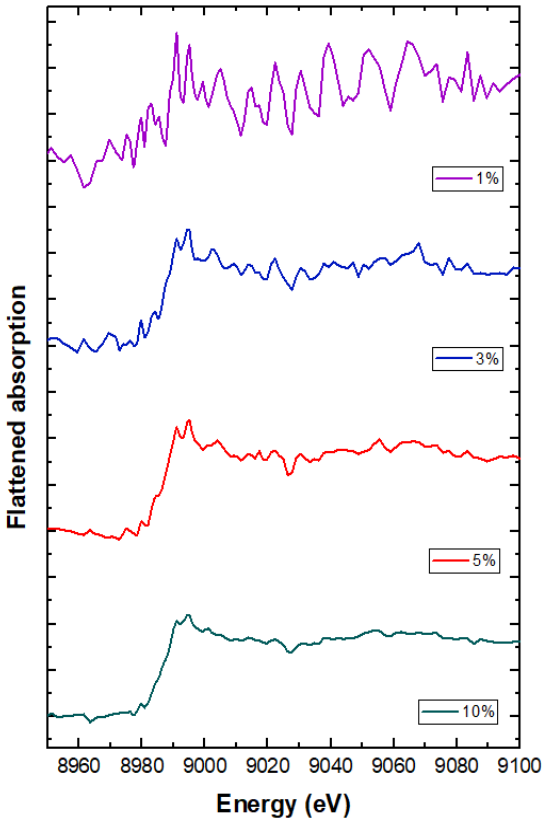

Figure 48 Cu K-edge XAS spectra of pellets with varying concentration of $Cu(phen)Cl_2$

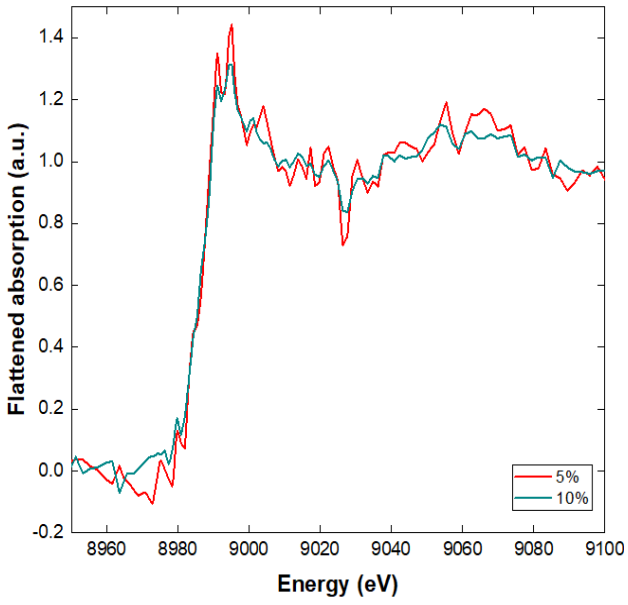

Figure 49 Cu K-edge XAS spectra of pellets containing $Cu(phen)Cl_2$ in concentration 5 and 10 wt.%

The additional aspect is the fact, that in the case of the synthesized compound, its amount is very limited by the efficiency of the synthesis, therefore any savings of the material are highly desired. Moreover, in the applications, this compound will be injected in low concentrations into the body of the patient. Therefore studies on the complexes dissolved in a solvent, mimicking the human body, should be performed for diluted samples. Since such experiments were planned, it occurred a need to have also spectra for low-concentrated references. Taking all the above into account, the concentration of 5 wt.% of the compound in all solid samples was chosen for further comparison of the results in this thesis.

4) XAS spectra for copper referential samples

The pellets with chosen compounds, as a reference for Cu^{2+}, and a copper foil, as a reference for Cu^{0}, were examined. The obtained spectra are presented in **Figure 50**.

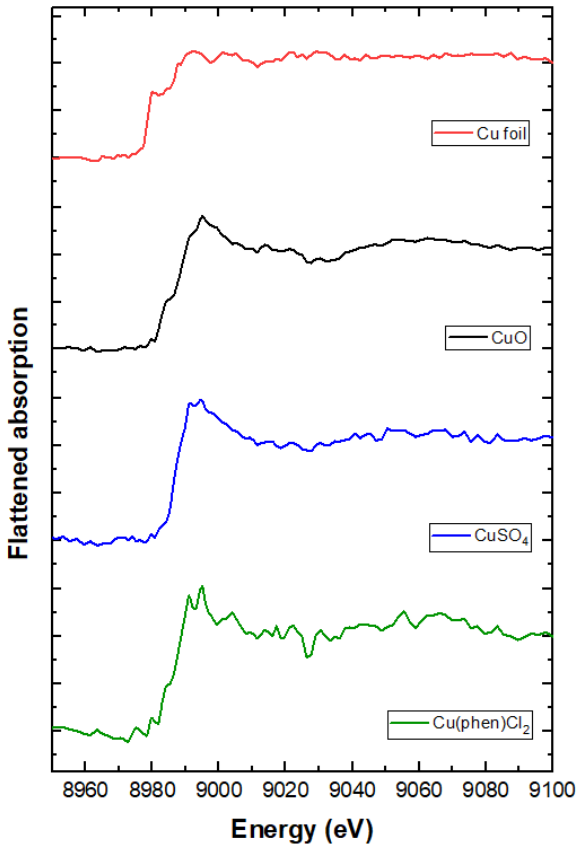

Figure 50 Laboratory Cu K-edge XAS spectra of copper foil and pellets, containing 5 wt.% of copper compound

For the spectrum of copper foil, it is easily visible that in the XANES region, there is visible an absorption edge with a peak at 8981 eV and a characteristic double shoulder above 8990 eV, which are also found on the spectra from the literature [27]. For the XANES spectra for pellets, the peak within the edge region is not visible, only for CuO at 8986 eV and $Cu(phen)Cl_2$ at 8985 eV respectively, there might be a shoulder. Instead of the double shoulder above, for all copper complexes, there is observed a prominent peak, called in the literature the "white line", suggesting a higher oxidation number for copper than 0.

The next step was to determine the energy of the absorption edge, so the energy needed for the dipole transition of electrons from the 1s to 4p orbital. There are some mathematical procedures to estimate this energy from the XAS spectrum. The first possibility is to determine the maximum of the first derivative of the spectrum, so the position on the energy scale where the growth in

the absorption coefficient is the most intensive. The second is taking the value of energy where the second derivative crosses the X-axis, so meets 0. The third possibility is to determine the energy for a point that matches half of the height of the absorption edge. All attempts were essayed and are reported below:

a) First and second derivative

To obtain the values with this attempt, the first and second derivatives of the XAS spectra were determined. It can be done both manually in the OriginLab program and the XAS Viewer. To present the data, the results of the normalized first derivative, second derivative, and XAS spectrum, were prepared in the first program, and the results are presented in **Figures 51-54**.

By analyzing the results, it is visible that for all samples, the maximum of the first derivative can be easily determined. The point where the second derivative crosses the OX axis was chosen in the region after its maximum value, which was also the region where the maximum of the first derivative was found. Taking into account the uncertainty of the measurement, both attempts provided the same value of the energy, that are listed in **Table 3**.

Table 3 Determined values of the energy of the absorption edge obtained by analyzing the derivatives of the XAS spectra

Compound	**The energy of the absorption edge [eV]**
Cu foil	8979 ± 1
CuO	8983 ± 1
$CuSO_4$	8986 ± 1
$Cu(phen)Cl_2$	8983 ± 1

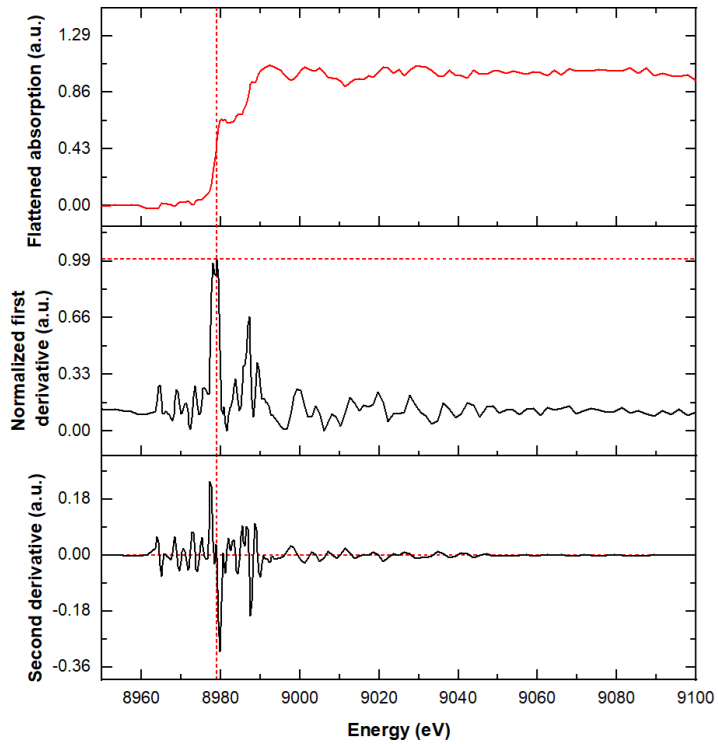

Figure 51 Laboratory Cu K-edge XAS spectrum of Cu foil (top), with the first (middle) and second derivative (down). With a vertical dashed line the energy of the maximum of the first derivative and the point crossing zero of the Y axis of the second derivative were marked. With horizontal dashed lines the value of the absorption totaling 1 and 0 respectively was marked

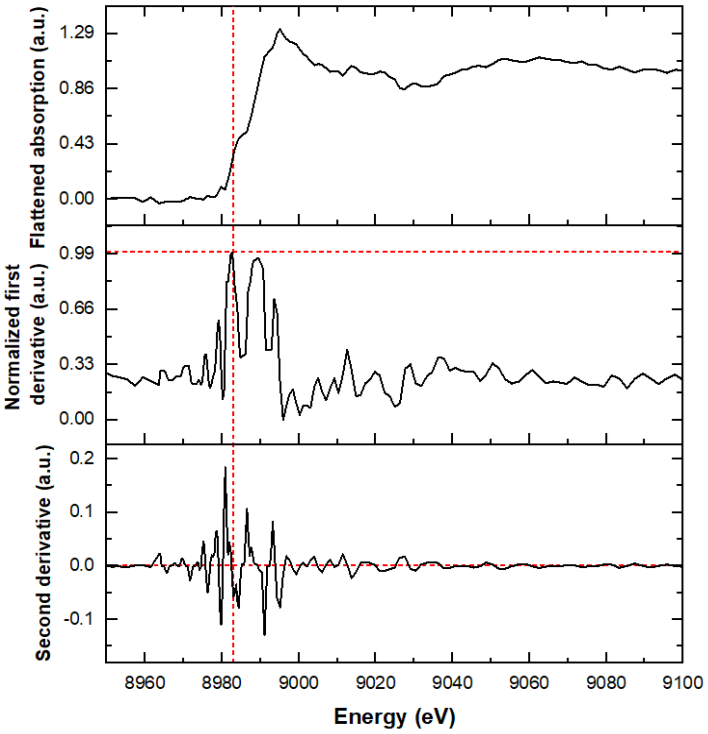

Figure 52 Laboratory Cu K-edge XAS spectrum of CuO pellet (top), with the first (middle) and second derivative (down). With a vertical dashed line the energy of the maximum of the first derivative and the point crossing zero of the Y axis of the second derivative were marked. With horizontal dashed lines the value of the absorption totaling 1 and 0 respectively was marked

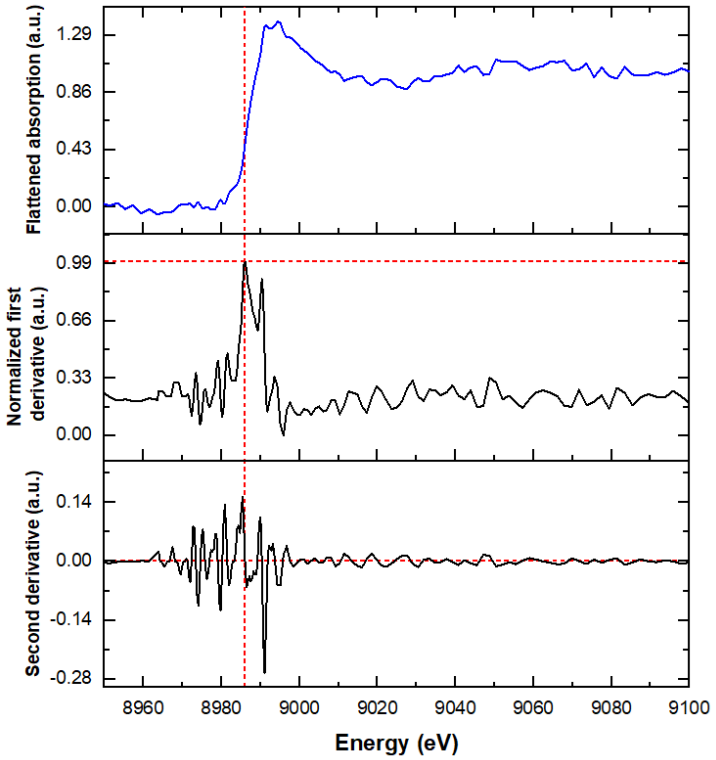

Figure 53 Laboratory Cu K-edge XAS spectrum of $CuSO_4$ pellet (top), with the first (middle) and second derivative (down). With a vertical dashed line the energy of the maximum of the first derivative and the point crossing zero of the Y axis of the second derivative were marked. With horizontal dashed lines the value of the absorption totaling 1 and 0 respectively was marked

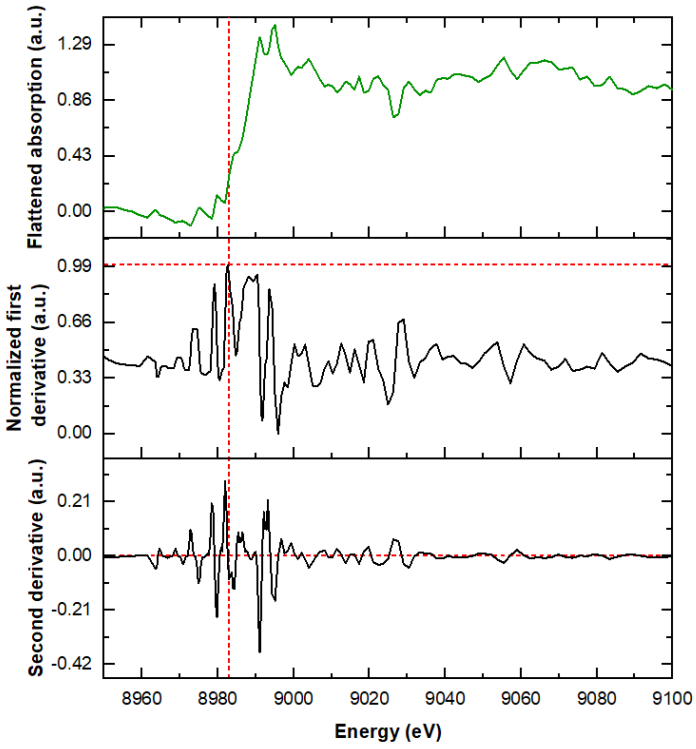

Figure 54 Laboratory Cu K-edge XAS spectrum of $Cu(phen)Cl_2$ pellet (top), with the first (middle) and second derivative (down). With a vertical dashed line the energy of the maximum of the first derivative and the point crossing zero of the Y axis of the second derivative were marked. With horizontal dashed lines the value of the absorption totaling 1 and 0 respectively was marked

b) Half of the height of the absorption edge

To obtain the values of the points, that mark out the region where absorption starts to rise and the value where it reaches its maximum within a XANES region (white line or first shoulder), all measurement points before the absorption edge were averaged, and the closest point to the averaged one was chosen. After that, these 2 values of the energy were subtracted and the result was divided by 2 to find half of the height of the absorption edge. Obtained values for all samples were listed in **Table 4**, and spectra with marked regions were presented in **Figures 55-58**.

Table 4 Determined values of energy of the absorption edge from taking the energy of the point in half of the height of the edge

Compound	**The energy of the absorption edge [eV]**
Cu foil	8979 ± 1
CuO	8988 ± 1
$CuSO_4$	8987 ± 1
$Cu(phen)Cl_2$	8987 ± 1

This attempt required the highest number of actions, that needed to be carried out by data analysts in comparison to the previous ones. These results give for all of the compounds very similar value of the energy of the absorption edge, even if their chemical structure significantly differs.

Since, the determination of the absorption edge energy from the first derivative involves the lowest number of actions, and this derivative can be easily calculated in programs used for processing XAS data, this method was chosen to be used in further analysis.

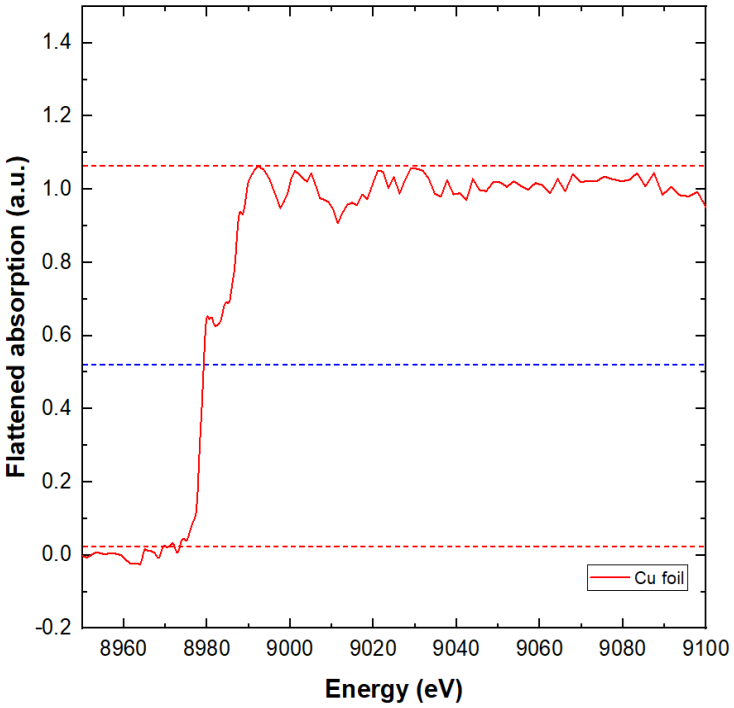

Figure 55 Laboratory Cu K-edge XAS spectrum of the Cu foil. With red dashed lines regions of the chosen beginning and end of the rising edge were marked, and with blue one the determined its half of the height

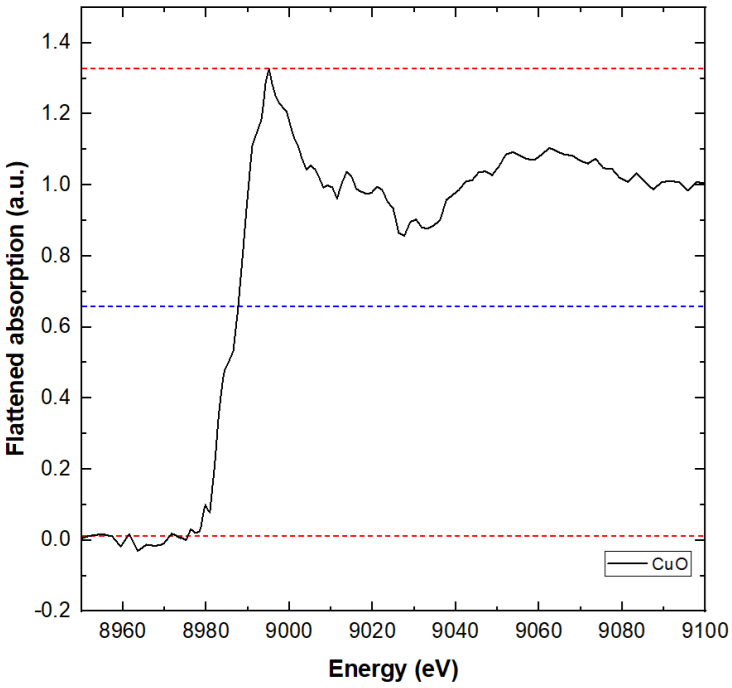

Figure 56 Laboratory Cu K-edge XAS spectrum of the CuO pellet. With red dashed lines regions of the chosen beginning and end of the rising edge were marked, and with blue one the determined its half of the height

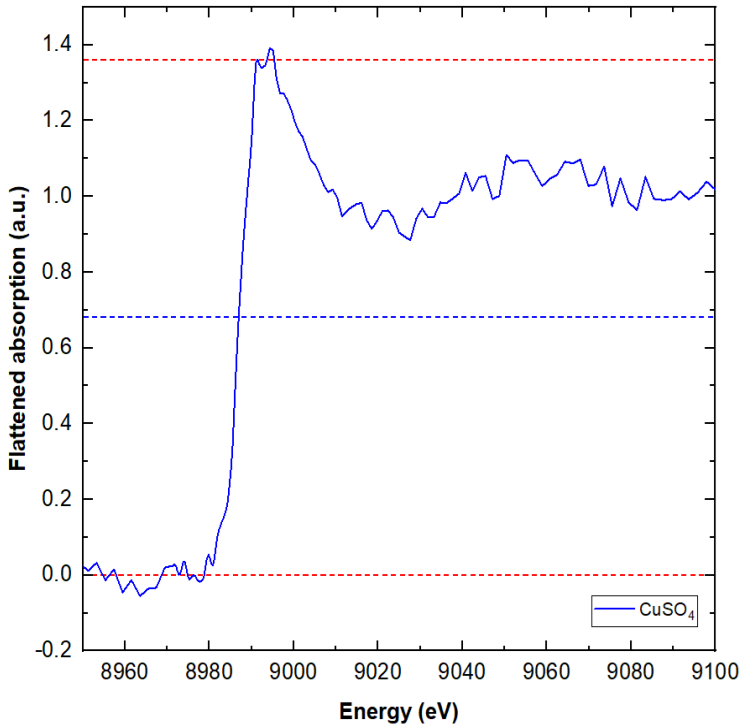

Figure 57 Laboratory Cu K-edge XAS spectrum of the $CuSO_4$ pellet. With red dashed lines regions of the chosen beginning and end of the rising edge were marked, and with blue one the determined its half of the height

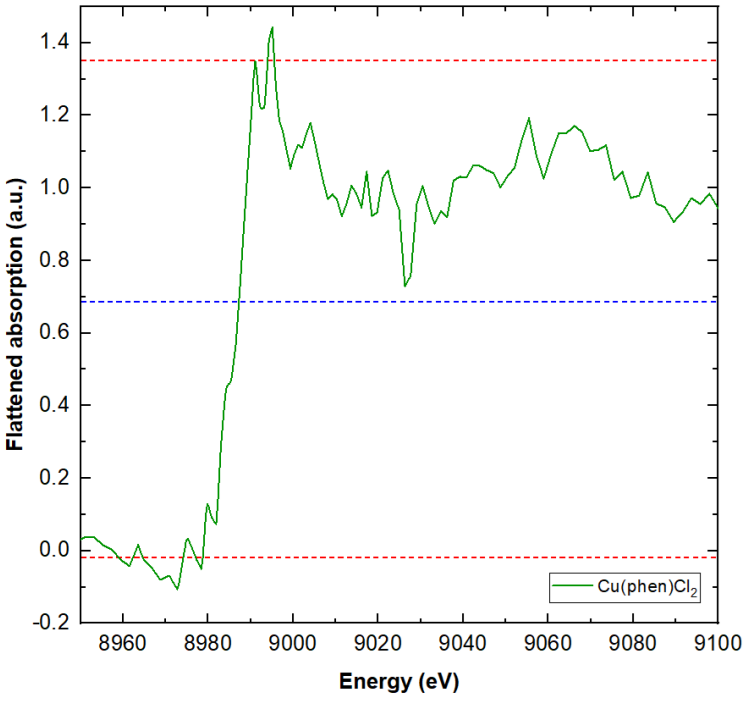

Figure 58 Laboratory Cu K-edge XAS spectrum of the $Cu(phen)Cl_2$ pellet. With red dashed lines regions of the chosen beginning and end of the rising edge were marked, and with blue one the determined its half of the height

2.5. XAS measurements of copper solid samples at synchrotron facilities

2.5.1. Setup preparation

The first synchrotron examination of copper-based compounds within the presented project was performed at the Swiss Light Source at the SuperXAS beamline. All the pellets were covered with the Kapton foil and attached to the holder, which was presented in **Figure 59**.

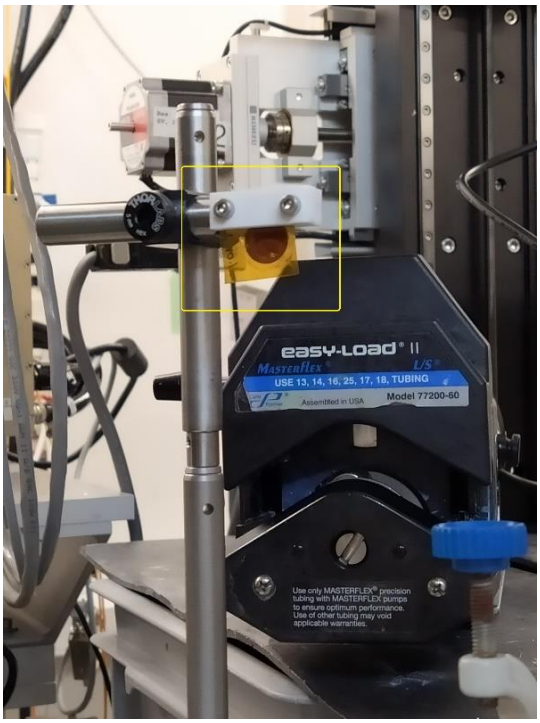

Figure 59 View on the sample holder with attached pellet (marked with a yellow square) on the SuperXAS experimental table

12 freshly-prepared pellets, containing one from the chosen copper(II) compounds: CuO, $CuSO_4$, and Cu(1,10-phenanthroline)Cl_2 in varying concentrations were examined. Because there was no available glove box to prepare copper(I) compound pellet protected from ease oxidization, such a reference for Cu^{1+} was not used. To decrease the radiation damage process, the size of the beam was changed to 100 μm x 1.1 mm. Also, an Al-160 attenuator was inserted into the beam. The SDD Vortex detector was chosen to register the signal in total fluorescence yield mode. The energetic steps of the scans were: 1 eV before the absorption edge: 8965 - 8976 eV, 0.5 eV for the region around the edge: 8976 - 8990 eV, 1 eV for 8990 - 9021 eV, and 2 eV for the EXAFS region: 9021 - 9149 eV. Three

scans per pellet were registered, which took around 21 minutes of data acquisition (7 minutes per scan, 3.5 seconds per point).

The second synchrotron examination was performed in the DESY facility at the P65 beamline. Data for pellets was acquired in a transmission mode, for which an ionization chamber was used as a detector. Pellets were mounted to the holder owned by the beamline, presented in **Figure 60**. From this moment, also Cu(phen,triaz)Cl_2 pellet was examined, since the synthesis of this complex was finally completed. The size of the beam totaled approximately 1.5 mm. Parallel to the detection of the signal from the sample, the signal from the copper foil was registered by the second ionization chamber. The energetic step was set to 0.3 eV for all regions of spectra in the energy range 8831 – 9580 eV, with the time to measure one spectrum totaling around 3 minutes (0.05 s per point), repeated twice per sample.

Figure 60 Holder for pellets from the P65 beamline

Figure 61 Pellet attached to the holder from ASTRA beamline

The third study was performed at the ASTRA beamline of the SOLARIS synchrotron. The transmitted signal through each pellet was measured by an ionization chamber, to which the signal from the copper foil was also acquired simultaneously by a second ionization chamber. The size of the beam was set to 1 x 8 mm, which gave a rectangle cross-section, which covered a significant volume of the pellet that was irradiated. Each pellet was attached to the holder with the use of Kapton foil (**Figure 61**), and the whole holder was stuck to the manipulator dedicated to the sample chamber. Chosen energetic steps were: 2 eV for 8900 – 8960 eV region, 1 eV for 8960 – 8975 eV region, 0.2 eV for 8975 – 9010 eV region, 0.5 eV for 9010 – 9025 eV region, and finally 1 eV for 9025 – 9200 eV region. It took 11 minutes to perform one scan, 1 second per point. Three scans for each pellet were gathered. Additionally, since the motor of the sample holder has not yet been available to change the spot of the measurement after each scan, any radiation damage process could be checked by comparison of the spectra obtained after different periods of time. Since after a quick comparison of gathered spectra, no significant differences in XAS spectra features were identified, one deduced that the chosen compounds, especially copper-phenanthroline ones, did not undergo visible radiation damage for the chosen experimental conditions.

In the case of all synchrotron (and laboratory) examinations, copper solid samples had the form of pellets and were performed accordingly to the procedure and in concentrations reported in Subchapter 2.4.1.

2.5.2. XAS data analysis

For data analysis of all synchrotron XAS spectra, the XAS Viewer program was used. To normalize the spectra, the fitting of the polynomial function to the pre-edge and post-edge regions was used. Then spectra (3 for each sample) were merged in intensity, to obtain one resultant spectrum for further comparison. Then the normalization was corrected, by adjusting the value of energy of the absorption edge (**E0**) to the determined maximum of the first derivative. The value of the absorption edge energy was set to 8979 eV by shifting the spectra with the difference between the obtained value from the experimental data and this tabularized one. Accordingly, all of the rest XAS spectra were shifted with the same value for energetic calibration. After that, data was rebinned and deconvoluted, according to the manner described in Subchapter 2.4.3. There was only one difference - a pre-edge

region in rebinning started from E0 - 140 eV energy value, because more points were gathered before the edge. As a measurement uncertainty value, the value of the chosen energetic step around the edge region was taken.

For easier comparison of the spectral features, the data was flattened to align spectra in the Y axis, especially the EXAFS regions.

For analysis of the pre-edge peaks, the ”Pre-edge Peak” extension of the XAS Viewer program was used. To the normalized spectra, a convolution of the Linear and Lorentzian functions was fitted to determine the baseline. Secondly, the region where the pre-edge was found was chosen and the Voigt function was fitted, to obtain the value of the peak area and position of the center.

In data analysis of the results from ASTRA beamline, there was a need to perform the interpolation of the data, since there were found issues with the monochromator operation. It was observed, that for the same parameters of the performed scans of the same pellet, the monochromator for some determined Bragg angles could not repeat the same positions in each scan, therefore it was found that the energetic steps differed in the sets of data for the same sample. As a result, after merging the normalized spectra, the fluctuations in some regions of spectra were visible, that were not connected to the process of the absorption in the sample, but issues in the monochromator movement. An example

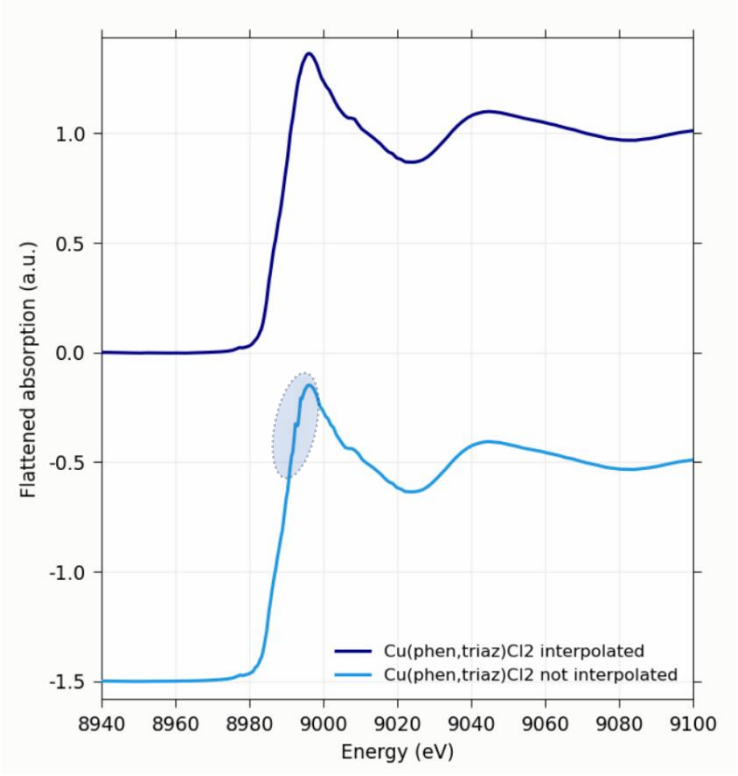

Figure 62 Comparison of the results of interpolation, between the Cu K-edge XAS spectra of Cu(phen,triaz)Cl_2 pellet. With blue marked area indicating the region with disturbed data by monochromator issues

was shown in **Figure 62**, for the obtained XAS spectra for Cu(phen,triaz)Cl_2 pellet, after merging three scans. To remove that problem, simple linear interpolation in the OriginLab program was performed, by choosing one set of the energetic points from the first scan, to which other sets were interpolated. After that, normalization and merging of the corrected spectra gave an XAS spectrum without such fluctuations.

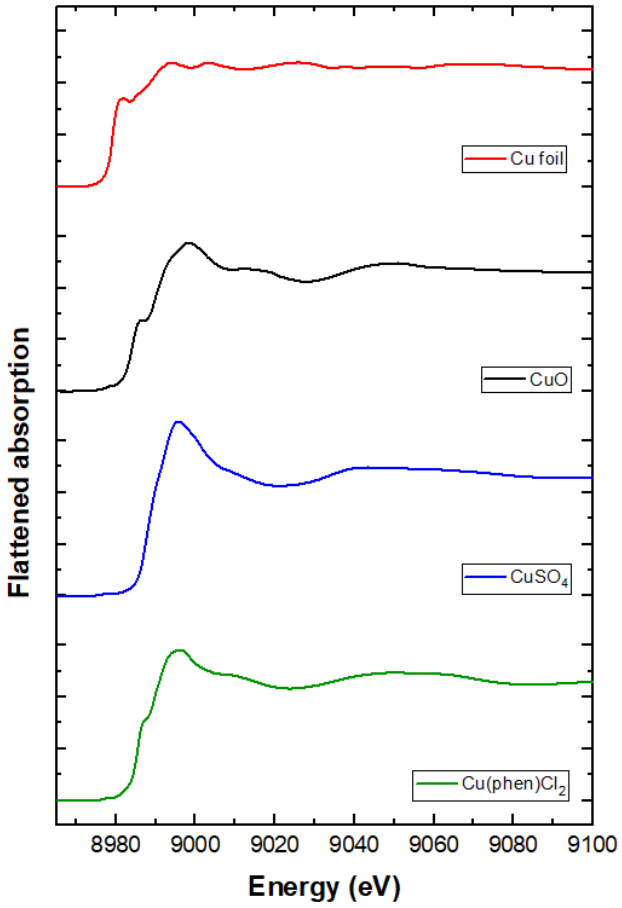

Figure 63 Synchrotron Cu K-edge XAS spectra of copper foil and pellets, containing 5 wt.% of a given copper complex

2.5.3. Results

In **Figure 63**, XAS spectra obtained from the measurements of pellets at the SuperXAS beamline were presented, that contained 5 wt.% of one from the copper(II) compounds, and a copper foil. From the spectrum of copper foil, where copper is the only neighboring element to other copper atoms, and has a Cu^{0+} oxidation state, the absorption edge with a characteristic peak around 8982 eV can be distinguished, and further a double shoulder, instead of one prominent peak. For the spectra of two other references, there can be observed a characteristic white line, confirming the presence of Cu^{2+}. For CuO and Cu(phen)Cl_2 a shoulder in the edge region can be also found, around 8986 eV and 8987 eV respectively. This feature also indicates the presence of Cu^{2+}, since for Cu^{1+}, there would be a peak instead of the shoulder, slightly shifted towards lower energies [27].

The presence of the white line is not the only indicator of the Cu^{2+}. As was mentioned in the previous subchapter, since 3d orbital is non-filled and for all of these complexes the ligands around the metallic center are present, the quadrupole transition from 1s to 3d orbital could be noted, resulting in the creation of the pre-edge peak structure before the absorption edge. For all chosen complexes this structure was observed and presented in **Figure 64**. The position of the center of the pre-edge peak and its intensity

were found to be sensitive to the geometry of the chosen compound [28]. Therefore, to investigate such an effect, the analysis of the pre-edge region for three spectra was performed (**Table 5**).

Table 5 Determined values characteristic for pre-edge peaks of Cu K-edge XAS spectra of copper complexes with the indication of its crystallographic system

Compound	Position of the centroid of the pre-edge peak [eV]	The area under the pre-edge peak	Crystallographic system	Space group
CuO	8978.19 ± 0.03	0.036 ± 0.003	Monoclinic [15]	C2/c
$CuSO_4$	8977.39 ± 0.02	0.037 ± 0.002	Orthorhombic [29]	Pnma
$Cu(phen)Cl_2$	8977.88 ± 0.06	0.035 ± 0.005	Monoclinic [30]	P21/c

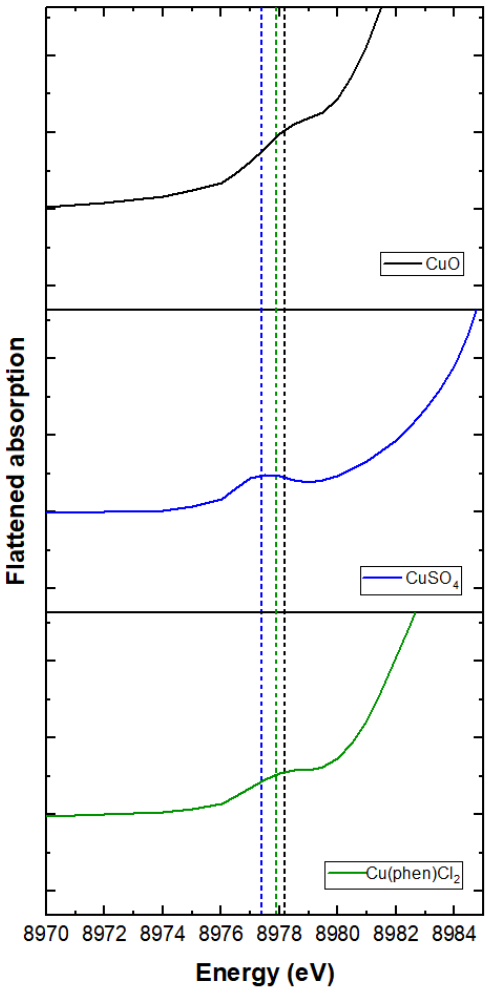

Figure 64 Pre-edge region of the Cu K-edge XAS spectra of copper complexes

By comparing the area under the pre-edge peaks, significant differences cannot be found between the samples, that might indicate the differences in the geometry of complexes. What can be found, are different positions of the center of the peak, in the

following order: $CuSO_4$, $Cu(phen)Cl_2$, and CuO. Additionally, these values seem to be very low. Taking into consideration, that all of the examined compounds have a centrosymmetric geometry, only quadrupole transition contributes to the occurrence of the pre-edge peak. Dipole transition from 1s to hybridized 3d orbital, which could give a significant rise of the intensity, is not observed, since the mixing of 4p-3d orbitals can occur when centrosymmetry is distorted [31]. Therefore, these results support the results from crystallography measurements.

Table 6 Determined values of the energy of the absorption edge for copper samples

Compound	**The energy of the absorption edge [eV]**
CuO	8984.0 ± 0.5
$CuSO_4$	8988.0 ± 0.5
$Cu(phen)Cl_2$	8985.5 ± 0.5

The differences in the energy of the absorption edge were also found (**Table 6**). The lowest value is observed for CuO, then for $Cu(phen)Cl_2$, ending with the value for $CuSO_4$. The order is reversed to this of positions of the centre of the pre-edge peaks.

2.5.4. Verification of XAS results obtained in laboratory conditions

To verify the usability of the laboratory setup to study copper(II) compounds for future chemotherapy purposes, the comparison between laboratory and synchrotron XAS setup was evaluated. The results were also already published in the paper by the author of this thesis [32].

Normalized and flattened for better comparison in the XAS Viewer spectra were exported, and with the OriginLab program, both sets of spectra from the laboratory and synchrotron studies were presented together in **Figure 65**. At first sight, the spectra obtained with the synchrotron source appear to be like a fitting function to the laboratory data, since their features match quite well, yet the first ones are significantly less noisy. In most of the cases, the absorption edge is aligned for both studies, only for the $CuSO_4$ sample there is a slight shift of the spectrum from synchrotron towards higher energies.

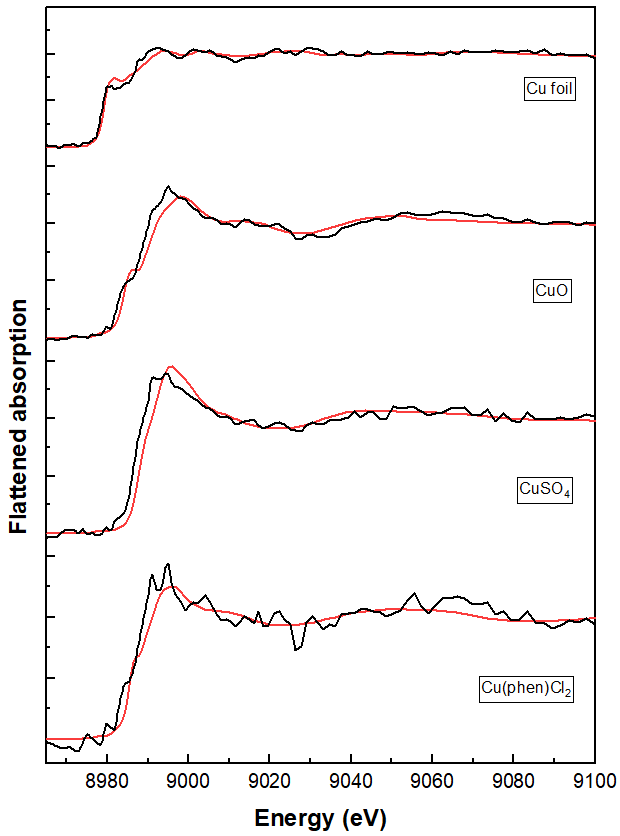

Figure 65 Cu K-edge XAS spectra of copper samples obtained in synchrotron (red) and laboratory (black) conditions

The biggest difference in the quality of spectra can be observed for the $Cu(phen)Cl_2$, which was also the most complex compound examined in this study. This fact did not affect the quality of the XAS spectra for the synchrotron study, while for the laboratory it is quite visible, that the concentration of the copper atoms in this complex is lower, while the proportions of the copper compound with cellulose was constant for all samples. Looking therefore on the concentration factor, since it was determined as a weight concentration, the differences in the copper itself differed between the samples and totals as follows: for CuO it totaled 5.97 mg, $CuSO_4$: 2.99 mg, and for $Cu(phen)Cl_2$: 1.525 mg. If one would like to have the same amount of Cu in each pellet, therefore, when choosing the amount that was in the CuO pellet, the new weight of the compounds would be $CuSO_4$: 29.95 mg, and $Cu(phen)Cl_2$: 58.72 mg. For $Cu(phen)Cl_2$ this mass value is quite high, and since this compound is purchased, the costs of the study would increase. Also for other, more complex hybrid compounds, like $Cu(phen,triaz)Cl_2$ described in Chapter 1, it would be very hard to obtain such high mass after synthesis, to use it even to make only one pellet.

Another significant difference was found in the pre-edge region, where the pre-edge peak can occur, indicating the transition of the electrons from the 1s to 3d hybridized

orbital. This also supports the information about the presence of Cu^{2+}. On laboratory spectra, this feature cannot be distinguished due to the level of the noise, while on synchrotron ones it can be easily found, as it was presented in the previous subchapter.

2.6. Comparison of copper-complexes XAS spectra obtained with different radiation sources

After completing the adjustments of the laboratory setup to study copper(II) samples, the examination of the synthesized Cu(phen,triaz)Cl_2 was started. The spectrum for this compound was significantly noisier than these for referential samples, and the noise much affected even the region of the white line, which is especially important for the determination of the maximum of the first derivative. Because of that, data with the use of the XAS Viewer program was smoothed, choosing the convolution method and the Gaussian function. This operation resulted in the meaningful improvement of the quality of spectra, presented in **Figure 66**, enabling more accurate data analysis and revealing the absorption edge region. After that, to compare the results of studies of this compound with referential samples, the rest of the laboratory spectra were also smoothed accordingly.

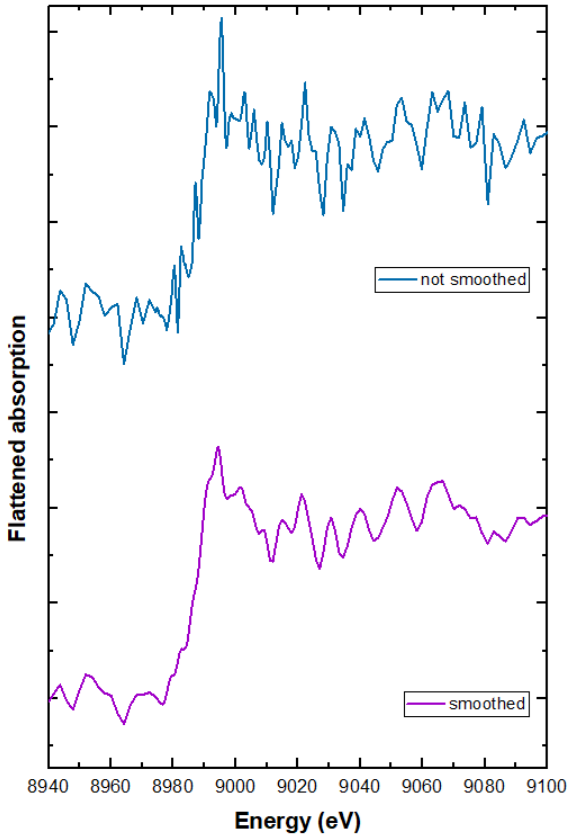

Figure 66 Comparison of the not smoothed and smoothed Cu K-edge XAS spectra of Cu(phen,triaz)Cl_2 5 wt.% pellet

It is already known, that there could be differences between the results of examination of the same samples, with the application of the same (XAS) method, due to different environmental parameters (pressure, atmosphere) or absorbed dose of radiation [33]. Therefore, all data obtained in three synchrotron facilities (DESY, ASTRA, SLS) and the laboratory was compared, which are presented in **Figures 67-71**.

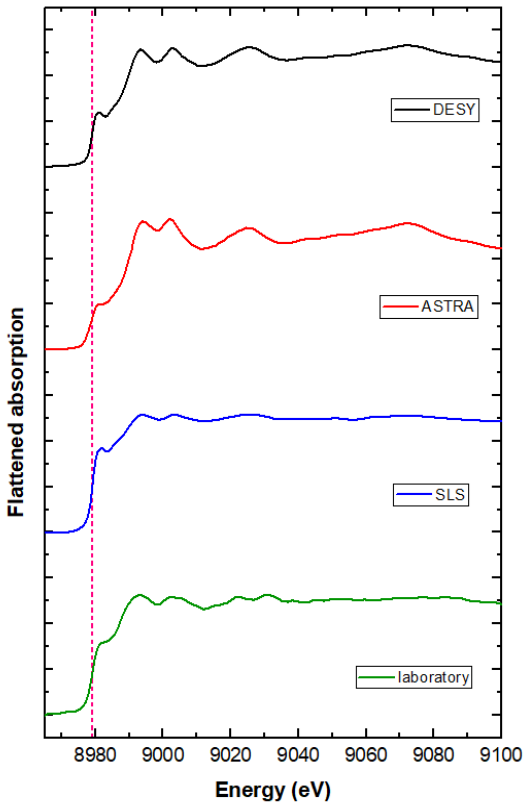

Figure 67 Cu K-edge XAS spectra of Cu foil, with marked with dashed line energy of the absorption edge

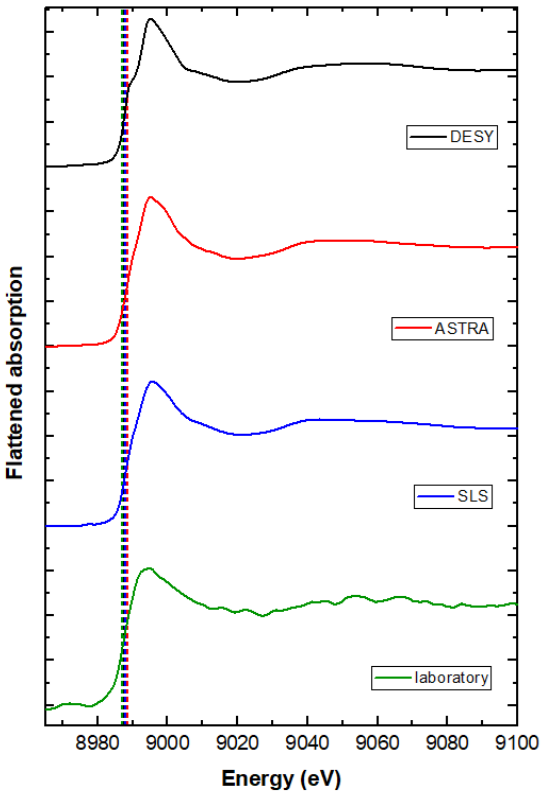

Figure 68 Cu K-edge XAS spectra of $CuSO_4$ pellet, with marked with dashed lines determined energy of the absorption edge for each spectrum

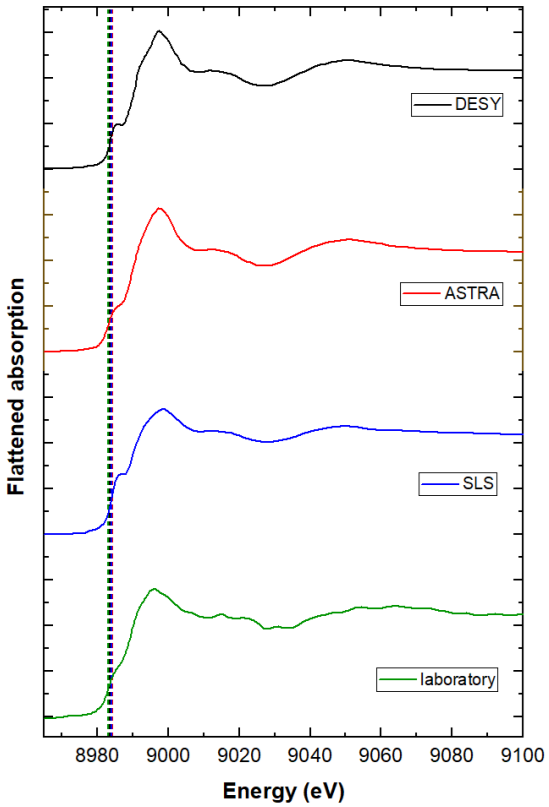

Figure 69 Cu K-edge XAS spectra of CuO pellet, with marked with dashed lines determined energy of the absorption edge for each spectrum

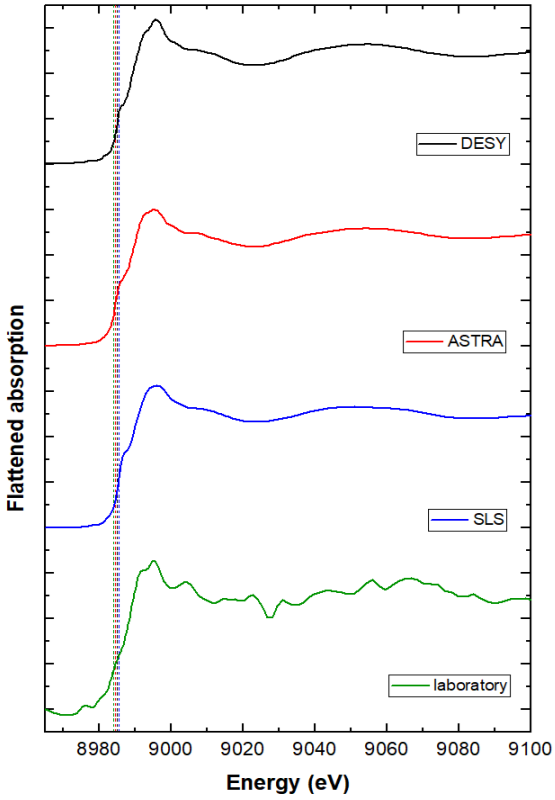

Figure 70 Cu K-edge XAS spectra of $Cu(phen)Cl_2$ pellet, with marked with dashed lines determined energy of the absorption edge for each spectrum

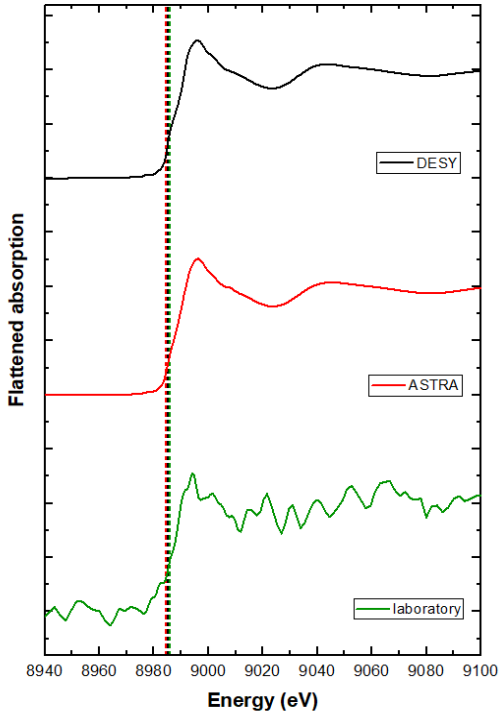

Figure 71 Cu K-edge XAS spectra of $Cu(phen,triaz)Cl_2$ pellet, with marked with dashed lines determined energy of the absorption edge for each spectrum

Starting with the first reference, the spectra of $CuSO_4$ pellets have a prominent white line with a maximum around 8995 eV, and a matching shape of the EXAFS region. In the XANES range some minor differences can be observed - only the spectrum obtained in DESY has a visible shoulder in the edge region around 8989 eV, while the rest have only very slight inflection in this area. The white line is also the narrowest for the result from DESY, while the widest is for the spectrum obtained in laboratory conditions. The results for the second reference - CuO are also very alike. Spectra from all synchrotron beamlines have a visible shoulder in the edge region around 8985 eV, while from the laboratory one, there is only an inflection. White lines in spectra from DESY and ASTRA are narrow and have a higher intensity than results from SLS and laboratory. In the case of the SLS result, since it was acquired in a fluorescence mode, probably self-absorption led to the drop in the intensity of the spectrum.

Spectra from synchrotrons of $Cu(phen)Cl_2$ pellets possess shoulder in the absorption edge region around 8986 eV, and a visible white line, with a maximum around 8995 eV. Spectrum from DESY, has also a slight inflection nearby its maximum. The laboratory spectrum, especially in the EXAFS region, is significantly affected by the noise.

The last was a comparison of results for $Cu(phen,triaz)Cl_2$. The shape of XAS spectra from synchrotrons looks very similar to spectra of $CuSO_4$, but the shoulder in the spectrum for DESY, and inflection in the spectrum from ASTRA, occurs here in a lower energy region, around 8986 eV, so in the same region as for $Cu(phen)Cl_2$. Similarly to the previous copper-phenanthroline complex, EXAFS region is disturbed even more by the occurring noise.

Determined values of the energy of the absorption edge from the first derivative were listed in **Table 7**. Taking into consideration the measurement uncertainty, results from laboratory study match well the values of absorption edge energy obtained in synchrotron facilities (with one exception - $CuSO_4$ ASTRA results). The biggest discrepancy in results can be observed for the compared pair, that is DESY and ASTRA data.

Table 7 Comparison of the obtained energies of the absorption edge for all copper(II) samples, determined from he results of the measurements using different sources of X-rays

	Energy of the absorption edge (eV)			
Radiation source / **Copper(II) compound**	**SLS**	**DESY**	**ASTRA**	**Laboratory X-ray tube**
CuO	8984.0 ± 0.5	8983.5 ± 0.3	8984.2 ± 0.2	8983 ± 1
$CuSO_4$	8988.0 ± 0.5	8987.8 ± 0.3	8988.7 ± 0.2	8987 ± 1
$Cu(phen)Cl_2$	8985.5 ± 0.5	8985.1 ± 0.3	8984.5 ± 0.2	8984 ± 1
$Cu(phen,triaz)Cl_2$		8985.1 ± 0.3	8985.0 ± 0.2	8986 ± 1

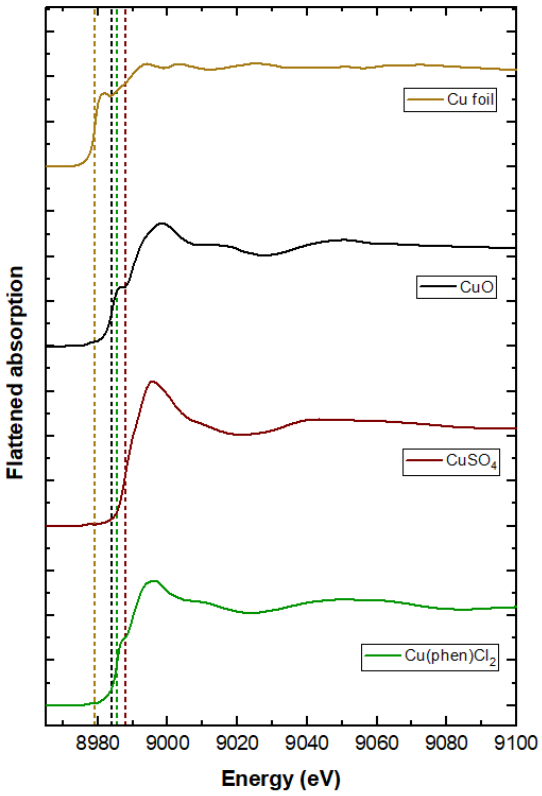

Figure 72 Cu K-edge XAS spectra of chosen copper samples, that were obtained with SLS synchrotron radiation. With dashed lines of colours matching the corresponding spectra, the values of the determined energy of absorption edge were marked

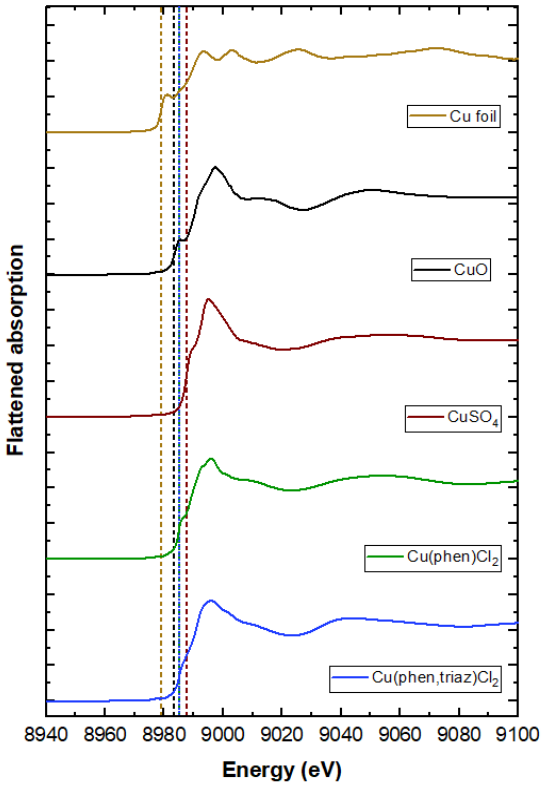

Figure 73 Cu K-edge XAS spectra of chosen copper samples, that were obtained with DESY synchrotron radiation. With dashed lines of colours matching the corresponding spectra, the values of the determined energy of absorption edge were marked

The next step involved the comparison of the chemical shifts of spectra. In **Figures 72-75**, XAS spectra were presented for each study, with marked values of the absorption edge energy. For all of the samples it is visible, that values of this energy are placed in the region of the shoulder or the inflection within the edge region.

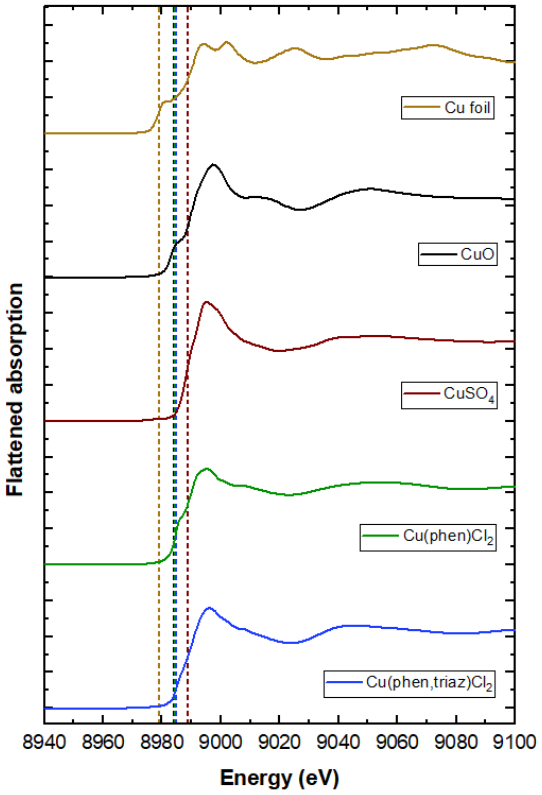

Figure 74 Cu K-edge XAS spectra of chosen copper samples, that were obtained with ASTRA synchrotron radiation. With dashed lines of colours matching the corresponding spectra, the values of the determined energy of absorption edge were marked

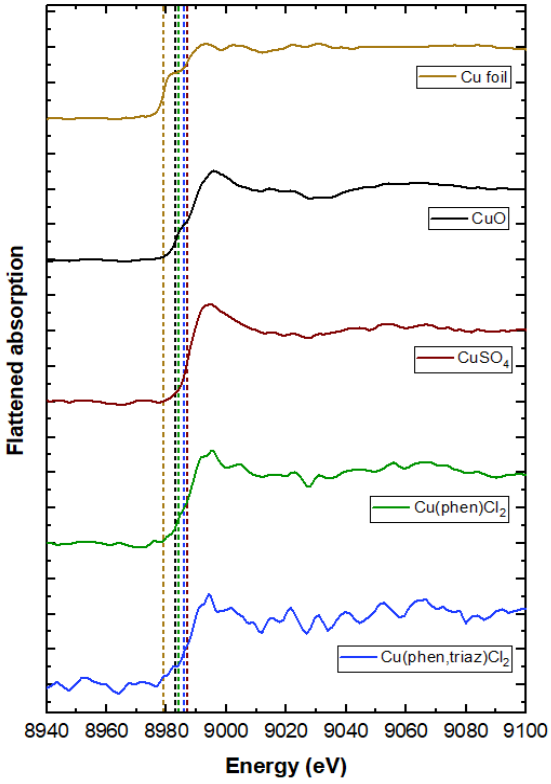

Figure 75 Cu K-edge XAS spectra of chosen copper samples, that were obtained with radiation emitted by the X-ray tube. With dashed lines of colours matching the corresponding spectra, the values of the determined energy of absorption edge were marked

For SLS and DESY results, there is observed the following order of increasing chemical shift in comparison to the copper foil spectrum - CuO: 5 ± 0.5 eV and 4.5 ± 0.3 eV, $Cu(phen)Cl_2$: 6.5 ± 0.5 and 6.1 ± 0.3 eV, ending with $CuSO_4$: 9 ± 0.5 and 8.8 ± 0.3 eV, respectively. Additionally, for the DESY study, the chemical shift of $Cu(phen,triaz)Cl_2$ spectrum, like for other phenanthroline complex, totalled 6.1 ± 0.3 eV. For the ASTRA study, there is a little difference – the closest are both CuO: 5.2 ± 0.2 eV and $Cu(phen)Cl_2$: 5.5 ± 0.2 eV, then $Cu(phen,triaz)Cl_2$: 6 ± 0.2 eV, and as last $CuSO_4$: 9.7 ± 0.2 eV, with the biggest observed shift from all of the obtained results. For the laboratory study obtained results were as follows - CuO: 4 ± 1 eV, $Cu(phen)Cl_2$: 5 ± 1 eV, $Cu(phen,triaz)Cl_2$: 7 ± 1 eV, and $CuSO_4$: 8 ± 1 eV. A significant difference can be observed between the two first samples and $CuSO_4$.

To determine the possible oxidation state of copper in both copper-phenanthroline complexes, values of the absorption edge energy for all of the examined samples were compared and presented in **Figure 76**. It is visible, that these values lie between values for referential CuO and $CuSO_4$ samples, or at least are very close. Since CuO and $CuSO_4$

samples have a known value of the copper's oxidation number, that is 2+, the obtained results confirm the presence of Cu^{2+} also in both complexes of interest.

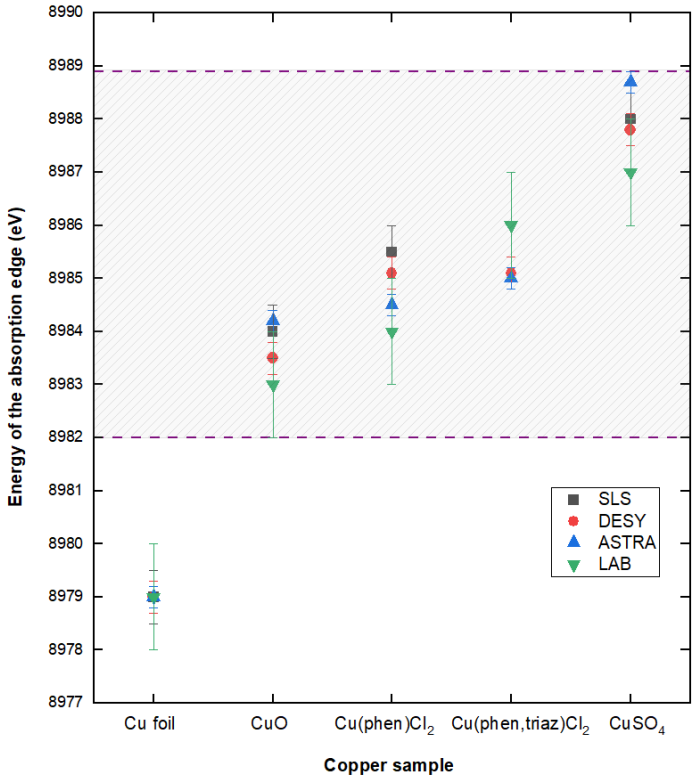

Figure 76 Comparison of the values of energy of the absorption edge for different copper samples and used radiation sources. With the hatched area the region of the values for Cu^{2+} compounds was marked

To supplement the above results, analysis of the pre-edge peak for data from the DESY study was performed, since the obtained spectra possessed the most distinguished features from all gathered sets of synchrotron data (**Table 8, Figure 73**). It was expected to obtain also the small value of the intensity of the pre-edge peak for Cu(phen,triaz)Cl_2, like in the analysis of the rest compounds from the Subchapter 2.5.3., since the synthesized compound is also centrosymmetric, and only quadrupole transition can undergo.

Table 8 Determined values of parameters characteristic for pre-edge peaks of XAS spectra of copper complexes with the indication of its crystallographic system

Compound	Position of the centroid of the pre-edge peak [eV]	The area under the pre-edge peak [a.u.]	Crystallographic system	Space group
CuO	8977.70 ± 0.10	0.016 ± 0.003	Monoclinic [15]	C2/c
$CuSO_4$	8976.88 ± 0.04	0.018 ± 0.001	Orthorhombic [29]	Pnma
Cu(phen)Cl_2	8977.30 ± 0.10	0.015 ± 0.002	Monoclinic [30]	P21/c
Cu(phen,triaz)Cl_2	8977.30 ± 0.10	0.011 ± 0.003	Monoclinic [34]	P21/n

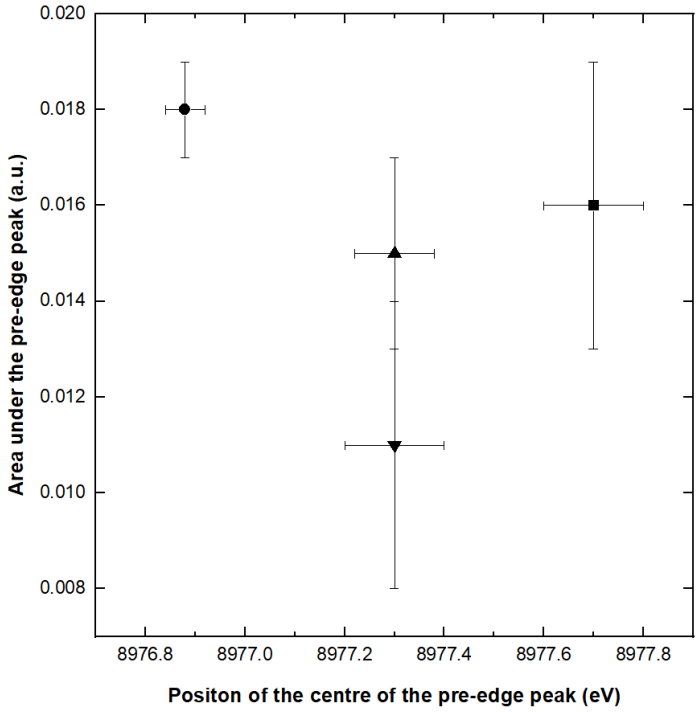

Figure 77 Position of the center of pre-edge peaks in a function of their area under peak

As it was presented in **Figure 77**, from the position of the pre-edge peak's center, the copper phenanthroline samples can be distinguished from the $CuSO_4$ and CuO samples, yet not one from another. The shift of the pre-edge peak maximum is in the opposite manner to the chemical shift of the absorption edge, because for $CuSO_4$ reaches the lowest and for CuO the highest value of energy. It is hard to find any significant differences in the area under the peak, since after taking into consideration the uncertainties of the analysis, it cannot be said that there are meaningful differences caused by different geometry, affecting this parameter.

However, the geometry is in fact not that different, since all of the compounds are centrosymmetric, three of them crystalize to a monoclinic system, and the coordination number for copper in most of them, apart from triazole complex where it totals 5, is 4. Therefore, also this analysis confirms results from crystallographic measurements.

2.7. Discussion

All of the referential materials and copper-phenanthroline synthesized complex were measured with two types of X-ray radiation sources – an X-ray tube and a synchrotron. Laboratory XAS setup operation was optimized, with adjustments of the parameters of data acquisition. It was found, that the optimal acquisition time is 8 hours per sample, the concentration of the compound should total around 5 wt.% in a pellet, and measurement of

the I_0 signal is best performed by registering the signal transmitted through a pure cellulose pellet.

Yet, the problems occur when measuring the more complex compounds, like organic copper-phenanthroline ones. While other referential compounds can be easily measured in a concentration of 5 wt.%, for a compound with triazole, it was found that the signal was observably less intensive and spectrum noisier. Due to the limited accessible amount of this copper-phenanthroline compound, the other possible way was not to change the concentration of it in a pellet, but to add an additional step of data analysis, which was smoothing the spectrum. It resulted in the originating of the edge and a white line on the spectrum.

Comparison of the spectra obtained in laboratory and synchrotron conditions led to the conclusion, that laboratory XAS setup can be used to great effect to obtain satisfactory in quality spectra for preliminary analysis of solid samples. However, for a more detailed analysis, it would be worth to transfer the studies to synchrotron facilities. By this approach, not only the time for data acquisition will be significantly shorter, but also very low-intensive features, like pre-edge peaks, could be observed. Nevertheless, due to the common overbooking of the beamlines, long waiting time to perform examination, and limitation of samples that can be taken with experimenters, it is very convenient to have own XAS setup. Not only test measurements could be performed, which could give first information concerning the electronic structure of new materials, but also many elements of the setup, like holders or cells, could be checked. Experimenters can also verify the stability of the samples in planned experimental conditions, that could be subjected to a photoreduction process or another type of radiation damage.

Another raised subject was a comparison of the spectra acquired in synchrotron facilities, to verify whether the slight differences between beamlines affect the shape or quality of XAS data. Happily, additional peaks or significant shifts of the absorption edge energy were not found, which could indicate the undergoing photoreduction or significant radiation damage. In fact, most of the data stand in agreement, including the values from laboratory examination.

Three possible approaches to determine the energy of the absorption edge were tested. It was found that choosing the maximum of the first derivative or a point passing zero in the second derivative around the edge region, gives exact and reliable values. However, choosing the point in the energy range that stands in the middle of the edge, seems to give misleading values. Therefore, the first approach was chosen to be used in further data analysis.

Additionally, the analysis of the pre-edge peaks was undertaken. It provided information about the undergoing quadrupole transition of electrons from 1s to 3d orbital, and missing dipole transition from 1s to 4p-3d hybridized orbital, what proves that all of the studied compounds possess a centrosymmetric geometry. The presence of this small peak and comparison of the energies of the absorption edge for copper-phenanthroline complexes and other copper compounds also confirmed the presence of Cu^{2+} in all samples.

Summing all the above up, the goals 2-4 were achieved, and moving to examination of liquid samples could start.

2.8. Materials and used programs

1) **Chemicals:**
   a) Copper foil – Goodfellow Cambridge Limited, cat. nr: LS397006, thickness: 0.01mm, purity: 99.9%, CAS: 7440-50-8
   b) Copper(II) oxide (CuO) – Sigma-Aldrich, cat. nr: 544868-5G, nanopowder with particles diameter < 50 nm, CAS: 1317-38-0
   c) Copper(II) sulfate ($CuSO_4$) – Fluka™, Honeywell, cat. nr: 12852-250G, CAS: 1317-38-0
   d) Dichloro(1,10-phenanthroline) copper(II) (Cu(1,10-phenanthroline)Cl_2) – Sigma-Aldrich, 98%, cat. nr: 362204-1G, CAS: 14783-09-6
   e) Dichloro-(1,10-phenanthroline)-(1H-1,2,4-triazole-1-yl)-copper(II) monohydrate (Cu(1,10-phenanthroline)-(1H-1,2,4-triazole-1-yl)$Cl_2 \cdot H_2O$) – synthesized
   f) Cellulose $(C_6H_{10}O_5)_n$ – Sigma-Aldrich, cat. nr: 310697-500G, microcrystalline powder, particles diameter: 20 μm, CAS: 9004-34-6
2) **Programs for data acquisition in laboratory conditions:**
   a) Andor SOLIS 64-bit for Imaging: X-0000 – dedicated to the detector operation
   b) X-BEAM Utility Version 0.92 – dedicated to the X-ray tube operation
   c) XILab 1.17.19 – dedicated to the operation of the motors
   d) Wolfram Mathematica 12.3 – dedicated to the visualization of the detector-registered signal
3) **Programs used for data analysis:**
   a) XAS Viewer [35] – program from the Larch package, developed by Matthew Newville, which is based on the commonly known Athena program [36], used for data analysis of XAS data. It was written in a Python programming language and has a public license.
   b) OriginLab 2021

2.9. Bibliography

[1] Hirayama, Hideo. "Lecture note on photon interactions and cross sections." *KEK, High Energy Accelerator Research Organization*, Oho, Tsukuba, Ibaraki, Japan (2000).

[2] Nilsson, Anders, et al. "Catalysis in real time using X-ray lasers." *Chemical Physics Letters* 675 (2017): 145-173.

[3] Willmott, Philip. An introduction to synchrotron radiation: techniques and applications. John Wiley & Sons, (2019).

[4] Bunker, Grant. "Introduction to XAFS: a practical guide to X-ray absorption fine structure spectroscopy." *Cambridge University Press*, (2010).

[5] Stańczyk, Wiktoria, and Joanna Czapla-Masztafiak. "The use of the X-ray absorption spectroscopy laboratory setup in the examination of copper (II) compounds for biomedical applications." *Nuclear Instruments and Methods in Physics Research Section B: Beam Interactions with Materials and Atoms* 497 (2021): 65-69.

[6] Błachucki, Wojciech, et al. "A laboratory-based double X-ray spectrometer for simultaneous X-ray emission and X-ray absorption studies." *Journal of Analytical Atomic Spectrometry* 34.7 (2019): 1409-1415.

[7] Huang, Juanjuan, et al. "Simultaneous two-color X-ray absorption spectroscopy using Laue crystals at an inverse-compton scattering X-ray facility." *Journal of Synchrotron Radiation* 28.6 (2021): 1874-1880.

[8] Mobilio, Settimio, Federico Boscherini, and Carlo Meneghini. “Synchrotron Radiation.” *Springer-Verlag Berlin An* (2016).

[9] Newville, Matthew. "Fundamentals of XAFS." *Reviews in Mineralogy and Geochemistry* 78.1 (2014): 33-74.

[10] Parratt, L. G., C. F. Hempstead, and E. L. Jossem. " " Thickness Effect" in Absorption Spectra near Absorption Edges." *Physical Review* 105.4 (1957): 1228.

[11] Trevorah, Ryan M., Christopher T. Chantler, and Martin J. Schalken. "Solving self-absorption in fluorescence." *IUCrJ* 6.4 (2019): 586-602.

[12] Carboni, Roberta, et al. "Self-absorption correction strategy for fluorescence-yield soft X-ray near edge spectra." *Physica Scripta* 2005.T115 (2005): 986.

[13] De Groot, Frank, György Vankó, and Pieter Glatzel. "The 1s x-ray absorption pre-edge structures in transition metal oxides." *Journal of Physics: Condensed Matter* 21.10 (2009): 104207.

[14] Honkanen, Ari-Pekka, et al. "Johann-type laboratory-scale x-ray absorption spectrometer with versatile detection modes." *Review of Scientific Instruments* 90.3 (2019).

[15] Ching, W. Y., Yong-Nian Xu, and K. W. Wong. "Ground-state and optical properties of Cu_2O and CuO crystals." *Physical Review B* 40.11 (1989): 7684.

[16] Fanselow, Rafał, et al. "Performance of a laboratory von Hámos type x-ray spectrometer in x-ray absorption spectroscopy study on 3d group metals." *X-Ray Spectrometry* (2022).

[17] https://www.esrf.fr/home/UsersAndScience/Experiments/EMD/ID26/Characteristics.html (accessed: 11.01.2024)

[18] https://www.psi.ch/en (accessed: 11.01.2024)

[19] https://www.psi.ch/en/sls/superxas/optics-0 (accessed: 11.01.2024)

[20] https://www.psi.ch/en/sls/superxas/optics-0 (accessed: 11.01.2024)

[21] https://petra4.desy.de/index_eng.html (accessed: 11.01.2024)

[22] https://photon-science.desy.de/facilities/petra_iii/index_eng.html (accessed: 11.01.2024)

[23] Szlachetko, Jakub, et al. "SOLARIS national synchrotron radiation centre in Krakow, Poland." *The European Physical Journal Plus* 138.1 (2023): 1-10.

[24] https://www.esrf.fr/id26 (accessed: 11.01.2024)

[25] XAS spectra database, that is available at: https://xaslib.xrayabsorption.org/elem/Cu/

[26] Parratt, L. G., C. F. Hempstead, and E. L. Jossem. "" Thickness Effect" in Absorption Spectra near Absorption Edges." *Physical Review* 105.4 (1957): 1228.

[27] Gaur, A., B. D. Shrivastava, and S. K. Joshi. "Copper K-edge XANES of Cu (I) and Cu (II) oxide mixtures." *Journal of Physics: Conference Series*. Vol. 190. No. 1. IOP Publishing, 2009.

[28] Shimizu, Ken-ichi, et al. "Ligand field effect on the chemical shift in XANES spectra of Cu (II) compounds." *Physical Chemistry Chemical Physics* 3.5 (2001): 862-866.

[29] Kokkoros, P. A., and P. J. Rentzeperis. "The crystal structure of the anhydrous sulphates of copper and zinc." *Acta Crystallographica* 11.5 (1958): 361-364.

[30] Liu, Y-Q. "Dichlorido (1, 10-phenanthroline) copper (II)." *Acta Crystallographica Section E: Structure Reports Online* 63.12 (2007): m2991-m2991.

[31] Kroll, Thomas, et al. "Effect of 3d/4p Mixing on 1s2p Resonant Inelastic X-ray Scattering: Electronic Structure of Oxo-Bridged Iron Dimers." *Journal of the American Chemical Society* 143.12 (2021): 4569-4584.

[32] Stańczyk, Wiktoria I., et al. "Comparison between laboratory and synchrotron X-ray absorption spectroscopy setup examination of Cu (II) complexes with prospective anticancer properties." *Nuclear Instruments and Methods in Physics Research Section B: Beam Interactions with Materials and Atoms* 543 (2023): 165100.

[33] Van Schooneveld, M. M., and S. DeBeer. "A close look at dose: Toward L-edge XAS spectral uniformity, dose quantification and prediction of metal ion photoreduction." *Journal of Electron Spectroscopy and Related Phenomena* 198 (2015): 31-56.

[34] Tabassum, Sartaj, et al. "Synthesis and characterization of copper (II) and zinc (II)-based potential chemotherapeutic compounds: their biological evaluation viz. DNA binding profile, cleavage and antimicrobial activity." *European Journal of Medicinal Chemistry* 58 (2012): 308-316.

[35] Newville, Matthew. "Larch: an analysis package for XAFS and related spectroscopies." *Journal of Physics: Conference Series*. Vol. 430. No. 1. IOP Publishing (2013).

[36] Ravel, Bruce, and Matthew Newville. "ATHENA, ARTEMIS, HEPHAESTUS: data analysis for X-ray absorption spectroscopy using IFEFFIT." *Journal of Synchrotron Radiation* 12.4 (2005): 537-541.

Chapter 3

BioXAS

3.1. Studies of interactions of metal complexes with biomolecules

With the aim to design a drug that will target cancer cells, there is a need to study its possible interactions with the biomolecules, which will decide on its cytotoxicity. Taking cisplatin as an example, this compound binds covalently to nucleotides, what results in the creation of the stable complex, where cisplatin handicaps DNA replication and transcription processes [1]. There are also compounds, including copper-phenanthroline ones, which interact noncovalently with DNA by fitting inside the groove, blocking access for DNA polymerase [2]. Such interactions can stop cells' division, since without replication mitosis cannot undergo. Therefore, while designing a new prospective chemotherapeutics, aiming to target DNA molecules, these interactions need to be studied.

The first widely used method of such investigation is UV-Vis absorption spectroscopy. With this method, absorption spectra of DNA or a drug alone are gathered and compared with the spectrum where these two are combined in one sample, enabling their interaction. In the case of focusing on the prospective drug, solutions of this compound in fixed concentration with increasing concentration of the DNA can be prepared. By comparing changes in the intensity of the spectrum of the drug alone and after the addition of DNA, one can determine the mode of the interaction. For intercalation, where the complex fits between two adjacent pairs of nucleotides in double-stranded DNA, the decrease in the intensity of the chosen band can be observed (hypochromism) and the shift of its maximum towards higher wavelengths (bathochromism) [3]. In contrast, for a groove binding, the increase in the intensity of the visible band might be observed (hyperchromism) [4].

Another commonly applied method of interaction investigation is fluorescence emission spectroscopy measurements, especially affected by occurring quenching processes. For complexes possessing aromatic groups, there can be registered a fluorescent signal from their deexcitation, which is significantly higher than that emitted by DNA [3]. While fixing the concentration of the examined compound and increasing amounts of DNA in a liquid solution, there can be distinguished modes of their interaction, basing on the changes in the intensity of the fluorescence. For intercalation, the increase in the fluorescence signal is observed, since the position of the complex within the DNA

molecule enhances this mode of deexcitation, while for free compound undergoes a quenching process, affected by rotation [4]. For groove binding, a decrease in the fluorescence can be observed.

All the above methods focus on the examination of interactions between DNA and a given prospective drug in specially prepared solutions, optimized for these studies in terms of chosen solvent, pH, etc. Yet in real body conditions, before the drug will even have an opportunity to bind to DNA complex, it probably would interact with the components of blood first, to which might be introduced. In blood, there are many proteins, especially human serum albumin, which is responsible for the transportation of many drugs. Therefore, when studying a new prospective chemotherapeutic drug, it seems reasonable to examine its possible interaction with this protein [5]. In many studies, instead of the human serum albumin, a bovine serum albumin (BSA) is used, since it is cheaper and structurally alike [6]. Also, for studies involving albumins, both fluorescence emission and UV-ViS absorption spectroscopies can be applied.

Starting with the first mentioned method, the quenching effect in fluorescence emission spectroscopy is investigated, but this time focusing on the detection of the signal from the BSA molecule, while increasing the concentration of the drug. In this case the fluorescence signal from biomolecule is preferred, since BSA possesses some amino acids, especially tryptophan, that are known to be fluorophores. For interactions between compound and BSA, there can be observed a decrease in the fluorescence, being an implication of the BSA-drug conjugate creation [5]. For UV-Vis spectroscopy studies, also the absorption spectra for BSA are being gathered while changing the concentration of the studied compound. There can be seen a hyperchromism effect, suggesting the interaction between BSA and prospective drug, e.g. by electrostatic interaction [7]. With a comparison of the bands with absorption spectra of the given amino acid present in the protein structure, with which it could interact, one can determine the possible site of the drug's docking [8].

Apart from the two mentioned experimental methods for drug-biomolecule interaction investigation, also others can be applied, including FTIR spectroscopy, circular dichroism, or cyclic voltammetry studies. All these methods have specifications from the sample preparation point of view, including the state of matter of the sample, its volume, or suitable solvents. Therefore the same compound in different environmental conditions will be hard to be studied with only one of these methods.

Yet, there is a method that might provide not only information about the presence of drug-biomolecule interactions, but also enable examination of many types of samples

(both solids or liquids) and provides flexibility concerning applied temperature, used solvents, pressure, or even a stage of the given physical/chemical reaction. Additionally, it can probe the environment around a specific atom and changes of its oxidation state while undergoing redox reactions. And this method was already mentioned – X-ray Absorption Spectroscopy, which was chosen to investigate the copper-phenanthroline complexes structure and possible interactions with two biomolecules - bovine genomic DNA and bovine serum albumin.

3.2. XAS examination of biological samples - BioXAS

Growth in the application of the X-ray Absorption Spectroscopy to study biological samples resulted in the creation of a separate term for such type of studies – BioXAS. One of the deeply investigated group of samples are metalloproteins. Especially, since the XAS is sensitive to the changes in the oxidation state of the chosen element, it is widely used in structural biology studies on enzymes involved in catalytic reactions [9]. Another important application, is an examination of metal-containing drugs, including chemotherapeutics. For example, there are reports about new platinum-based complexes' behavior in aqueous solutions, to determine the mechanism of their cytotoxicity and stability in different conditions [10].

Biological samples are usually more complex than pure solids, since they might consist of different compartments. In the case of cells or tissues, they have a mix of biomolecules, like DNA or proteins, covered in water-containing substance (cytosol). For structural studies on one biomolecule at a time, like enzymes, an aqueous solution containing the chosen complex might be prepared. In drug discovery research, many developed compounds hardly dissolve in water, giving as a result very diluted solutions [11]. In such samples, probed element may occur in a low concentration, limiting the strength of the XAS signal. Therefore, for BioXAS studies, some improvements in the experimental setup need to be implemented.

The first adjustment is to focus on the fluorescence signal registration, since the detected radiation would come mostly from the element of interest, which constitutes only a small part of the sample. Another implementation is to optimize the beam flux and measurement time, which can be tested after starting with the minimum possible time and lower flux than available, which can be gradually increased until any changes indicating radiation damage on the XAS spectrum start to be identified [12]. Yet the flux, due to the low concentration of element, might need to be higher for diluted samples than applied for

more concentrated ones to obtain satisfactory XAS spectra. For some studies, to decrease the measurement's time, the applied energy range narrows to only the XANES region, since EXAFS' signal-to-noise ratio value often is not enough for proper analysis, or the needed information can be determined from the XANES region only.

The other aspect of planning a BioXAS study is to take into consideration undesirable effects that can occur after irradiation of biological samples. X-ray radiation is known to ionize matter, not only by inducing the ejection of electrons after its absorption, but also indirectly, via interactions of these electrons with other molecules. In aqueous solutions, there can be observed a process of radio-hydrolysis, where water molecules absorb photons, what leads to the creation of so-called hydrated electrons (e^-_{hydr}) and free radicals [12] (**Equations 38-39**):

$$H_2O \rightarrow e^-_{hydr} + H_2O^+ \quad (38)$$

$$H_2O + H_2O^+ \rightarrow OH^\circ + H_3O^+ \quad (39)$$

Production of other reactive species, like H_2O_2, can be also observed. These electrons, ions, and free radicals can then react with all present molecules in a sample, leading to the secondary ionization of the examined matter. The ionization by the reactive species and electrons can even occur faster than the ejection of electrons, being an outcome of an X-ray absorption [13]. A result especially affecting the XAS examination is a process of photoreduction of metallic center in a given complex, which will give a misleading change in the XAS spectrum [12]. Other meaningful processes are heat dissipation or bond breaking [14].

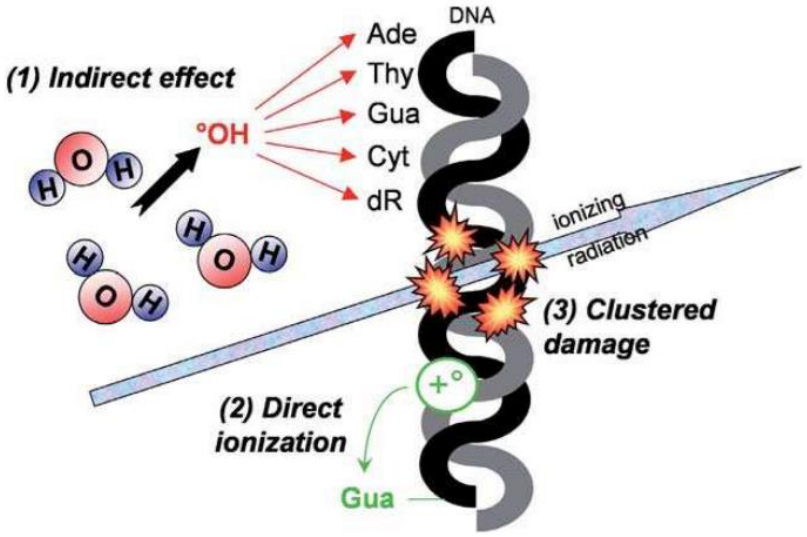

Figure 78 Damaging processes of the DNA structure after irradiation [15]

Apart from the photoreduction of the examined compound, there is a possibility that the chosen biomolecule will undergo radiation damage (**Figure 78**). From the mentioned ions and radicals, hydroxyl radical was found to intensively interact with DNA, causing lesions, even more than direct ionization caused by radiation [15]. Therefore, not only investigated complex should be protected from destruction during studies involving X-ray irradiation, but also the solvent and given biomolecule.

To prevent such situations, some applications are being commonly implemented. The first is cooling the samples to very low temperatures (cryocooling), to reduce the mobility of hydrated electrons and radicals. However, to protect the sample from damage caused by freezing, some additional substances might be added, like glycerol [16]. Another widely known possibility is to develop a setup in which the liquid will be in constant movement [12, 17]. It can be done by designing a special cell, where the beam will hit the closed in it sample, or a liquid-jet setup, where the liquid escapes from the closed parts for a moment for measurements [18]. Such an application significantly reduces the time of irradiation of the given volume, since every time X-rays incident on a fresh portion of liquid being in a movement. Another implemented solutions are closing a beam shutter to remove unnecessary exposure to radiation in a moment when the measurements are not ongoing, or to enlarge the diameter of an incident beam, to reduce the dose absorbed by a given volume [12].

Why the above effects are important for the described in this thesis study, is that if the given biomolecule's structure was destroyed by the X-rays, the interaction of the prospective drug with it, probed by XAS, could be interrupted. On the other hand, if the mentioned photoreduction process of the studied drug occurred, the analyzed differences of spectra between the samples incubated with and without a given biomolecule might give a biased result, where it would be hard to decide whether the reduction was caused by the generated in the solvent free radicals or was it an outcome of the direct X-ray ionization. Therefore, one decided to focus on developing a liquid delivery setup to measure aqueous solutions of both copper-phenanthroline complexes with and without the chosen biomolecule, when the sample will be in a constant flow. The reason for not choosing the cooling the sample is that the interactions of the biomolecules with complexes would be stopped during the experiment, since the movement of molecules will be significantly slowed, and also there might be a change in the spatial conformation of any compound-biomolecule conjugate as a result of freezing. Closing a shutter before and after measurement was also applied.

3.3. Development of the setup for the delivery of liquids

Three different types of setups for the delivery of liquids for XAS examination were tested. The first one was tested during an internship at the ID26 beamline of the ESRF synchrotron, and to this setup, some minor yet important changes were applied. To reduce the minimum amount of liquid needed to fill the whole setup while circulation, the primary setup had to be slightly modified. It was proposed to choose the funnel as a container, what resulted in a reduction of the length and number of setup elements, in comparison to those that were used at the beamline (**Figures 79-80**). As a result, the sample was first injected into the pipe connected to the magnetic pump, to fill the clutch. This pipe was then connected via a connector to the pipe connected to the funnel, to close this part. The rest of the liquid was simply introduced to the funnel. Then the pump was turned on and the circulation started. The pipe connected to the output of the pump transferred the liquid to the glass capillary, from which the liquid left the closed part of the setup, enabling hitting the X-rays only the sample itself. Then the solution was dropping into the plastic funnel, connected to the pipe entering the magnetic pump. The only part when the solution was outside the setup, was the moment of flowing from the capillary and entering the slot of the funnel.

Figure 79 Photography of the simple liquid delivery setup, that was tested before the experiment

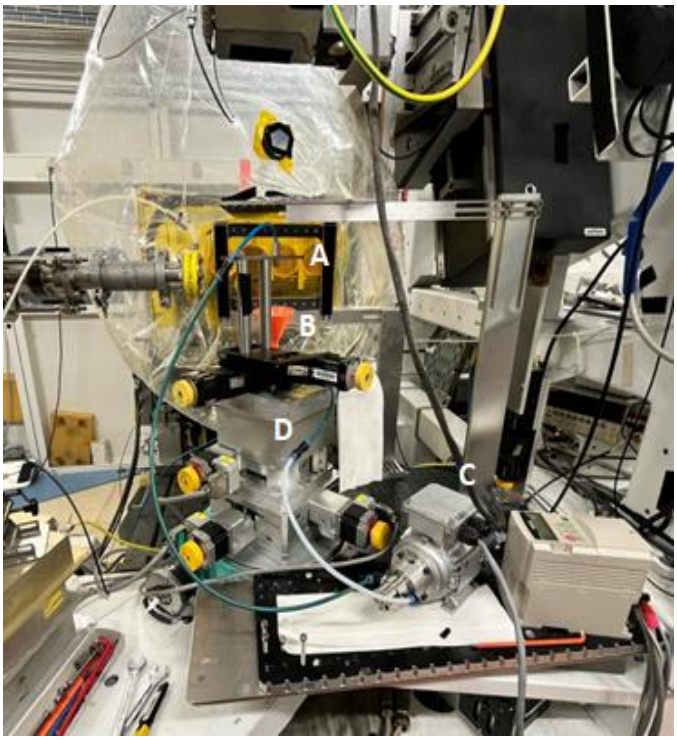

Figure 80 Liquid delivery setup mounted on the experimental table of the ID26 ESRF beamline. With letters were marked: A- glass capillary, B- funnel, C- magnetic pump, D – connector with pipes

This one part of the setup, when the liquid was escaping from the capillary and flowing to the funnel, was found to be the crucial problem that was met while running testing XAS measurements. Since the solution was exposed to the air at that very moment, it also was evaporating. After around 3 hours, a few milliliters of the liquid were lost due to that effect. It also led to the creation of air bubbles and breaks in the constant flow, because the whole setup was not filled fully with the solution anymore. Taking this into consideration, there was a need to develop a new setup for a liquid delivery, which would diminish the contact of liquid with air to the possible minimum.

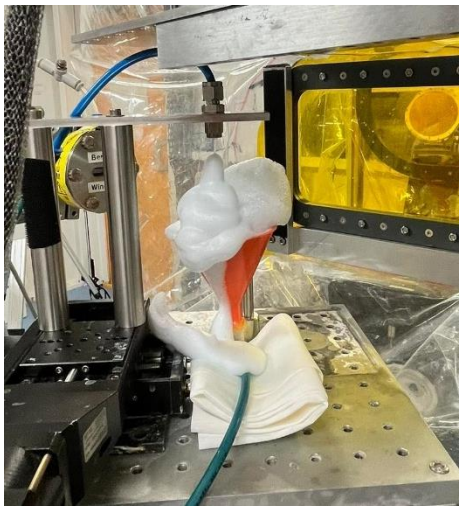

Figure 81 Created foam made from albumin as a result of the aerification

The other problem that was found, was the effect of aeration of the sample, in which albumin was added, to study the interaction of the copper(II) complexes with this protein. As a result, the creation of the stiff foam, like a meringue from the whites of an egg in the kitchen, was observed (**Figure 81**). It led to the loss of the XAS signal when the foam covered the capillary and eclipsed the liquid. Because of that, it was concluded that such an open part of the setup should be eliminated in the case of albumin-containing samples, to prevent such a problematic

situation in the future.

Therefore for further studies, it was decided to focus on testing other setups. The first one was provided by the P65 beamline from the DESY synchrotron, during the obtained beamtime. The biggest difference to the previous setup was the application of the liquid cell, through which the sample was passing. The window was made as a round opening in the cell covered with Kapton foil, through which the X-rays were transmitted to the detector (**Figure 82**).

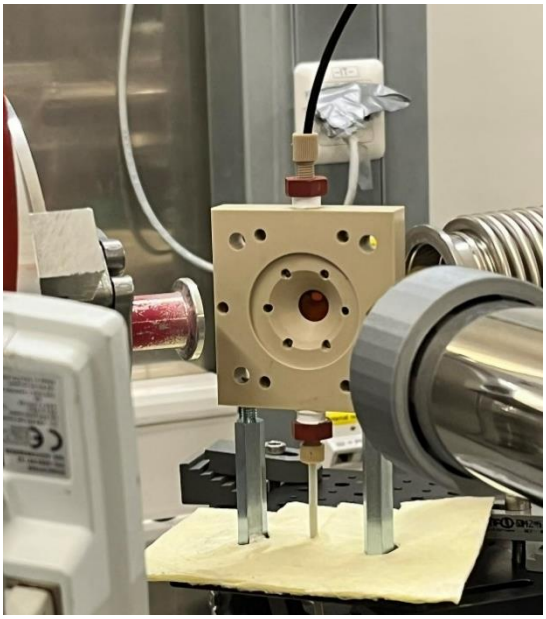

Figure 82 Liquid cell for experiments with the circulating sample

Since for the diluted samples, the preferred mode of data acquisition is a fluorescence mode, the cell was rotated 45 degrees to the direction of the beam and the detector position, as required (**Figure 83**).

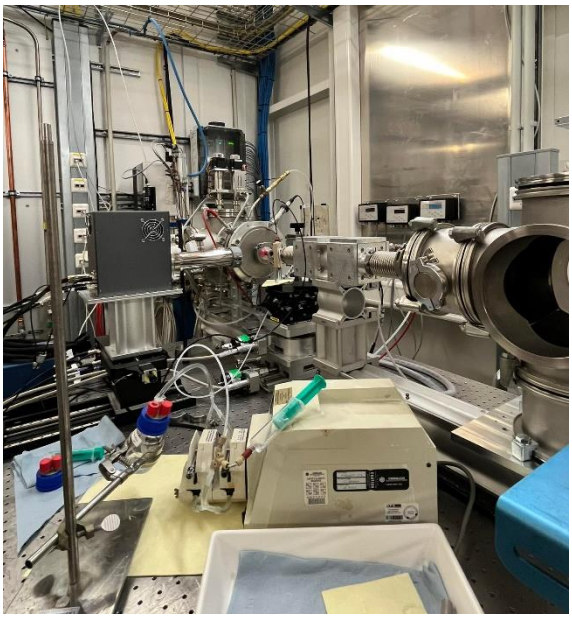

Figure 83 Liquid delivery setup mounted on the P65 beamline of DESY synchrotron

To provide the liquid into the setup, one pipe was taking the sample from the closed container, and the second one was collecting it from the rest of the setup. With the usage of the container, the liquid was not evaporating that much, what led to the situation where this effect was no longer creating any problem and not affecting the acquisition time. Yet, still, some obstacles were identified. Firstly, because there was only one cell available and each sample was passing through it, there was a need to wash the whole setup with a significant amount of water to remove the residues.

Taking into consideration experiences with the above setups, a new type of liquid delivery setup was designed at the IFJ PAN and tested in the ASTRA beamline of the SOLARIS synchrotron during the obtained beamtime. Since the beamline operates without the hatch, there was a need to provide the constant flow of the liquid, with a part of the sample that was irradiated placed inside the closed chamber. As a result, the cell was designed, which was rotated 45 degrees from the origin position, to operate the measurements in the fluorescence and transmission mode at the same time. Since there was not enough space and pipes needed to have an external diameter of the classic tubes for HPLC measurements (around 3.2 mm) the magnetic pump was switched to the small and easily transferable peristaltic pump. To provide a sample to the setup, liquid was poured into the plastic part of the syringe, to which the end of the tube was connected. Then the other end was connected to the cell closed in the chamber, and another pipe was collecting the liquid and pouring it into the syringe (**Figures 84-85**).

Figure 84 Part of the liquid delivery setup, with presented container from the part of syringe, and little peristaltic pump controlled by the microcontroler

Figure 85 Liquid delivery setup, which was mounted on the ASTRA beamline of SOLARIS

3.4. BioXAS examination of copper(II) compounds interactions with biomolecules

3.4.1. Data acquisition and analysis

Due to the fact, that the planned concentration of the copper complex in solution was 4 mM, so very diluted, it was decided to focus only on the fluorescence mode of XAS data acquisition in synchrotron centers. In laboratory setup, this mode is unavailable, since the applied X-ray source is polychromatic and a monochromator is not available. Additionally, the minimum concentration that might be measured in the laboratory was estimated to be 200 mM [19], so 50 times higher than was planned. Therefore, all experiments with copper-phenanthroline compounds with biomolecules were performed with the use of the synchrotron radiation source.

The first study focused on the examination of both copper-phenanthroline complexes, incubated with bovine genomic DNA, at the P65 beamline in DESY. The energetic range was set to 8833 - 9581 eV, with 0.4 eV step, 0.1 second/point. At least, 30 scans per sample were acquired, and with 4 minutes to take one scan.

The second examination with bovine serum albumin (BSA) was conducted in ASTRA beamline. Chosen energetic steps were set as follows: 2 eV in the range 8900 - 8960 eV, 1 eV in 8960 - 8975 eV, 0.2 eV in 8975 - 9010 eV, 0.5 eV in 9010 - 9025 eV, and 1 eV in 9025 -9200 eV. At least 3 scans per sample were acquired, what took around 1 hour to complete 1 scan, with 8 seconds per energetic step.

All the data was analyzed with the XAS Viewer program, with the same procedure as described in Chapter 2, with minor changes: for DESY data, 30 scans were merged for better statistics, and for ASTRA all that were registered for a given sample. Data for ASTRA was interpolated as for pellets. To determine whether the interaction of the given complex with the biomolecule occurred, an analysis of the difference between the XAS spectra of the compound incubated with the biomolecule and the compound alone was performed. To obtain such difference, spectra were subtracted with the XAS Viewer program and the result was normalized for easier comparison. To increase the quality of the data from ASTRA studies and obtain better clarity, data was smoothed with the convolution method and Gaussian function. The energy of the absorption edge was determined from the chosen maximum of the first derivative in the region of the edge, after comparison with the first derivative of XAS spectra of corresponding pellets.

3.4.2. Comparison of the XAS spectra of solid and liquid copper(II) samples

To verify whether there occurs a difference in the chemical neighborhood of the copper in a solid state of copper-phenanthroline complex and after dissolving it, XAS spectra of both types of samples were compared. As a solid sample, a 5 wt.% pellet with one of the copper-phenanthroline complexes was chosen, and as a liquid sample, a 4 mM aqueous solution of the same compound (proportions are given in the next subchapter). For this analysis, results from the DESY study were chosen for examination, which are presented in **Figures 86-87**.

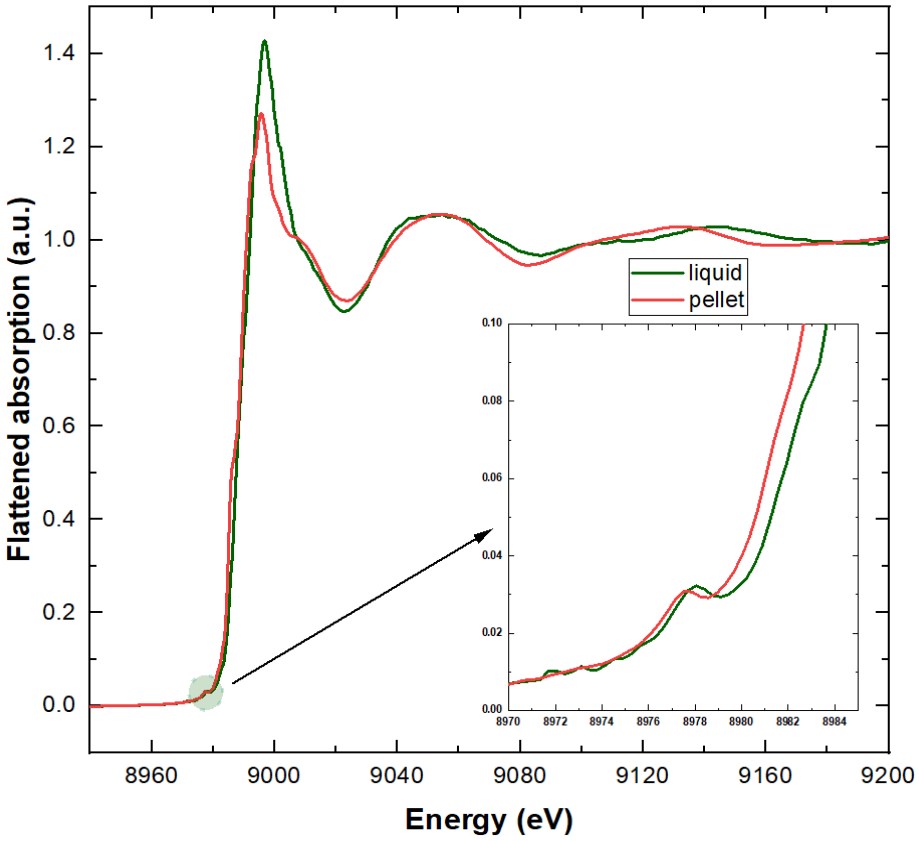

Figure 86 Synchrotron Cu K-edge XAS spectra of liquid and solid sample containing $Cu(phen)Cl_2$**.** With green circle the pre-edge region was marked, enlarged and inserted on the right bottom corner to show pre-edge peak

Starting from the XANES region, in all XAS spectra there is a visible pre-edge peak in the region 8976 - 8990 eV. A slight shift (around 0.5 eV) of its position towards higher energies is observed for liquid samples. Any significant increase in its intensity is not visible, which means that the centrosymmetry is not broken, and like in the case of pellets, a quadrupole transition still contributes to the presence of this spectral feature.

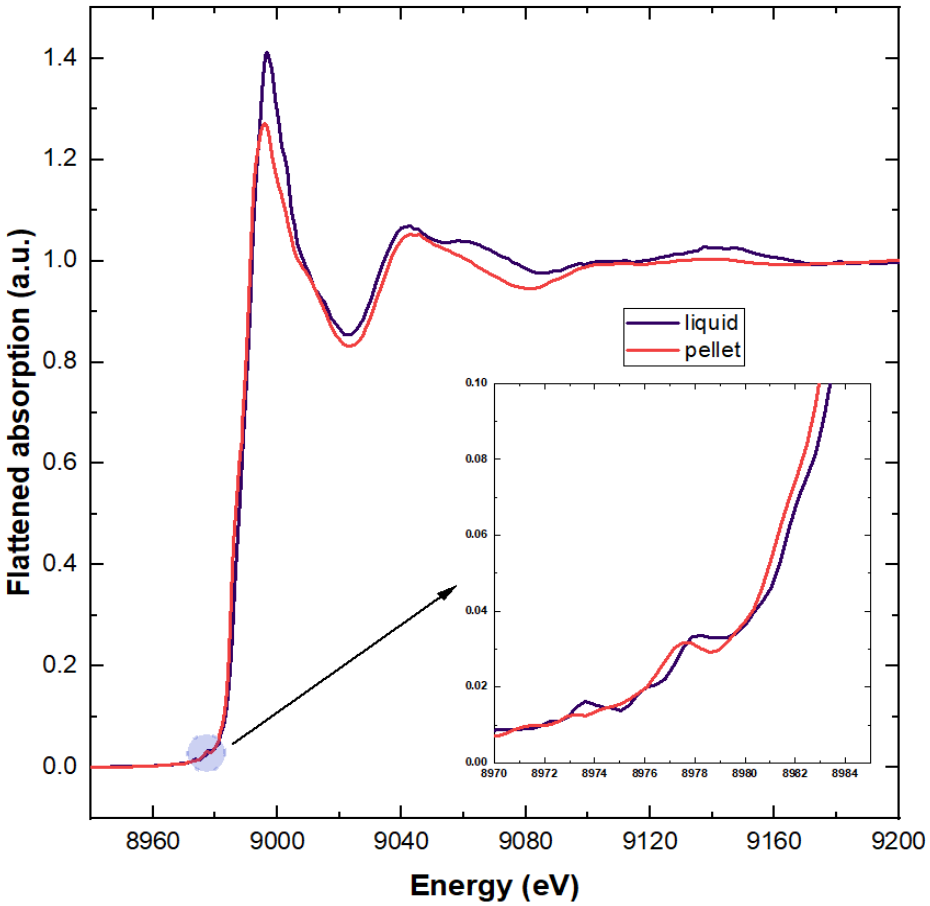

Figure 87 Synchrotron Cu K-edge XAS spectra of liquid and solid sample containing Cu(phen,triaz)Cl_2**.** With light blue circle the pre-edge region was marked, enlarged and inserted on the right bottom corner to show pre-edge peak

The next step involved the determination of the maximum of the first derivative of XAS spectra. For both complexes, there can be visible a double peak within the XANES energy range (**Figures 88-89**), therefore derivatives of spectra of pellets and liquids were compared to decide which maximum should be chosen.

For Cu(phen)Cl_2 samples, for both derivatives, the maximum of the first peak was higher than the other. For the Cu(phen,triaz)Cl_2 spectrum of the pellet, the first maximum is higher than the second, while for the liquid sample, the opposite one. Therefore, both values of maxima were identified on the spectrum of the liquid and were marked in **Figure 90** for further investigation.

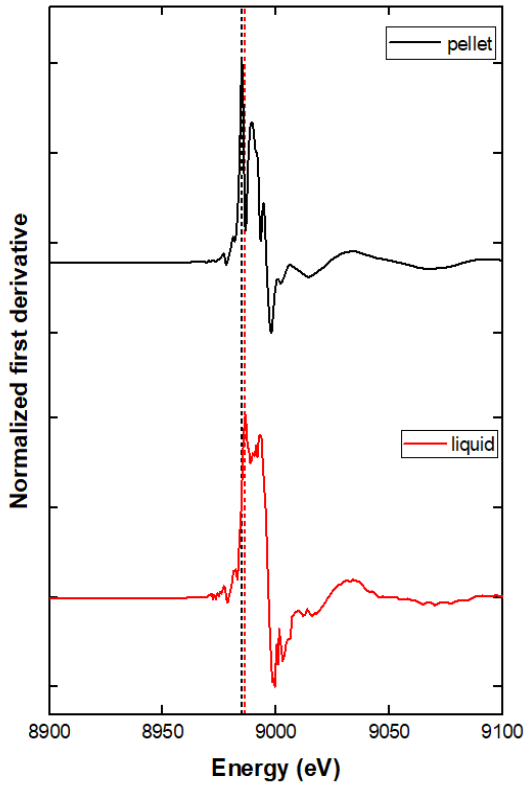

Figure 88 First derivative of Cu K-edge XAS spectra of Cu(phen)Cl_2 pellet and its 4 mM aqueous solution. With dashed lines maxima of both derivatives were marked, that determine the energy of the absorption edge

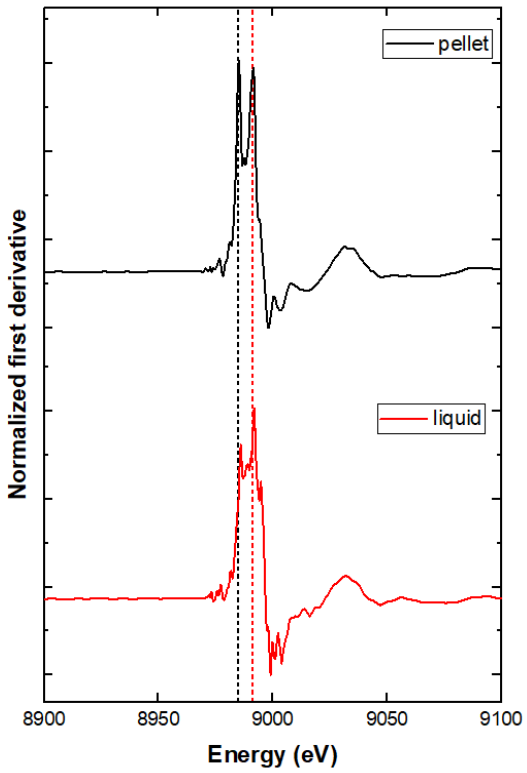

Figure 89 First derivative of Cu K-edge XAS spectra of Cu(phen,triaz)Cl_2 pellet and its 4 mM aqueous solution. With dashed lines maxima of both derivatives were marked, that determine the energy of the absorption edge

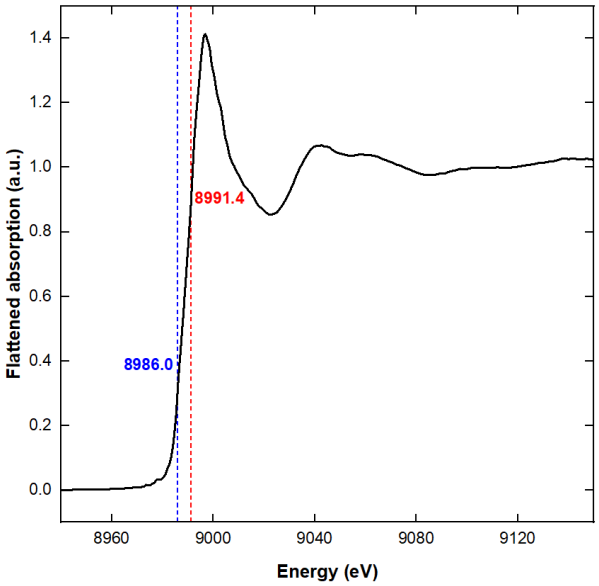

Figure 90 Cu K-edge XAS spectrum of Cu(phen,triaz)Cl_2 solution, with marked with dashed lines values of maxima of two peaks of the first derivative of spectrum within the XANES region

It can be seen, that the maximum of the second peak of the derivative (8991.4 eV) can be identified closer to the white line. Also, there are two slight inflections in the XANES region of this spectrum, that probably led to the generation of these two observed maxima. Additionally, if the second maximum has been chosen, it would suggest that there is a significant shift of the edge totaling around 6 eV from this of the pellet, which can not be even seen in **Figure 87**. Therefore, after this verification, it was decided to choose the maximum of the first peak, since probably for such a low concentrated sample, the height of both peaks might be affected by noise, and taking right away the highest value might not be in this case the most reliable choice.

For all results presented in the next subchapters, the determination of the energy of the absorption edge was also based on a prior comparison of the spectra of pellets and liquids, to choose the most appropriate maximum.

After verification of the maxima of the first derivatives, in the **Table 9** determined values of energies of the absorption edge for tested samples were listed.

Table 9 Determined values of the energy of the absorption edge for solid and liquid copper-phenanthroline samples

Complex	The energy of the absorption edge [eV]
$Cu(phen)Cl_2$ - pellet	8985.1 ± 0.3
$Cu(phen)Cl_2$ - solution	8986.5 ± 0.4
$Cu(phen,triaz)Cl_2$ - pellet	8985.1 ± 0.3
$Cu(phen,triaz)Cl_2$ - solution	8986.0 ± 0.4

For both complexes, a shift of spectra of liquids, totaling around 1 eV towards higher energies, can be seen. Since any photooxidation to Cu^{3+} seems to not be a good explanation, because this state is not stable, it can be suspected, that ligands around copper could change. In the case when the new ligand has a higher electronegativity, there can be observed a chemical shift towards higher energies, while the probed element's oxidation number stays the same [20]. For studied complexes, there is a probability that Cl atoms were exchanged to more electronegative ligands, like -OH or $-OH_2$ groups, after dissolving the complexes in aqueous solutions. Such a situation was already observed for some platinum chemotherapeutic compounds, including cisplatin, where hydrolysis occurred and Cl atoms were exchanged [21, 22].

To verify that hypothesis, the theoretical calculations of XAS spectra in the FEFF9 program, of liquid complexes with Cl atoms, or them substituted with other ligands, were performed in collaboration with dr Michał Nowakowski from the University of Paderborn. For these calculations, cif. files, that were obtained from [23, 24] were used, and the crystallographic data was prior optimized in terms of the position of atoms, by conducting additional ab initio calculations with ORCA 5.0 program package. For comparison with experimental spectra, all presented in this thesis theoretical spectra were shifted by a value of the shift of the absorption edge from the edge of the corresponding experimental spectrum, which aligned both absorption edges and white lines. Results of FEFF calculations were presented in **Figures 91-92**.

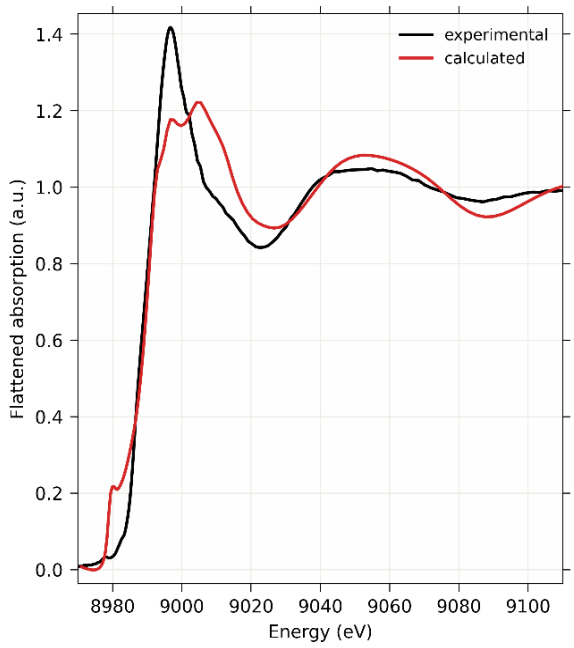

Figure 91 Experimental and calculated Cu K-edge XAS spectra of Cu(phen)Cl_2 solution

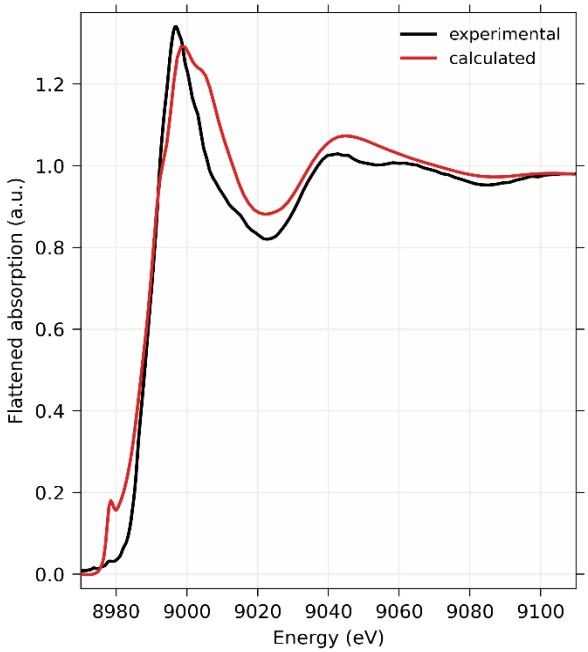

Figure 92 Experimental and calculated Cu K-edge XAS spectra of Cu(phen,triaz)Cl_2 solution

As can be observed, theoretical calculations for both compounds, which were performed with data considering preservation of the chemical structure of their solid state, did not match well the experimental data. The white line is wider and consists of a shoulder/inflection, while for experimental spectra the white line is narrow and sharp. Also, the EXAFS region features are not aligned. Therefore, calculations were performed, taking into consideration other ligands bound to copper atom, which were two -OH groups, or one -OH and one -OH_2 group (**Figures 93-96**).

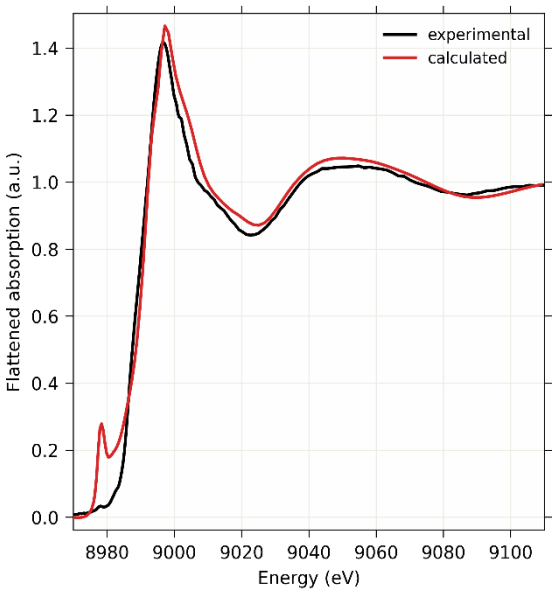

Figure 93 Experimental and calculated Cu K-edge XAS spectra of copper-phenanthroline complex solution, after substitution of two Cl atoms with two -OH groups

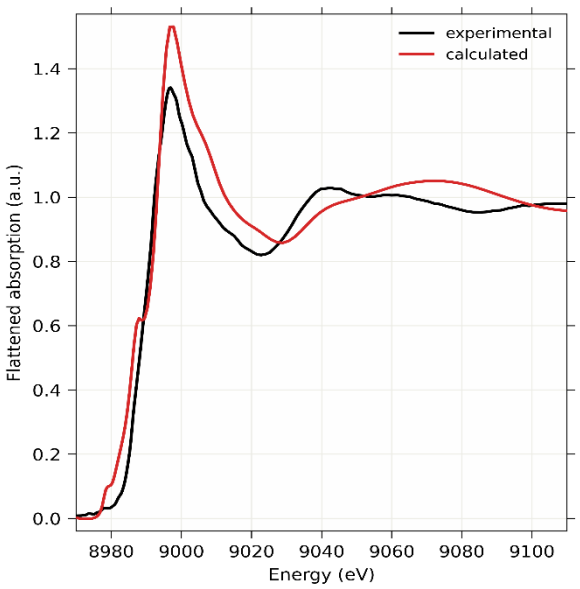

Figure 94 Experimental and calculated Cu K-edge XAS spectra of copper-phenanthroline-triazole complex solution, after substitution of two Cl atoms with two -OH groups

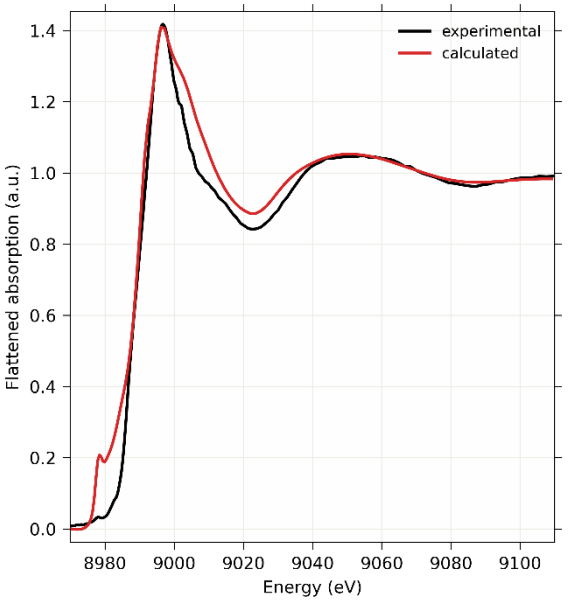

Figure 95 Experimental and calculated Cu K-edge XAS spectra of copper-phenanthroline complex solution, after substitution of two Cl atoms with one -OH and one -OH_2 group

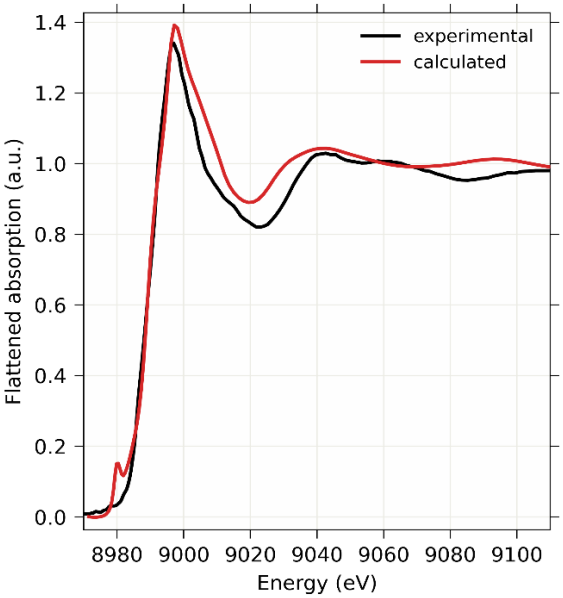

Figure 96 Experimental and calculated Cu K-edge XAS spectra of copper-phenanthroline-triazole complex solution, after substitution of two Cl atoms with one -OH and one -OH_2 group

Taking for comparison results for the first copper-phenanthroline complex, it can be observed, that both spectra, which were calculated for the compound after ligands substitution, have white lines and EXAFS regions well aligned with experimental spectra. For the spectrum considering exchange to two -OH groups, the pre-edge peak is more intensive, while for the second, the white line possesses a slight, but noticeable inflection.

For the second complex, the spectrum, which was calculated for this compound with substituted Cl atoms with -OH groups, possesses an additional shoulder in the edge region, and the EXAFS region has a different shape from this of the experimental. The second result of simulations, concerning exchange to -OH and -OH_2 group, provides a spectrum with a matching shape of the absorption edge and white line, yet, a little different EXAFS region.

Taking all the above into consideration, theoretical calculations confirm, that the change in the chemical structure of both complexes undergoes, after dissolving them in aqueous solutions. For the first copper-phenanthroline compound, both substitution of Cl atoms with two -OH groups and one -OH and one -OH_2 seems to be probable, while for the second, more likely the second type of the exchange may occur.

Another difference can be visible by comparing the intensities of experimental spectra only. In both cases, the intensity of the white line of spectra for liquid samples was higher than for pellets. The reason lies probably in the mentioned “thickness effect”, since in the pellet there was a higher amount of the compound in the measured spot, than in penetrated by radiation volume of its diluted solution. There are also noticeable differences in the EXAFS region, confirming different chemical surroundings for these two states of the sample, especially for the triazole complex.

3.4.3. Examination of copper(II)-phenanthroline complexes’ interactions with DNA

A study of the prospective interactions of both copper-phenanthroline complexes with DNA was undertaken at the DESY P65 beamline. To verify whether the chosen compound interacts with this biomolecule, the solutions with and without DNA were prepared, to identify differences between both XAS spectra, being a result of such a process. Solutions were made, using the below proportions presented in **Table 10**, resulting in obtaining the concentrations of reagents: 4mM concentration of copper(II) complex and 20 mM of HEPES.

Table 10 Proportions of the used materials to prepare sample with copper-phenanthroline complex with DNA for incubation

Compound	Mass of the compound [mg]	HEPES [ml]	DNA [ml]	Distilled water [ml]
$Cu(phen)Cl_2$	37.76	0.6	0.35	29.05
$Cu(phen,triaz)Cl_2$	48.21			

Liquids were incubated at 37°C and stirred constantly by the magnetic stirrer. To sustain a chosen temperature of samples, closed bottles with liquids were put inside a water bath, that was made from the deep crystallizer, which was put on the plate of the stirrer and to which water was poured. The temperature was measured with the thermocouple and was adjusted by the stirrer's heating system. Incubation lasted around 20 hours, so close to one day.

Next, a given solution was transferred to the liquid cell, that was described earlier in this chapter, and measurements were started. After completing the acquisition of all scans, the sample was removed from the setup, which was then flushed many times with a big portion of water.

The results of the XAS measurements of solutions of compounds alone, with DNA and the differential signal after their subtraction were presented in **Figures 97-98**.

Table 11 Determined values of the energy of the absorption edge for liquid copper-phenanthroline samples with or without DNA

Complex	The energy of the absorption edge [eV]
$Cu(phen)Cl_2$	8986.5 ± 0.4
$Cu(phen)Cl_2$ + DNA	8988.0 ± 0.4
$Cu(phen,triaz)Cl_2$	8986.0 ± 0.4
$Cu(phen,triaz)Cl_2$ + DNA	8986.3 ± 0.4

Determined values of the energy of the absorption edge, based on the first derivatives of spectra, were presented in **Table 11**. There is observed approx. 1.5 eV shift towards higher energies of the energy of the absorption edge of $Cu(phen)Cl_2$ sample incubated with DNA to this energy of the sample incubated alone. For the second complex, there is not observed difference in this value between the two types of sample.

Taking into consideration the shape of the XAS spectra, at first sight, there are no visible differences between the spectrum of the sample incubated alone and with DNA.

The differential signal is very similar for both complexes, suggesting their similar behavior in the presence of DNA. There can be observed a drop in the intensity in the region of the absorption edge, which suggests a drop in the density of the unoccupied 4p states. This fact could be explained by taking into consideration electrostatic interactions, that might be generated after the substitution of two Cl atoms, that are in fact negative ions, with at least one neutral group, like mentioned -OH_2. In that situation, both complexes gain a positive charge from the Cu^{2+}, which can be attracted by negatively charged DNA molecules. This mechanism was not mentioned nor considered in the publication, where the synthesis of Cu(phen,triaz)Cl_2 and the mechanism of its interaction with DNA were characterized [25]. However, the results from XAS studies, generate a hypothesis, that such a substitution and additional type of interaction may occur.

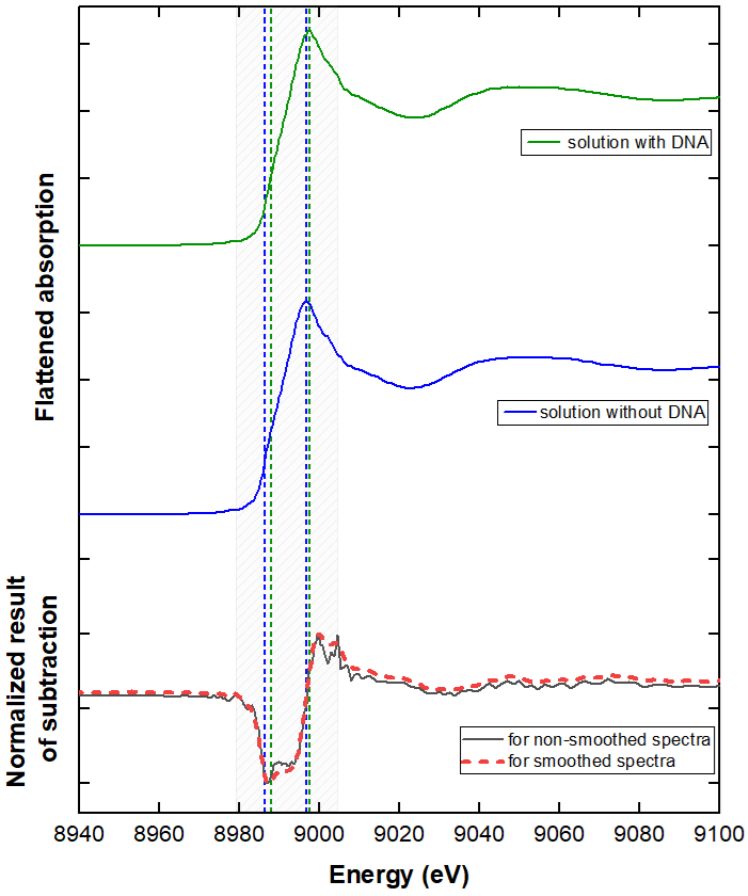

Figure 97 Cu K-edge XAS spectra of incubated 4 mM Cu(phen)Cl_2 solutions, with DNA (dark green) and alone (dark blue). Result of their subtraction was presented with a black line at the bottom. With dashed lines, in the same colours as the corresponding spectra, marked the values of the energy of the absorption edge and maxima of the white lines. Additionally, with the red dashed line on the bottom graph, the subtraction of the smoothed spectra is presented, to ease the analysis

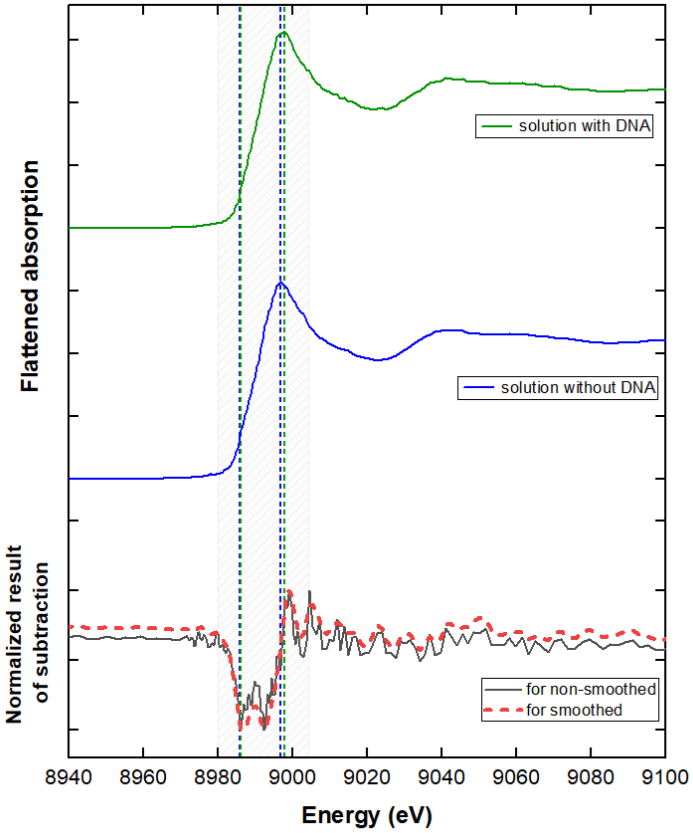

Figure 98 Cu K-edge XAS spectra of incubated 4 mM Cu(phen,triaz)Cl_2 solutions, with DNA (dark green) and alone (dark blue). Result of their subtraction was presented with a black line at the bottom. With dashed lines, in the same colours as the corresponding spectra, marked the values of the energy of the absorption edge and maxima of the white lines. Additionally, with a red dashed line on the bottom graph, the subtraction of the smoothed spectra is presented, to ease the analysis

Therefore, results of theoretical calculations of XAS spectra of both complexes incubated with DNA, having Cl atoms substituted with two -OH groups, or one -OH and one -OH_2 group, that were preformed in cooperation with dr Nowakowski, were performed and presented in **Figures 99-102**.

Similarly to the comparison of theoretical calculations, that were performed for solutions without DNA, for the first copper-phenanthroline complex, both variants of substitution taken in simulations provided quite aligned spectra with experimental ones. For the copper-triazole compound, again the exchange to -OH and -OH_2 groups gave better fitting results and favored this kind of exchange of ligands. Yet, both of these sets of simulations confirmed again, that the Cl atoms were substituted with other groups after dissolving the compounds. Taking into consideration, that in the chemical structures of both complexes, the Cl atoms are ions with a negative charge and they could be exchanged to at least one neutral ligand -OH_2, the electrostatic interaction between copper compounds and DNA, should also be taken into account.

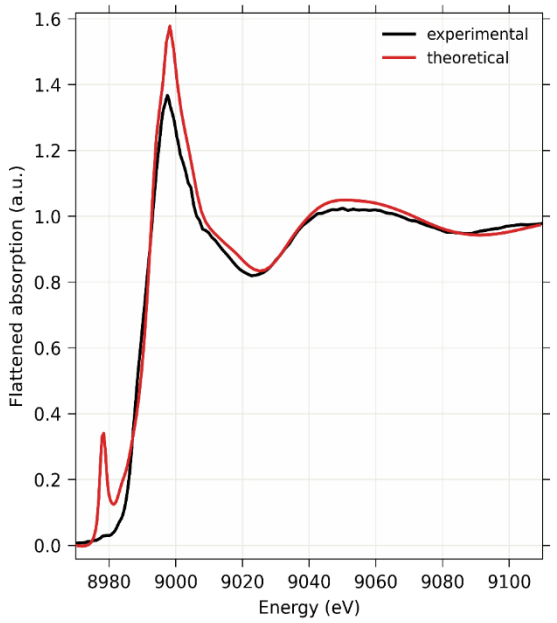

Figure 99 Experimental and calculated Cu K-edge XAS spectra of copper-phenanthroline complex solution with DNA, after substitution of two Cl atoms with two -OH groups

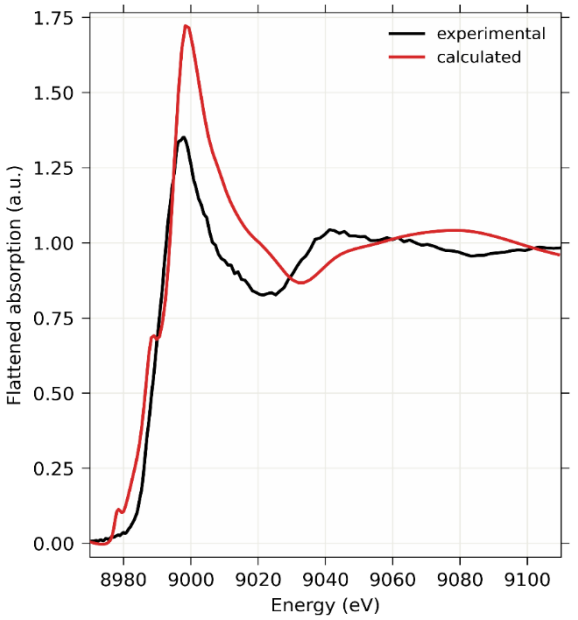

Figure 100 Experimental and calculated Cu K-edge XAS spectra of copper-triazole complex solution with DNA, after substitution of two Cl atoms with two -OH groups

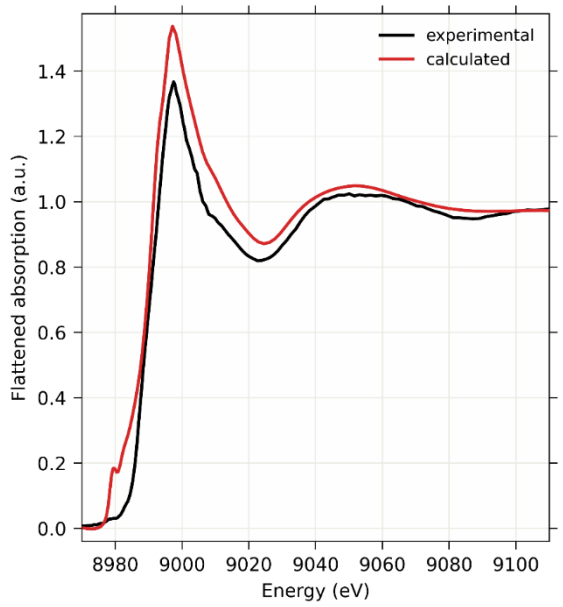

Figure 101 Experimental and calculated Cu K-edge XAS spectra of copper-phenanthroline complex solution with DNA, after substitution of two Cl atoms with one -OH and one -OH_2 group

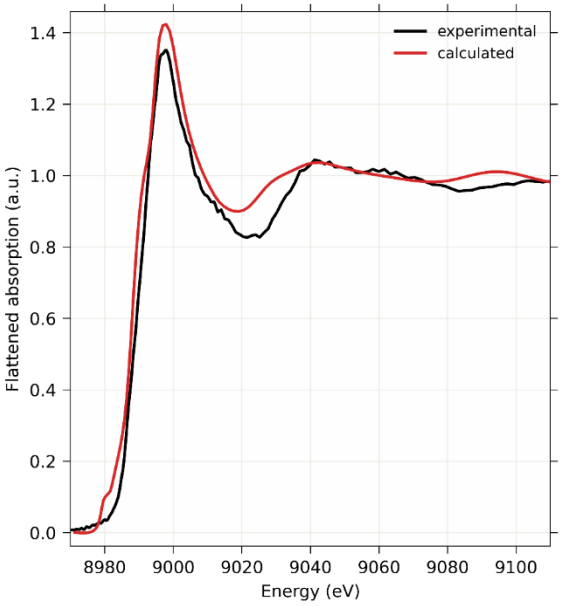

Figure 102 Experimental and calculated Cu K-edge XAS spectra of copper-triazole complex solution with DNA, after substitution of two Cl atoms with one -OH and one -OH_2 group

Another part of this study considered the analysis of the pre-edge peak. On spectra of both $Cu(phen)Cl_2$ solutions with and without DNA, there is a visible pre-edge peak. However, for the first complex, there is observed its slight shift toward higher energies,

and probably the pre-edge peak consists of two, imposed peaks (**Figure 103**). This change suggests a change in the neighborhood of the copper, which could be originated from the intercalation into the minor groove. For the spectrum of Cu(phen,triaz)Cl_2 solution with DNA, unfortunately, this time the noise affected significantly this region, therefore it is hard to recognize whether there are some pre-edge peaks present (**Figure 104**).

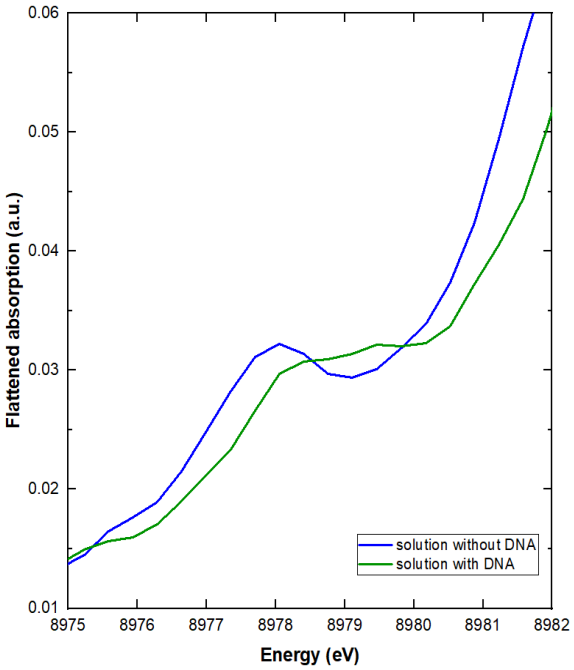

Figure 103 Pre-edge region of the Cu K-edge XAS spectra of copper-phenanthroline solutions, that were incubated without and with DNA

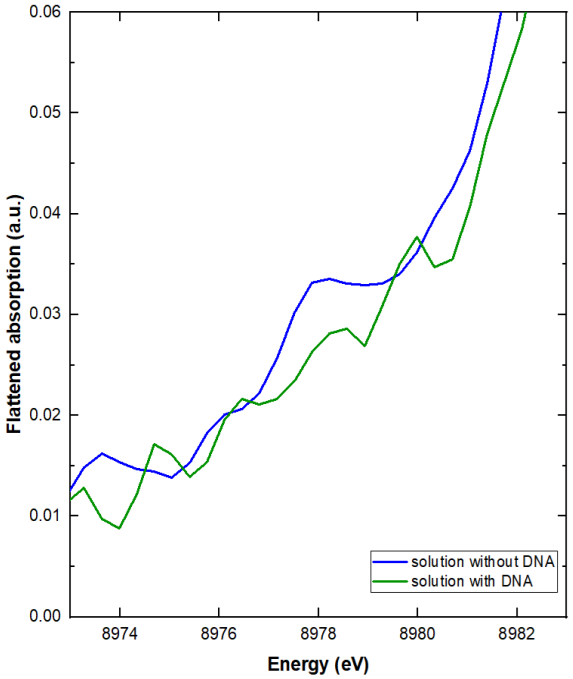

Figure 104 Pre-edge region of the Cu K-edge XAS spectra of copper-triazole solutions, that were incubated without and with DNA

All above results seem to confirm the presence of expected weak interactions between copper-complexes with DNA, which were described in the mentioned publication about Cu(phen,triaz)Cl_2 [25], that involve intercalation into the minor groove and interactions with DNA groups via van der Waals and hydrophobic forces. The chemical structure of the complexes seems to be maintained, since there are no observed additional spectral features or big shifts of the values of energy of the absorption edge, that would implicate the presence of stronger interactions. However, the difference between the XAS spectra of complexes incubated without and with DNA shows, that the change in the electronic structure of both compounds occurs after the addition of DNA to the solutions, which can originate from the undergoing interactions between compounds and biomolecules. One study on a platinum-based compound, that revealed its interactions with DNA via hydrogen bonds, also noted small differences between spectra of the complex alone and in the presence of DNA, which follows the above interpretation [22].

In Chapter 1 the possible undergoing redox reactions were mentioned, where a copper changes its oxidation number from 2+ to 1+ and in reverse, during which some free radicals can be generated. From the determined values of the energy of the absorption edge, it can not be concluded that for set parameters of XAS measurements, concentrations, and composition of solutions, such reactions are undergoing, since there are no shifts towards lower energies, which could indicate reduction to Cu^{1+}. Yet, basing on the literature, this kind of reaction could be promoted, when introducing some reducing agents, like ascorbic acid or 3-mercaptopropionic acid [26].

3.4.4. Examination of copper(II)-phenanthroline complexes' interactions with BSA

Studies on interactions between copper-phenanthroline complexes and bovine serum albumin (BSA) were performed at the ASTRA SOLARIS beamline. Since the chosen protein tends to easily create a foam during stirring of the solution, the procedure of preparing a liquid for examination slightly differed from that with DNA. Firstly, the weighted portion of BSA was gently transferred to the surface of distilled water. When the protein dissolved, the rest of the reagents were added, and the bottle with the liquid was put into a water bath for incubation overnight. The proportions to obtain 15 ml of the solution were listed in **Table 12**.

Table 12 Proportions of the used materials to prepare sample with copper-phenanthroline complex and BSA for incubation

Compound	**Mass of the compound [mg]**	**HEPES [ml]**	**BSA [mg]**	**Distilled water [ml]**
$Cu(phen)Cl_2$	18.88	0.3	37.5	14.7
$Cu(phen,triaz)Cl_2$	25.19			

After incubation, the given sample was transferred to the container made from a syringe, and its flow was forced by the pump. After the liquid passed through all the elements, which were a cell and pipes, and returned to the container, measurements could start. It was found after a few hours, that some of the protein sedimented in the container, suggesting that the amount of protein was in excess. However, a significantly higher amount of protein than the amount of compound provided the situation, for which all molecules of the compound could react with BSA. After completing the cycle of scans, the setup was flushed many times with a big portion of water, to remove the residual sample.

To determine whether the interaction between the copper complex and BSA occurred, like for the DNA study, the XAS spectrum of the sample incubated with BSA was subtracted from this for the incubated solution with the compound alone. Results were presented in **Figures 105-106**.

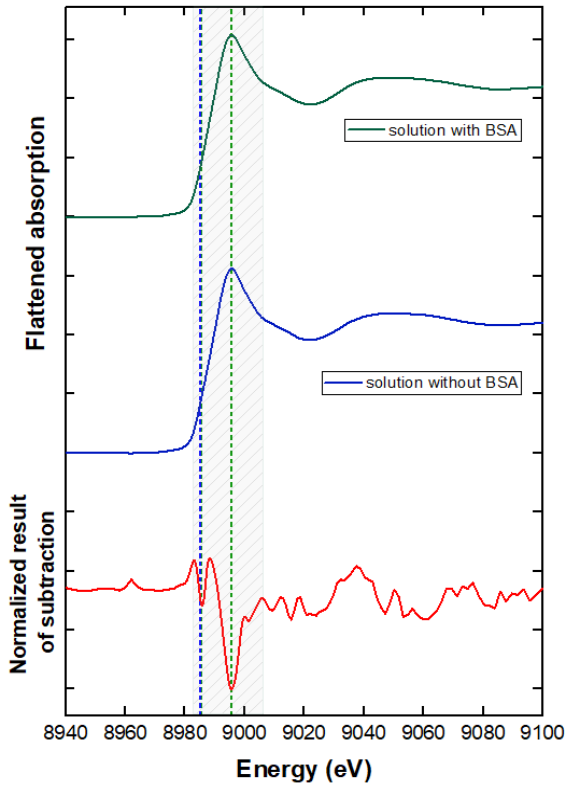

Figure 105 Cu K-edge XAS spectra of incubated 4 mM copper-phenanthroline solutions, with BSA (dark green) and alone (dark blue). Result of their subtraction was presented with a red line at the bottom.

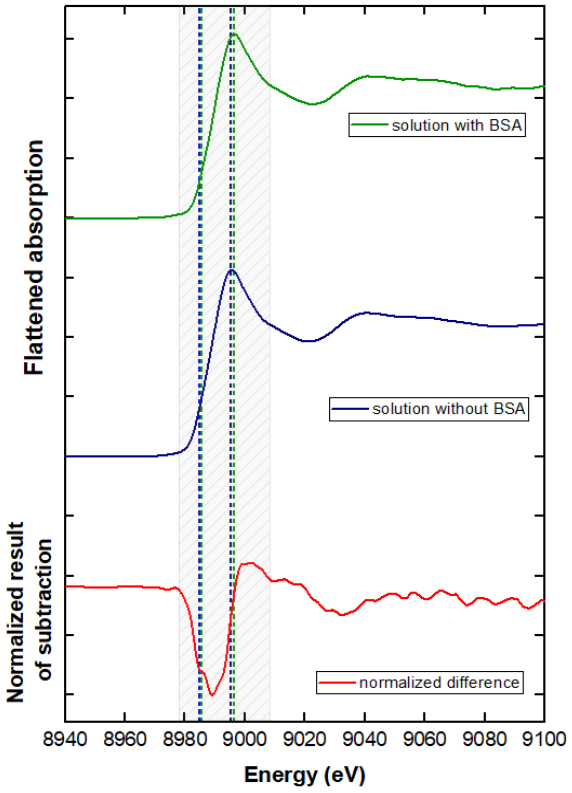

Figure 106 Cu K-edge XAS spectra of incubated 4 mM copper-triazole solutions, with BSA (dark green) and alone (dark blue). Result of their subtraction was presented with a red line at the bottom.

As can be seen, the differential spectra vary between complexes. Yet, the drop in the intensity of the white line is observed for both samples after incubation with BSA, suggesting a drop in the electron density.

From the determined values of absorption edge energy, from the first derivative of spectra (**Table 13**), there can be seen a similar slight shift towards higher energies for both complexes, totaling around 0.5 eV.

Table 13 Determined values of the energy of the absorption edge for liquid copper-phenanthroline samples with or without BSA

Complex	The energy of the absorption edge [eV]
$Cu(phen)Cl_2$	8985.1 ± 0.2
$Cu(phen)Cl_2$ + BSA	8985.7 ± 0.2
$Cu(phen,triaz)Cl_2$	8984.9 ± 0.2
$Cu(phen,triaz)Cl_2$ + BSA	8985.6 ± 0.2

A possible mechanism of interaction of copper-phenanthroline complexes might be suspected, basing on some reports from the literature. From fluorescence emission spectroscopy measurements, there are reports describing interactions between metal complexes with BSA, via hydrophobic interactions in the hydrophobic pocket of the subdomain IIA [27, 28]. The flat geometry of the organic groups seems to enhance such an interaction [29]. For both studied complexes, there is a planar 1,10-phenanthroline group, and for the synthesized complex, there is an additional 1,2,4-triazole one, which might interact in the mentioned subdomain.

From the values of the energy of the absorption edge, determined from the first derivative, for both complexes there is observed a small shift towards higher energies, totaling approx. 0.5 eV. The shape of the spectrum for samples after incubation with BSA was preserved, yet the subtraction revealed slight changes. Unlike in the case of studies of solutions with DNA, the subtraction results differ between complexes. There can be seen a drop in the intensity within the absorption edge region, however, more pronounced for copper complex with triazole. Therefore, while it can not be decided whether the first complex does not interact with BSA or if this interaction is very weak, the second seems to exhibit an interaction. That could be enhanced by the presence of the second organic group, which might also interact via hydrophobic interaction in the expected subdomain.

Additionally, following the results from the studies with DNA, also for this case electrostatic interactions could take place. In pH around 7.4 (in this experiment pH was also around that value), the amino acids residues from BSA get a negative charge from the ionization processes [30]. Since taking into consideration the mentioned previously substitution of Cl^- ions with other ligands, especially $-OH_2$, both copper-phenanthroline complexes might gain a positive charge, and also in this case the attraction between BSA sites and compounds can undergo.

Unfortunately, for data obtained at the ASTRA beamline, the pre-edge peaks were not well pronounced, after choosing the smallest possible energetic step, even if from the

study performed at the DESY facility it was known, that for both incubated liquids without biomolecule in the same conditions it was observed (and described in the previous subchapter). As a result, attempts to compare the geometry around copper in the presence and absence of BSA could not be performed.

3.5. Discussion

This chapter concentrated on the examination of liquid samples, especially those containing one out of two copper-phenanthroline-based complexes, which were incubated with chosen biomolecules – DNA or bovine serum albumin.

The first obstacle to solve was the development of the setup for the delivery of solutions, that will also prevent possible radiation damage. It also had to provide constant mixing of the complex with biomolecules and their proper distribution in volume, enabling their interactions. It was found, that not only the general construction, like the choice and number of elements, played a key factor in reducing the needed volume of solution and masses/volumes of reagents, to obtain expected concentrations, and to fill all of the components with the sample. Also, the contact of the liquid with air and resulting evaporation was a parameter limiting the acquisition time of a few scans, before losing a significant amount of the sample and generation of the air bubbles affecting the XAS signal. Moreover, for solutions containing BSA, the contact with air and with the funnel resulted in the aerification and obtaining a stiff foam, which led to the loss of the XAS signal. Taking all the above into consideration, the closed setups were applied, which were tested and enabled successful measurements of the samples with and without biomolecules for a time of a few hours, nondisturbed by evaporation.

After the efficient setup was developed, there came a possibility to study solutions of both copper-phenanthroline complexes, and to compare their results with those for pellets, which were described in the previous chapter. For both complexes, a shift of the absorption edge towards higher energies of spectra for their solutions was observed. Also, the changes in the EXAFS signal were noticed, which suggested changes in the geometry around the copper. The probable exchange of the Cl atoms was confirmed by the results of theoretical calculations, which supported the possible substitution of Cl atoms with -OH or/and -OH_2 groups. There is still a possibility to explore a probable substitution to other groups or combinations, including two OH_2 groups. Nevertheless, XAS experiments, supplemented by simulations of XAS spectra, already provided information, which was lacking in the literature, that a change occurs in the chemical structure of Cu(phen)Cl_2 and

$Cu(phen,triaz)Cl_2$ after dissolving them in aqueous solution. As a result, this eschange may enhance their interaction with biomolecules.

Simulations of XAS spectra of complexes incubated without and with DNA, and with substituted ligands, matched well the experimental spectra. For both compounds, results of spectral subtraction and comparison of the spectral shape suggest their similar behavior in the presence of DNA and undergoing weak interactions, which were described in the literature. After substitution with one -OH (principally OH^-) and one $-OH_2$ group, both complexes would gather a positive charge from Cu^{2+}, which was balanced in their solid state with two negatively charged Cl ions. Therefore, taking into consideration that the DNA molecule possesses a negative charge, the electrostatic interaction between DNA and copper-phenanthroline complexes should also be considered, which might take part in the formation of a DNA-compound conjugate in the minor groove.

Results of the examination of both copper compounds with BSA provided information, that preferably $Cu(phen,triaz)Cl_2$ exhibits interactions with this biomolecule. The probable explanation of this kind of higher activity than the other complex relies on the fact, that this compound possesses an additional organic group, that could also be involved in the expected hydrophobic interactions. To this mechanism, also electrostatic interaction should be taken into account, between negatively charged residues of amino acids and positively charged copper complex, after the exchange of two Cl^- to at least one neutral ligand. Moreover, it would be worth repeating the XAS examination of $Cu(phen)Cl_2$, to confirm that the results were not affected by any unnoticed events during beamtime at the ASTRA beamline.

Summing above discussion, all three set goals (5-7) were met, which involved tests of the liquid delivery setups, XAS studies of dissolved copper-phenanthroline complexes with and without chosen biomolecules, and finally complex data analysis.

3.6. Materials

1) **Chemicals:**
   a) Copper foil – Goodfellow Cambridge Limited, nr cat. LS397006, thickness: 0.01mm, purity: 99.9%, CAS: 7440-50-8
   b) Copper(II) oxide (CuO) – Sigma-Aldrich, cat. nr: 544868-5G, nanopowder with particles diameter < 50 nm, CAS: 1317-38-0
   c) Copper(II) sulfate ($CuSO_4$) - Fluka™, Honeywell, cat. nr: 12852-250G, CAS: 1317-38-0
   d) Dichloro-(1,10-phenanthroline)copper(II) (Cu(1,10-phenanthroline)Cl_2) – Sigma-Aldrich, 98%, cat. nr: 362204-1G, CAS: 14783-09-6
   e) Dichloro-(1,10-phenanthroline)-(1H-1,2,4-triazole-1-yl)-copper(II) monohydrate (Cu(1,10-phenanthroline)-(1H-1,2,4-triazole-1-yl)$Cl_2 \cdot H_2O$) - synthesized
   f) Cellulose $(C_6H_{10}O_5)_n$ – Sigma-Aldrich, cat. nr: 310697-500G, microcrystalline powder, particles diameter: 20 μm, CAS: 9004-34-6
   g) Bovine genomic DNA – Novagen ®, EMD Millipore Corp., cat. nr: 69231-3, 100 μg in TE Buffer (10mM Tris-HCl pH 8.0, 1mM EDTA)
   h) Bovine serum albumin (BSA) – Sigma-Aldrich, cat. nr: A9418-5G, lyophilized powder, BioReagent, suitable for cell culture, CAS: 9048-46-8
   i) HEPES (N-(2-Hydroxyethyl)piperazine-N'-(2-ethanesulfonic acid) – Sigma-Aldrich, cat. nr: H0887-20ML, 1 M, pH 7.0-7.6, sterile-filtered, BioReagent, suitable for cell culture, CAS: 7365-45-9

2) Programs:
   a) XAS Viewer [31]
   b) OriginLab 2021
   c) ORCA 5.0 – a program package for ab initio calculations for quantum chemistry, involving the DFT approach [32]
   d) FEFF9 – a program that is used for calculating theoretical XAS spectra, which documentation can be found here [33-35].

3) Laboratory equipment:

a) Magnetic stirrer: Heidolph Instruments GmbH & Co. KG, MR Hei-Tec, nr. 505-30000-00-4, voltage: 230 – 240 V, frequency: 50/60 Hz, power: 825 W, 100-1400 r.p.m.

3.7. Bibliography

[1] Jamieson, Elizabeth R., and Stephen J. Lippard. "Structure, recognition, and processing of cisplatin− DNA adducts." *Chemical Reviews* 99.9 (1999): 2467-2498.

[2] Barone, Giampaolo, et al. "DNA-binding of nickel (II), copper (II) and zinc (II) complexes: Structure–affinity relationships." *Coordination Chemistry Reviews* 257.19-20 (2013): 2848-2862.

[3] Rehman, Sayeed Ur, et al. "Studying non-covalent drug–DNA interactions." *Archives of Biochemistry and Biophysics* 576 (2015): 49-60.

[4] Sirajuddin, Muhammad, Saqib Ali, and Amin Badshah. "Drug–DNA interactions and their study by UV–Visible, fluorescence spectroscopies and cyclic voltametry." *Journal of Photochemistry and Photobiology B: Biology* 124 (2013): 1-19.

[5] Sułkowska, Anna. "Interaction of drugs with bovine and human serum albumin." *Journal of Molecular Structure* 614.1-3 (2002): 227-232.

[6] Wang, Chun, et al. "Study of the interaction of carbamazepine with bovine serum albumin by fluorescence quenching method." *Analytical Sciences* 22.3 (2006): 435-438.

[7] Korkmaz, Filiz, Deniz Altunoz Erdogan, and Şeniz Özalp-Yaman. "Interaction of a novel platinum drug with bovine serum albumin: FTIR and UV-Vis spectroscopy analysis." *New Journal of Chemistry* 39.7 (2015): 5676-5685.

[8] Ariga, Girish G., et al. "Interactions between epinastine and human serum albumin: Investigation by fluorescence, UV–vis, FT–IR, CD, lifetime measurement and molecular docking." *Journal of Molecular Structure* 1137 (2017): 485-494.

[9] Cząstka, Karolina, et al. "Enzymatic X-ray absorption spectroelectrochemistry." *Faraday Discussions* 234 (2022): 214-231.

[10] Nicolis, Ioannis, et al. "X-ray absorption spectroscopy of low-molar-mass metallic complexes in pharmacy." *Journal of Synchrotron Radiation* 10.1 (2003): 96-102.

[11] Lipinski, C. A. L. F. "Poor aqueous solubility—an industry wide problem in drug discovery." Am. Pharm. Rev 5.3 (2002): 82-85.

[12] George, Graham N., et al. "X-ray-induced photo-chemistry and X-ray absorption spectroscopy of biological samples." *Journal of Synchrotron Radiation* 19.6 (2012): 875-886.

[13] Błachucki, W., et al. "Inception of electronic damage of matter by photon-driven post-ionization mechanisms." *Structural Dynamics* 6.2 (2019).

[14] Garman, Elspeth F., and Robin Leslie Owen. "Cryocooling and radiation damage in macromolecular crystallography." *Acta Crystallographica Section D: Biological Crystallography* 62.1 (2006): 32-47.

[15] Belloni, J, Mostafavi, M, Douki, Th, and Spotheim-Maurizot, M. Radiation chemistry from basics to applications in material and life sciences. France: N. p., (2008) Web.

[16] Ascone, Isabella, Wolfram Meyer-Klaucke, and Loretta Murphy. "Experimental aspects of biological X-ray absorption spectroscopy." *Journal of Synchrotron Radiation* 10.1 (2003): 16-22.

[17] Rosi, Matthew, et al. "An automated liquid jet for fluorescence dosimetry and microsecond radiolytic labeling of proteins." *Communications Biology* 5.1 (2022): 866.

[18] Fuchs, Oliver, et al. "A liquid flow cell to study the electronic structure of liquids with soft X-rays." *Nuclear Instruments and Methods in Physics Research Section A: Accelerators, Spectrometers, Detectors and Associated Equipment* 585.3 (2008): 172-177.

[19] Błachucki, Wojciech, et al. "A laboratory-based double X-ray spectrometer for simultaneous X-ray emission and X-ray absorption studies." *Journal of Analytical Atomic Spectrometry* 34.7 (2019): 1409-1415.

[20] Hummer, Alfred A., and Annette Rompel. "X-ray absorption spectroscopy: a tool to investigate the local structure of metal-based anticancer compounds in vivo." *Advances in Protein Chemistry and Structural Biology* 93 (2013): 257-305.

[21] Lau, Justin Kai-Chi, and Bernd Ensing. "Hydrolysis of cisplatin—a first-principles metadynamics study." *Physical Chemistry Chemical Physics* 12.35 (2010): 10348-10355.

[22] Czapla-Masztafiak, Joanna, et al. "Mechanism of hydrolysis of a platinum (IV) complex discovered by atomic telemetry." *Journal of Inorganic Biochemistry* 187 (2018): 56-61.

[23] Liu, Y-Q. "Dichlorido (1, 10-phenanthroline) copper (II)." *Acta Crystallographica Section E: Structure Reports Online* 63.12 (2007): m2991-m2991.

[24] https://www.ccdc.cam.ac.uk/structures/search?id=doi:10.5517/ccw3fx9&sid=DataCite (accessed: 25.01.2024)

[25] Tabassum, Sartaj, et al. "Synthesis and characterization of copper (II) and zinc (II)-based potential chemotherapeutic compounds: their biological evaluation viz. DNA binding profile, cleavage and antimicrobial activity." European Journal of Medicinal Chemistry 58 (2012): 308-316.

[26] Bales, Brian C., et al. "Mechanistic studies on DNA damage by minor groove binding copper–phenanthroline conjugates." *Nucleic Acids Research* 33.16 (2005): 5371-5379.

[27] Samari, Fayezeh, et al. "Affinity of two novel five-coordinated anticancer Pt (II) complexes to human and bovine serum albumins: a spectroscopic approach." *Inorganic chemistry* 51.6 (2012): 3454-346

[28] Asadi, Mozaffar, et al. "Affinity to bovine serum albumin and anticancer activity of some new water-soluble metal Schiff base complexes." *Spectrochimica Acta Part A: Molecular and Biomolecular Spectroscopy* 133 (2014): 697-706.

[29] Topală, Tamara, et al. "Bovine serum albumin interactions with metal complexes." *Clujul Medical* 87.4 (2014): 215.

[30] Wang, Yan-Qing, et al. "Spectroscopic studies on the interaction between silicotungstic acid and bovine serum albumin." *Journal of Pharmaceutical and Biomedical Analysis* 43.5 (2007): 1869-1875.

[31] Newville, Matthew. "Larch: an analysis package for XAFS and related spectroscopies." *Journal of Physics: Conference Series*. Vol. 430. No. 1. IOP Publishing (2013).

[32] https://www.orcasoftware.de/tutorials_orca/index.html (accesed: 28.01.2024)

[33] Rehr, John J., et al. "Parameter-free calculations of X-ray spectra with FEFF9." Physical *Chemistry Chemical Physics* 12.21 (2010): 5503-5513.

[34] Rehr, John J., et al. "Ab initio theory and calculations of X-ray spectra." *Comptes Rendus Physique* 10.6 (2009): 548-559.

[35] https://feff.phys.washington.edu/feff/Docs/feff9/feff90/feff90_users_guide.pdf (accessed: 25.01.2024)

Final discussion

The motivation to study copper-based compounds as potential anticancer drugs came from the fact, that commonly used chemotherapeutics are still not giving expected treatment results for each type of cancer, or even can differ between patients, who have the same case of illness. Moreover, drugs that are based on platinum, can generate unwelcome side-effects, which affect not only physical health but also might disturb mental health, that also plays a significant factor in reviving. Copper being a micronutrient, spreads in the human body in a controlled process, with the involvement of transporters, like ceruloplasmin. Additionally, copper is significantly cheaper to possess than platinum, what reduces the costs of the production of chemotherapeutics. Therefore, also in described in this thesis project, it was decided to concentrate on complexes, which are based on this element.

Hybrid complexes, that have planar organic groups and metallic centres, can fit between parts of the DNA helix, blocking access for proteins that are involved in replication or transcription processes. Additionally, the presence of a transient metal like copper can induce the generation of free radicals in the neighborhood of this biomolecule, which might damage DNA structure. Both of these mechanisms might induce apoptosis processes, giving a promising therapeutic effect. In this thesis, two hybrid copper-phenanthroline complexes were described and examined, which were expected to interact noncovalently with DNA, and were tested, whether they might also interact with bovine serum albumin.

The decision to choose the X-ray Absorption Spectroscopy, instead of other, still more commonly used methods of investigation (like fluorescence emission or UV-Vis spectroscopies), was motivated by the fact, that this method probes both changes in the geometry around the chosen element, and changes in its oxidation number, during the same measurement. The first parameter can provide information on whether the complex fits within DNA or BSA structure, while another if any redox reaction undergoes. The ability to examine both solid and liquid samples with the same method, in different compositions, room temperature, and ambient atmosphere, made it possible to perform a wide examination of all copper complexes, including monitoring the changes in their chemical structure after dissolving in aqueous solution.

Two major aspects of the described research, that needed to be explored, were identified: technical and analytical. The first one involved :

a) optimization of parameters of the synthesis of Cu(phen,triaz)Cl_2, including the conditions in the laboratory, especially the temperature under the fume hood,

b) a proper choice and arrangement of the elements of the laboratory setup, including the type of crystal analyzer, distances between elements, etc.
c) parameters of measurements, like acquisition time and energy range,
d) a choice of the type of I0 signal for studies of pellets (a signal that passed through air or cellulose pellet), containing copper-compound and cellulose
e) concentration of the complex in the solid sample for measurements in a transmission mode, to optimize the intensity of the registered XAS signal,
f) a choice of the synchrotron beamlines and mounting setups, that were borrowed or developed on-site,
g) designing and testing the setups for measurements of liquids, to prevent radiation damage and enable constant mixing,
h) proper preparation of the liquid samples, including developing the water bath, careful dissolving of the compounds, and maintaining constant incubation conditions for over 20 hours.

The second aspect – analytical, involved:

a) a choice of the method for characterization of the products of the synthesis, that was ATR-FTIR spectroscopy and interpretation of the obtained results,
b) a proper choice of the referential spectra of copper foil from literature, to perform calibration of pixel number into energy of the registered photons for laboratory data,
c) a choice of the referential compounds and comparison of all gathered XAS spectra, that were obtained in laboratory and synchrotron conditions,
d) performing data analysis in a similar manner, which involved binning the laboratory data, calibration, normalization, and choosing the energy of the absorption edge on the basis of the maximum of the first derivative of spectra,
e) a decision, whether the laboratory setup is efficient to study copper-based compounds, and for which cases it would be better to apply the synchrotron radiation,
f) determination of the approach, that will enable the verification, of whether the compound present in a pellet and dissolved in an aqueous solution changes its chemical structure,
g) comparison of the spectra of the liquid, containing the chosen complex only and other incubated also with biomolecules, followed by their subtraction,

h) determination if gathered XAS spectra for chosen copper-phenanthroline complexes provide information that they interact with DNA in the manner described in the literature, or maybe other processes are undergoing,
i) another determination, if results support the idea, that copper-phenanthroline compounds might interact with BSA.

Results from Chapter 1 provided information, that the described in the publication procedure to obtain $Cu(phen,triaz)Cl_2$ lacks the important fact, that the parallel synthesis of the second compound undergoes for proposed conditions, reagents, and concentrations. Any chosen modification did not result in the elimination of the second product. Therefore, after repetitions of the synthesis, both products were verified by performing ATR-FTIR measurements and further analysis of the spectra. This study revealed, that these two products are: $Cu(phen)Cl_2$, which was already planned to be used as a reference to the $Cu(phen,triaz)Cl_2$, which seemed to be synthesized, as it was expected.

Chapter 2 was focused on the XAS examination of solid copper-containing samples, in both laboratory and synchrotron conditions. Significantly less intensive radiation, which was used in laboratory study, than derived from synchrotron, forced a longer process of optimization of the samples' preparation and of setting the measurement parameters, like concentration of the compound in a pellet or acquisition time. Another important approach, that was applied, was a choice of the origin of the I0 signal, which was a radiation that passed through the pellet, which was made from cellulose. This application reduced the detection of scattered radiation and also included the absorption by the cellulose itself, which improved at the end the quality of the XAS spectra of pellets.

An important part of the data analysis of laboratory results involved the process of verification of the most representative approach of absorption edge energy determination. From the three methods, that were mentioned in the literature, the probably most used one was chosen, which was taking the maximum of the first derivative of spectra. Additionally, for compounds richer in atoms (like copper-phenanthroline complexes) than used referentials, it was essential to perform smoothing of the spectra, to reveal the important for interpretation spectral features, especially white lines.

These operations provided spectra of copper-based compounds, which enabled the determination of the oxidation number of copper and to get acquainted with the shape of the spectra. Unfortunately, even after 8 hours of measuring the spectrum of one sample, it was still impossible to observe any less pronounced features, like pre-edge peaks, that

could give an insight into the geometry of the complexes. Therefore, higher emphasis was put on planning and executing the examination of these complexes with the use of synchrotron radiation.

In this thesis, results from the studies that were performed in 3 synchrotron facilities, were presented and compared to verify their repetitiveness for all chosen copper complexes. There were not found any significant discrepancies, even if beamlines differ in the applied radiation flux or design. In all obtained spectra, characteristic features, like inflections or pre-edge peaks, were present. Therefore, a process of photoreduction was excluded.

Some important conclusions from the results which were described in Chapter 2 can be formulated. The first one is that the laboratory setup can be useful in the preliminary examination of complex compounds and for testing conditions of examination before taking a trip to an external facility. Application of a more intensive X-ray beam revealed less intensive features, which were pre-edge peaks, that confirmed undergoing quadrupole transition of electrons and centrosymmetric crystallographic systems of all studied complexes. The similarity of the chemical structure between $Cu(phen)Cl_2$ and $Cu(phen,triaz)Cl_2$ was also noticed after comparison of their XAS spectra, yet minor differences were observed, that enabled distinguishing one from another.

After finishing the measurements of the complexes in a solid state of matter, studies on solutions containing compounds of interest could be started, which was widely described in Chapter 3. The first obstacle to overcome, was the development of the setup dedicated to the studies of solutions. It was found, that liquid which stays in contact with air during measurements, tends to evaporate in that manner, which leads to a significant loss of the sample and reduces the available time for data acquisition. As a result, the most efficient setups were those provided by the P65 beamline and made in cooperation with SOLARIS, in which the sample was closed inside a cell during irradiation. To prevent radiation damage and provide constant stirring of the liquids, the flow of the samples was forced by the applied pumps.

Since, these two compounds were (to the best of my knowledge) studied with XAS for the first time, to analyze and understand the results obtained for solutions, it was essential to obtain spectra of the solid samples, that provided insight about the possible shape, presence of characteristic spectral features, or position of the absorption edge. Moreover, the comparison of spectra of pellets and liquids provided very important information about the changes in the chemical structure of both copper-phenanthroline complexes, especially $Cu(phen,triaz)Cl_2$, which was not reported in the dedicated to this

complex publication. Chemical shifts towards higher energies of spectra of liquid samples to spectra of pellets suggested possible substitution of Cl atoms with more electronegative ligands, like -OH or -OH_2. Results of theoretical calculations of XAS spectra supported that explanation, by showing a misalignment between spectra calculated for preserved chemical structures of their solid state and corresponding experimental ones. While for the first chosen copper-phenanthroline complex, both possibilities of exchange of two Cl atoms to two -OH groups, or one -OH group and one -OH_2, seems to be equally possible, for the copper-triazole compound the second possibility appears to be more probable.

The most crucial part of this research was the studies of copper complexes with chosen biomolecules, which were DNA and bovine serum albumin. The first important aspect was the usage of the properly designed liquid delivery setup, that enabled performing measurements over a few hours, without losing the sample or whipping. The second was maintaining the expected incubation conditions, for about 20 hours, which demanded properly set parameters of the water bath. Finally, the results of the measurements needed to be compared with the results of the pellets and theoretical calculations, and an exchange of Cl atoms to other ligands had to be taken into account.

With the application of X-ray Absorption Spectroscopy, undergoing weak interactions between both copper-phenanthroline compounds and DNA were detected, by looking at the spectral subtraction results and its analysis. Results from XAS supported the description of the interaction mechanism from the literature, however, it needs to be corrected by the fact, that ligands change after dissolving. A substitution of Cl atoms with at least one -OH_2 group seems more likely to happen than for two -OH groups, which adds additional, electrostatic interaction to the description.

In the situation of a possible interaction of copper complexes with BSA, the additional organic group in the triazole complex probably enhances hydrophobic interaction between the complex and protein subdomains, what can be observed in the XAS spectra subtraction. Therefore, while both complexes similarly interact with DNA, the Cu(phen,triaz)Cl_2 exhibits stronger interactions with bovine serum albumin.

Summing up the above discussion, a few significant conclusions arising from this research should be emphasized:

1) The proposed procedure of synthesis of Cu(phen,triaz)Cl_2 by Tabassum et al. (2012), should be corrected, by adding the second product of the reaction – Cu(phen)Cl_2.

2) Laboratory XAS setup for studies on prospective copper-based drugs showed usefulness in the preliminary examination of these compounds for further, more advanced studies, that need to be conducted in synchrotron facilities.
3) All analyzed compounds are resistant to radiation damage, like photoreduction, since the results obtained in all XAS studies, which were performed with different radiation flux and acquisition times, gave similar results.
4) To study liquid samples, the most efficient setups are those containing dedicated cells and reducing contact of the liquids with air.
5) Both copper-phenanthroline compounds change their chemical structure after dissolving in an aqueous solution, probably by substitution of Cl with other groups, like -OH and/or -OH_2.
6) Only results from XAS provided information, that the structure of the studied complexes changes in aqueous solutions. That fact was not detected by other methods (like fluorescence emission spectroscopy), that were used in the characterization of the copper-triazole complex in the mentioned article.
7) Weak interactions of both complexes with DNA were confirmed by the XAS examination, with extension to the possible additional electrostatic interactions.
8) Cu(phen,triaz)Cl_2 seems to preferentially interact with BSA.

Finally, a thesis hypothesis: “The application of the X-ray Absorption Spectroscopy (XAS) gives the possibility to identify and describe interactions of two chosen copper-phenanthroline complexes with biomolecules” can be considered as confirmed, with an extension. XAS enabled not only observation of the weak interactions of both complexes with DNA, but also provided information about the changes in their chemical structure, that might enhance that process. For studies with BSA, results showed that the Cu(phen,triaz)Cl_2 preferably interacts with that molecule, possibly because of the presence of the additional planar group.

There are also some aspects of that research, that would be worth to be explored in the future. Firstly, some other copper-phenanthroline complexes, including those with more than one phenanthroline or other organic groups, would be worth to be investigated. Secondly, performing laboratory XAS study with a more intensive X-ray tube could decrease the level of the noise in the signal, and reduce acquisition times or needed concentrations of the complexes to obtain good-quality XAS spectra. It would be worth finding or formulating another method of determining the energy of the absorption edge,

since the maxima of the derivative of spectra are sensitive to noise and can be affected by other spectral features, what needs additional verifications.

Another possibility is to develop other liquid delivery setups, that might even more reduce needed volumes for constant, undisturbed flow. It would also be worth exploring other types of DNA molecules (other origins, short fragments, etc.) and proteins, with which copper-phenanthroline complexes might interact.

To explore the generation of the free radicals, induced by the undergoing redox reaction which copper from copper-phenanthroline complexes might undergo, it would be worthy to examine solutions with added reducing agents, like ascorbic acid.

All results and discussion of this research lead to the conclusion, that the characterization of the prospective chemotherapeutic drugs, containing copper or other metals, and examination of their interactions with biomolecules, can be conducted with great success with the application of the X-ray Absorption Spectroscopy. This method should be therefore considered by scientists working on therapeutic compounds, since it provides information that other methods, usually used in biology or chemistry fields, can not that easily detect.

List of scientific achievements

1) Publications:
   a) Wojtaszek, K., Błachucki, W., Tyrała, K., Nowakowski, M., Zając, M., Stępień, J., Jagodziński, P., Banas, D., **Stańczyk, W.,** Czapla-Masztafiak, J. and Kwiatek, W.M., 2021. Determination of Crystal-Field Splitting Induced by Thermal Oxidation of Titanium. *The Journal of Physical Chemistry A*, *125*(1), pp.50-56.
   b) **Stańczyk, W**. and Czapla-Masztafiak, J., 2021. The use of the X-ray absorption spectroscopy laboratory setup in the examination of copper (II) compounds for biomedical applications. *Nuclear Instruments and Methods in Physics Research Section B: Beam Interactions with Materials and Atoms*, *497*, pp.65-69.
   c) **Stańczyk, W.I.,** Czapla-Masztafiak, J., Błachucki, W. and Kwiatek, W.M., 2023. Comparison between laboratory and synchrotron X-ray absorption spectroscopy setup examination of Cu (II) complexes with prospective anticancer properties. *Nuclear Instruments and Methods in Physics Research Section B: Beam Interactions with Materials and Atoms*, *543*, p.165100.
2) Active participation in conferences
   a) **European XFEL and DESY Photon Science Users` Meeting 2020**; Hamburg, Germany; 29-31.01.2020; ***poster presentation***; title:“ Examination of copper (II) compounds with the use of laboratory XAS setup for biological applications”.
   b) **Joint Meeting of Polish Synchrotron Radiation Society and SOLARIS Users conference**; online; 9-11.09.2020; ***poster presentation***; title: “Examination of prospective chemotherapeutics with the use of the X-ray Absorption Spectroscopy”.
   c) **IV$_{th}$ Conference for PAN PhD students**; online; 23.11.2020; ***oral presentation***, title: „Badanie potencjalnych chemioterapeutyków przy pomocy Rentgenowskiej Spektroskopii Absorpcyjnej” („*Examination of prospective chemotherapeutics with the X-ray Absorption Spectroscopy*”).
   d) **DESY Photon Science Users' Meeting and European XFEL Users' Meeting 2021**; online; 25-29.01.2021; ***poster presentation***; title: „Examination of prospective chemotherapeutics with the use of the X-ray Absorption Spectroscopy”.
   e) **VIII$_{th}$ Internal Conference for Medical Physics students „FIZYKA DLA MEDYKA”**; online; 14-15.04.2021, ***oral presentation***; title: „Badanie związków

miedzi(II) do potencjalnego wykorzystania w chemioterapii przy pomocy Rentgenowskiej Spektroskopii Absorpcyjnej" („Examination of copper(II) compounds for prospective usage in chemotherapy with the use of X-ray Absorption Spectroscopy").

Additionally, during this conference, the presentation won **2nd place** in the contest for the best presentation.

f) **"XFELs for Beginners" workshop**; online; 27-28.04.2021; ***two oral presentations***; titles: „Preparing the sample for an XFEL campaign" and "Is my sample ready for XFEL experiment? - laboratory XAS verification".

g) **International Conference on X-Ray Absorption Fine Structure (XAFS2021 Virtual)**; online; 11-13.06.2021; ***oral presentation***; title: „Prospective copper(II) anticancer compounds' examination with the X-ray Absorption Spectroscopy".

h) **Zakopane School of Physics Breaking Frontiers: Submicron Structures in Physics and Biology**; Zakopane, Poland; 23-27.05.2023; ***oral presentation***; title: "BioXAS examination of copper-phenanthroline complexes in solutions with biomolecules".

3) Scientific internships

a) **FXE end-station, European X-ray Free Electron Laser (EuXFEL) GmbH**, Schenefeld, Germany; host: Christopher Milne, Ph.D.; 20.07-17.08.2021; financed from PROM NAWA program and grant nr 2016/21/D/ST4/00378 given by National Science Centre (NCN).

b) **ID26 beamline, European Synchrotron Radiation Facility (ESRF)**, Grenoble, France; host: Pieter Glatzel, Ph.D.; 1.06.2022-31.07.2022; financed from STER NAWA program for doctoral schools.

4) Study tours

a) **SuperXAS beamline, Swiss Light Source (SLS) synchrotron**, Paul Scherrer Institut (PSI), Villigen, Switzerland; 14-17.02.2020; XAS and XES measurements of Au and Cu-containing samples.

b) **Ultrafast optical spectroscopy station, The Extreme Light Infrastructure ERIC, ELI Beamlines Facility**, Dolní Břežany, Czech Republic; 20-24.09.2021; studies on copper-phenanthroline complexes by Transient Absorption (TA) Spectroscopy and Femtosecond Stimulated Raman scattering (FSRS) methods.

c) **CLÆSS beamline, ALBA synchrotron**, Cerdanyola del Vallès, Spain; 11-14.10.2021; XAS measurements of Cu-containing samples.

d) **PIRX beamline, SOLARIS synchrotron**, Kraków, Poland; 21-23.04.2022; XAS measurements of copper-phenanthroline complexes with referential compounds;

e) **P65 beamline; Deutsches Elektronen-Synchrotron (DESY) synchrotron**, Hamburg, Germany; 15-19.08.2022; XAS measurements of copper-phenanthroline complexes, including liquid samples with DNA.

f) **ASTRA beamline, SOLARIS synchrotron**, Kraków, Poland; 19-22.04.2023; XAS measurements of copper-phenanthroline complexes, including liquid samples with bovine serum albumin.

5) Other activities

a) **President of the Doctoral Council of the Institute of Nuclear Physics Polish Academy of Sciences**: November 2019- December 2021

b) **Member of the Scientific Council of the Institute of Nuclear Physics Polish Academy of Sciences**: November 2019- December 2021

c) **Member of the Polish Academy of Sciences Team of the Polish Association of Doctoral Candidates (KRD)**: February-December 2021

d) **President of the Doctoral Council of the Polish Academy of Sciences**: November 2021-November 2022

e) **Leader of the Organization Team of the 6th Conference for Ph.D. students of Polish Academy of Sciences KonDokPAN 2022**: August-October 2022

f) **Member of the Polish Association of Doctoral Candidates (KRD) Advisory Board**; since March 2023